AN INVESTIGATION OF CERTAIN THERMODYNAMIC LOSSES IN MINIATURE CRYOCOOLERS

FINAL REPORT

AUTHOR: Cryogenics Group, Oxford University
RESEARCH: Fast Response Temperature Measurements in Cryocoolers

REPORT FOR:	USAF AFRL
CONTRACT:	FA8655-06-1-3071
DATE:	02-May-2007
ADDITIONAL DOCUMENTS:	None.
NUMBER OF PAGES:	71
OUR REF:	LOS-FR3

REPORT DOCUMENTATION PAGE

Form Approved OMB No. 0704-0188

Public reporting burden for this collection of information is estimated to average 1 hour per response, including the time for reviewing instructions, searching existing data sources, gathering and maintaining the data needed, and completing and reviewing the collection of information. Send comments regarding this burden estimate or any other aspect of this collection of information, including suggestions for reducing the burden, to Department of Defense, Washington Headquarters Services, Directorate for Information Operations and Reports (0704-0188), 1215 Jefferson Davis Highway, Suite 1204, Arlington, VA 22202-4302. Respondents should be aware that notwithstanding any other provision of law, no person shall be subject to any penalty for failing to comply with a collection of information if it does not display a currently valid OMB control number.
PLEASE DO NOT RETURN YOUR FORM TO THE ABOVE ADDRESS.

1. REPORT DATE *(DD-MM-YYYY)*	2. REPORT TYPE	3. DATES COVERED *(From – To)*
08-05-2007	Final Report	21 July 2006 - 21-Mar-07

4. TITLE AND SUBTITLE

5a. CONTRACT NUMBER
FA8655-06-1-3071

5b. GRANT NUMBER

5c. PROGRAM ELEMENT NUMBER

6. AUTHOR(S)

Dr. Charles R. Stone

5d. PROJECT NUMBER

5d. TASK NUMBER

5e. WORK UNIT NUMBER

7. PERFORMING ORGANIZATION NAME(S) AND ADDRESS(ES)
University of Oxford
Parks Road
Oxford OX1 3PJ
United Kingdom

8. PERFORMING ORGANIZATION REPORT NUMBER
N/A

9. SPONSORING/MONITORING AGENCY NAME(S) AND ADDRESS(ES)

EOARD
Unit 4515 BOX 14
APO AE 09421

10. SPONSOR/MONITOR'S ACRONYM(S)

11. SPONSOR/MONITOR'S REPORT NUMBER(S)
Grant 06-3071

12. DISTRIBUTION/AVAILABILITY STATEMENT
Approved for public release; distribution is unlimited.

13. SUPPLEMENTARY NOTES

14. ABSTRACT

Measurements were made of gas temperatures and power losses for a compression volume that included a regenerative heat exchanger.
A fine wire resistance thermometer with a rapid response was used to measure the gas temperature for flows between the piston/cylinder volume and the regenerator. The temperature profiles exhibited features that varied with different gases and operating conditions. These results were interpreted in terms of a stratified tidal gas volume that is subject to thermal diffusion and flow turbulence effects. A few nitrogen results for high pressure and low frequency were very unstable with significant high frequency components. A tentative interpretation was that this behaviour was associated with the transition from laminar to turbulent flow conditions.
At the other end of the regenerator in a separate fixed volume, a twin thermocouple probe was used to investigate the performance of a compensation technique designed to improve the time response of the bare thermocouples. The technique involves arranging two thermocouples with different time constants such that they experience the same gas temperature variation. The gas temperature is reconstructed by using various approaches for estimating the response times. It is shown that this technique can be considered, provided that the noise levels are low enough. For the measurements described here the noise could only be sufficiently reduced by ensemble averaging. This would be a limitation in circumstances where the waveform is not very repeatable.
The power loss measurements showed that a loss existed that could be correlated by a combination of Reynolds number and the experimental parameters pressure, frequency and stroke. Attempts to formulate this in a non-dimensional form were not successful suggesting that key parameters have been missed. One aspect in particular that needs closer attention is the effect of phase angle between mass flow and pressure variation.
An interesting feature of this work is the general agreement between the resistance wire thermometry results and the power loss measurements. Both sets of results exhibit changes in behaviour consistent with the idea of a laminar to turbulent transition. Furthermore a region of transition defined by a Reynolds number suggested by the power measurements is reasonably supported by the thermometer results..

15. SUBJECT TERMS
Cryocoolers, Thermodynamics, Compressible Flows, EOARD

16. SECURITY CLASSIFICATION OF:			17. LIMITATION OF ABSTRACT	18, NUMBER OF PAGES	19a. NAME OF RESPONSIBLE PERSON
a. REPORT	b. ABSTRACT	c. THIS PAGE			BARRETT A. FLAKE
UNCLAS	UNCLAS	UNCLAS	UL	72	19b. TELEPHONE NUMBER *(Include area code)* +44 (0)1895 616144

1 CONTENTS

1 CONTENTS 2
2 EXECUTIVE SUMMARY 3
3 BACKGROUND 4
4 INTRODUCTION 4
5 EXPERIMENTAL SETUP 7
6 FINE WIRE RESISTANCE THERMOMETER MEASUREMENTS (HOT WIRE PROBE) 10
7 MEASUREMENTS MADE USING COMPENSATED THERMOCOUPLES 19
8 DESCRIPTION OF POWER LOSS MEASUREMENTS 22
9 OVERALL SUMMARY AND CONCLUSIONS 37
10 FUTURE WORK 38
11 REFERENCES 38

APPENDIX 1: PRESSURE DROP IN REGENERATOR 39

APPENDIX 2: REPORT ON COMPENSATED THERMOCOUPLE RESULTS 42

2 EXECUTIVE SUMMARY

Measurements were made of gas temperatures and power losses for a compression volume that included a regenerative heat exchanger.

A fine wire resistance thermometer with a rapid response was used to measure the gas temperature for flows between the piston/cylinder volume and the regenerator. The temperature profiles exhibited features that varied with different gases and operating conditions. These results were interpreted in terms of a stratified tidal gas volume that is subject to thermal diffusion and flow turbulence effects. A few nitrogen results for high pressure and low frequency were very unstable with significant high frequency components. A tentative interpretation was that this behaviour was associated with the transition from laminar to turbulent flow conditions.

At the other end of the regenerator in a separate fixed volume, a twin thermocouple probe was used to investigate the performance of a compensation technique designed to improve the time response of the bare thermocouples. The technique involves arranging two thermocouples with different time constants such that they experience the same gas temperature variation. The gas temperature is reconstructed by using various approaches for estimating the response times. It is shown that this technique can be considered, provided that the noise levels are low enough. For the measurements described here the noise could only be sufficiently reduced by ensemble averaging. This would be a limitation in circumstances where the waveform is not very repeatable.

The power loss measurements showed that a loss existed that could be correlated by a combination of Reynolds number and the experimental parameters pressure, frequency and stroke. Attempts to formulate this in a non-dimensional form were not successful suggesting that key parameters have been missed. One aspect in particular that needs closer attention is the effect of phase angle between mass flow and pressure variation.
An interesting feature of this work is the general agreement between the resistance wire thermometry results and the power loss measurements. Both sets of results exhibit changes in behaviour consistent with the idea of a laminar to turbulent transition. Furthermore a region of transition defined by a Reynolds number suggested by the power measurements is reasonably supported by the thermometer results.

3 BACKGROUND

This report describes work that is a continuation of previous studies reported in Los-FR1[1] and Los-FR2[2]. These investigations are intended to give a better understanding of thermodynamic losses that occur in miniature Stirling cycle coolers but which are not adequately explained by our existing models. It is hoped that the results of this study will be useful in two ways. Firstly the results will help to develop improved CFD models of processes that occur in these coolers; secondly that the results might produce ideas for reducing such losses.

Los-FR1 looked closely at methods for determining power input to the gas. The conclusion drawn was that the only reliable way was to determine the integral of $P.dV$ for the compression space. This approach is accurate providing that any phase changes introduced in the instrumentation electronics are corrected. It was found that there was too much uncertainty in the motor losses to allow the power input to the gas to be determined from the total input power.

Los-FR2 used the test rig configured as a simple gas spring to produce gas springs losses that could be compared with established results, in particular the work of Kornhauser[3,4]. It was found that the agreement was good for a wide range of gases and Peclet numbers, and that the results supported Kornhauser's modification to Lee's[5] original equation. For these measurements there was a significant gas leakage past the piston and the results also demonstrated that this seal leakage did not appear to affect the nature of the gas spring losses. Los-FR2 also briefly described an unsuccessful attempt to apply a compensated twin thermocouple sensor to the measurement of varying gas temperature.

The final part of LOS-FR2 looked at whether the measurement of compression losses could be used to deduce heat transfer coefficients in a regenerator for oscillating flow. A differential method was suggested but not implemented.

In the work described here, the areas of temperature measurement and gas spring power loss are again pursued, this time with a gas spring geometry that more closely resembles the geometry of a real Stirling machine.

4 INTRODUCTION

The understanding of the compression losses in Stirling cycle machines can be approached in two different ways:

- A Quantitive approach: Direct measurement of losses – Losses can be analysed to derive values for components that are not included in existing models. The behaviour of these residual losses can be investigated for varying compressor parameters

- A Qualitative approach: Measurement of cycle temperature variation at particular locations. Temperature measurements can indicate magnitudes of heat transfer and mixing processes.

These are not in principle entirely separate – accurate temperature measurements for enough points would allow the energy flows and hence losses to be determined. However, in reality it is not practical to do this – temperature sensors tend to be intrusive and only a limited number can be installed.

The emphasis that will be pursued here is a closer consideration of the problems involved with measuring varying gas temperatures in Stirling cycle machines. Two approaches were investigated: a fine wire resistance thermometer (RT) and a more sophisticated technique that will be referred to as a compensated thermocouple thermometer.

To provide a suitable test bed for the thermometry, the test rig was configured as a more complex gas spring that included a regenerative heat exchanger. Additional components were made to allow the different thermometers to be installed. The modified test rig is shown in Figure 1.

Figure 1. Compression Test Rig with New Configuration

Although the main focus of this work was the investigation of thermometry it was decided that it would also be worth measuring the gas spring losses for this more complicated configuration. The previous work on the simple gas spring demonstrated that the phase correction approach can give good results and this was an opportunity to obtain some additional data.

To summarize it is hoped that although information acquired with these measurements will not be enough to guarantee a clear description, they will nonetheless be useful in gaining a better understanding:

- Temperature measurements are point measurements so they cannot be used to determine energy flows without assuming particular temperature profiles. For these

oscillating flow conditions and the small mean differences that would have to be determined, assuming a temperature distribution is not justifiable – uncertainties would be too large for the results to be useful

- The cold wire RT has a fast response and will give temperature variation for a small volume near the regenerator. This will be useful for investigating the nature of the flows between the compression space and the regenerator.

- The twin thermocouple is expected to have insufficient response to follow temperature variation. However it is a useful test vehicle for the compensated thermocouple approach. It is not expected that it will give as much insight into oscillating flows as the cold wire RT because the flow here will be small. Nonetheless it will give experience that will help determine whether this technique can be applied to these types of measurements

- Power loss measurements will help understand whether losses can be characterised in a useful way. They will not necessarily be directly applicable to Stirling cycle machines but they will be considerably more realistic than those calculated on the basis of a simple gas spring model.

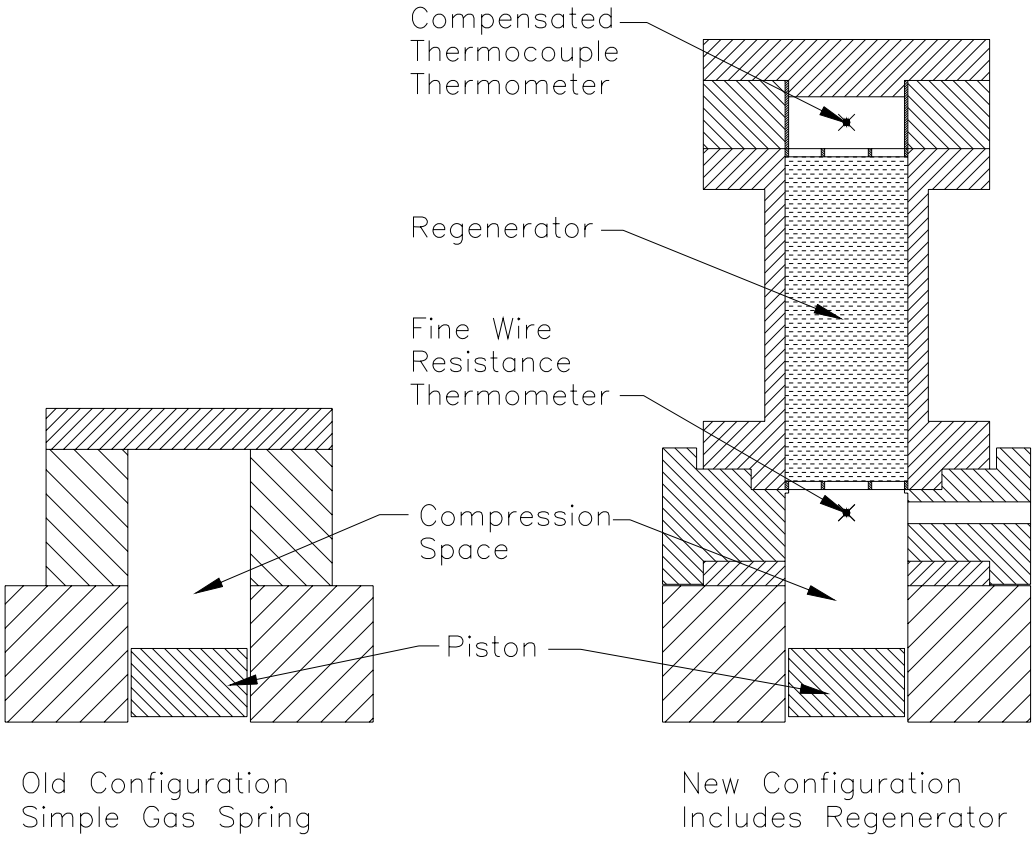

Figure 2. Comparison between Old and New Configurations

A cross section of the test rig used in this work is shown in section, together with the original simple gas spring in Figure 2. It will be seen that for the new configuration the compression space above the piston has been reduced in volume and is now attached to two additional

cylindrical volumes. The one closest to the compression space is filled with metal mesh so that it functions as a regenerative heat exchanger (i.e. a regenerator), the second added volume is free of any additional heat transfer surface.

The fine wire resistance thermometer was positioned slightly off centre in the top of the compression space (Volume A) close to the regenerator (Volume B). The temperature that will be measured will be a function of both the heat transfer conditions in the compression volume and the temperature of the gas flowing into the volume from the regenerator.
The compensated thermocouple thermometer was positioned approximately in the centre of the top volume (Volume C). The gas flow into the volume is very much smaller than for the volume A and it is expected that the temperature variation here will be less affected by the flow. Neither of these thermometers was purpose built for this application. The positioning was therefore mainly dictated by their existing installation requirements.

The power loss measurements were made by recording the instantaneous values of piston position and compression space pressure. After correcting for phase changes in the electronics the power loss is calculated from:

$$Power = f.\oint P.dV$$

The volume changes are calculated from the piston position and piston area

Temperature and power loss measurements were made for helium and nitrogen for varying pressures, frequencies and strokes. A Fylde 8 channel data acquisition system was used to collect the data. This will be described in more detail in the next section.

5 EXPERIMENTAL SETUP

A detailed diagram of the test rig volumes with dimensions is show in Figure 3. The principal additions are the regenerator volume and the two thermometer installations.

Regenerator
The regenerator volume was packed with circular mesh discs punched out from mesh sheet. For the measurements described only one type of mesh was used (see Table 1) but the rig could be repacked with other types of mesh if required.

Table 1.

Regenerator Material	Mesh Weave	Mesh Number (wires per inch)	Wire Diameter (mm)	Porosity* (void vol/total vol)
Stainless Steel	Plain Weave	#250	0.040	0.67

*The porosity was determined by weighing the regenerator assembly before and after packing. The mass of regenerator material and its density gives the volume of regenerator mesh.

Handling loose mesh discs can be problematic because the material as woven is very springy. To help with packing the regenerator the mesh was first annealed in a vacuum furnace. The annealed mesh was then packed in an assembly jig prior to being installed in the regenerator

housing. To prevent the regenerator from bowing out at its ends two supports were included as shown in Figure 4. The supports are designed to be as open as possible so as to avoid affecting the gas flows into and out of the regenerator. As it turned it was found that the annealing process caused a slight bonding of the meshes together so that they handled as slightly sintered blocks. The supports were therefore probably not really necessary.

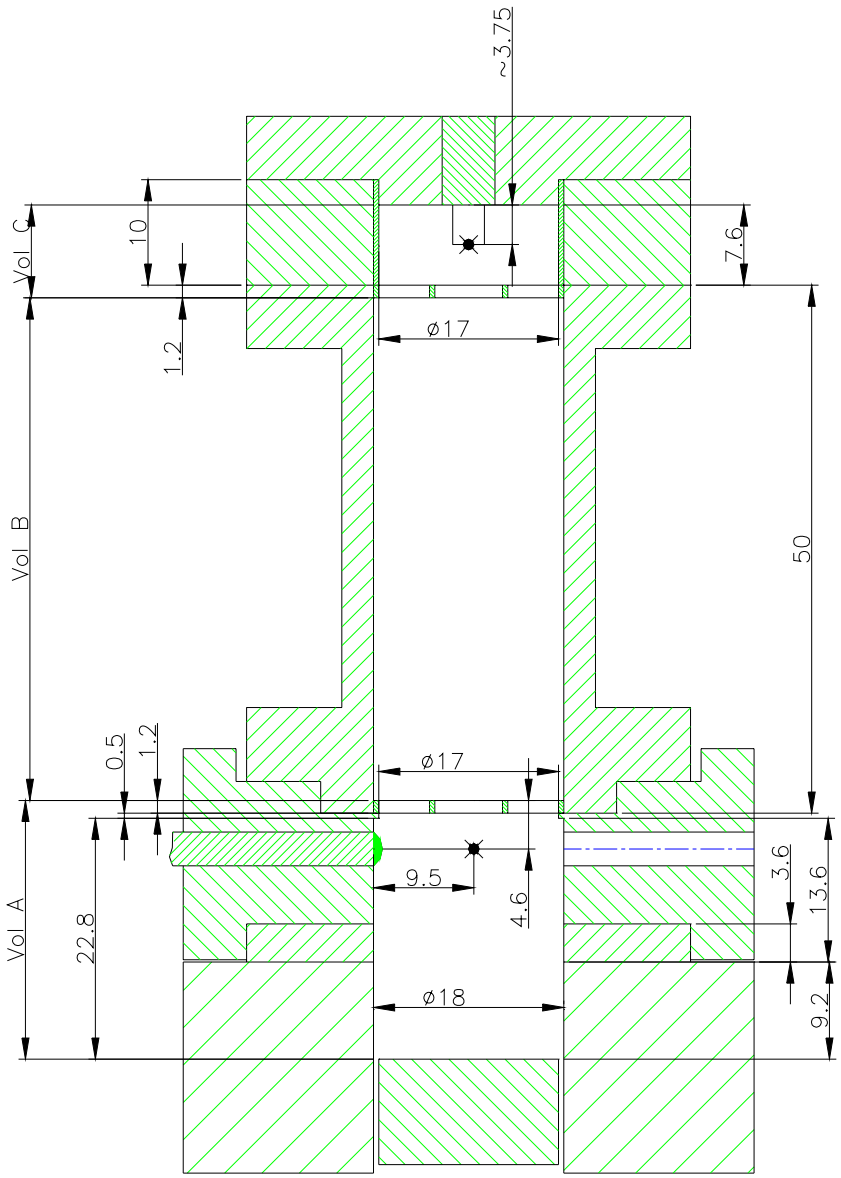

Figure 3. Details of New Configuration for Test Rig

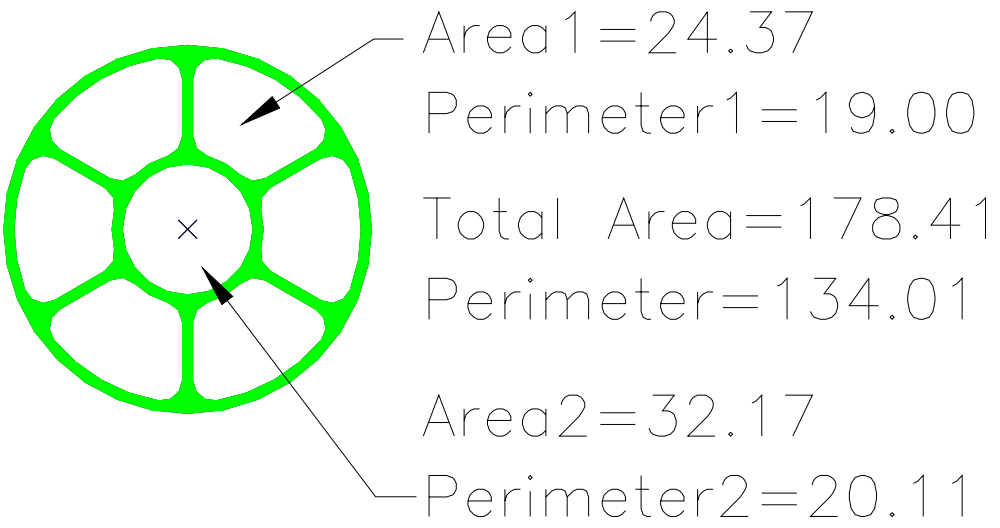

Figure 4. Regenerator Mesh Support

Thermometer installations
The thermometers required special adaptors to be made to allow them to be installed with the minimum of extra dead volume and intrusion into the gas flow. These are shown in figure 7.

Data Aquisition System
The data acquisition equipment used was the Fylde 8 channel unit used previously. The output of the Fylde unit is directly imported in to a Excel spread sheet for subsequent analysis. Because it was not intended to use the electrical input power for loss calculations, the instantaneous values for motor current and voltage measurements were no longer recorded. Additional inputs to the A/D were the thermometer outputs and an extra pressure channel to record the pressure variation at the end of the regenerator. The channel allocation with sensor details and calibrations are show in Table 2.

Table 2: Channel allocations for inputs into Fylde Data Acquisition system

Channel	Measurement Parameter	Sensor	Gain	Offset
1	Pressure in Volume A	Endevco	2.408 bar/V	6.0206 bar
2	Pressure in Volume C	Druck 200	1.9677 bar/V	15.444 bar
3	N/C			
4	Pressure in compressor body	Druck 820	6.0046 bar/V	8.3174 bar
5	Piston Position	Sch' LVDT	2.0884 mm/V	-5.5968 mm
6	Fine Wire Thermometer	TSI probe	10.296 K/V	38.379 deg C
7	TC 25 micron	Custom probe	4.00 K/V	24.00 deg C
8	TC 50 micron	Custom probe	4.00 K/V	24.00 deg C

Note: The Fylde data Acquisition unit digitises two channels at a time with 5 microsecond intervals hence channels 1 and 5 are at t=0, channels 2 and 6 are at t=5 microseconds etc

In addition to the cyclic variations recorded by the Fylde unit, information was also recorded manually:

Gas used
Frequency (from power analyser)
Total Input Power
Coil Current
Nominal Fill Pressure
Regenerator Body Temperature
Cold Junction Temperature (for TCs)
Amp7 zeros (V) TC50
Amp8 zeros (V) TC50
Resistance Thermometer current

Experimental Procedure
The procedure followed was to fill the test rig with the chosen gas to a prescribed pressure. The frequency was set and the stroke was increased to the required value by observing the LVDT output on a scope. The mean position of the piston was maintained approximately in its mid position by varying the dc current through the motor coil. When the compressor operation reached a steady state then the Fylde data acquisition system was used to record the variation of the parameters defined in the channel allocation above. The manual measurements were also recorded.

Two different setups were used. In one, the sampling period was fixed at 1 second with a sample rate of 5kHz. These measurements were used for the resistance thermometry and power measurements. For the compensated thermocouple measurements it was desirable to enable greater ensemble averaging. The sample rate was reduced to 2kHz and the sample period was increased to 15 seconds.

The measurements recorded in the Excel spreadsheet were the voltage outputs taken directly from the various instruments. Phase compensation and calibration factors are applied to these values to arrive at converted parameter values that can be used for analysis. This process of phase compensation and calibration is executed in additional Excel spreadsheets.

6 FINE WIRE RESISTANCE THERMOMETER MEASUREMENTS (HOT WIRE PROBE)

Description of Probe
The resistance thermometer measurements were made using a standard hot wire anemometer probe manufactured by TSI. The complete probe assembly consists of two parts, a sensor that incorporates the fine wire sensing element and a support into which the sensor component fits. The manufacturer's model numbers and details are as follows:

Hot Wire Sensor:	TSI Model 1210-T1.5 General Purpose Probe with wire sensor. (The wire is 3.8 microns in diameter and is tungsten with a protective platinum coating)
Probe Support:	TSI Model 1150 Single Sensor, Standard Probe Support (The probe supports come in three lengths, the model used was standard length = 6 inch version designated Model 1150-6)

Hot wire sensor and probe support are shown in Figures 5 and 6 respectively

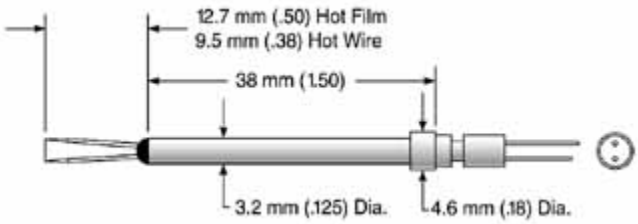

Figure 5. TSI Model 1210-T1.5 General Purpose Probe With Wire Sensor.

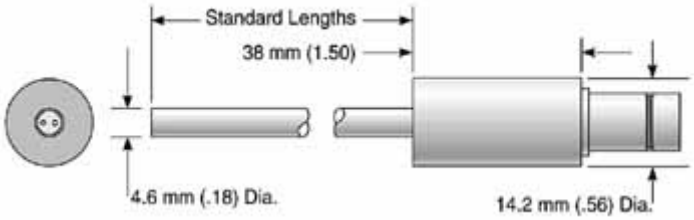

Figure 6. TSI Model 1150 Single Sensor, Standard Probe Support

For use as an anemometer this type of probe is usually operated with a varying current that maintains a constant temperature. However to operate it as a thermometer the sensor is energized with a constant current. For the results described here the current was 1mA. The choice of current is a compromise between sensitivity and errors produced by self heating. For the nitrogen at 1 bar, the self heating was found to be acceptably small by observing that there was no obvious change in temperature variation when the current was reduced to 0.5mA.

The output from the probe conditioning electronics is the voltage across the wire probe. Hence if the temperature/resistance characteristics of the probe are known then the temperature can be calculated. The nominal resistance is ~ 6 ohms and the sensitivity with 1 mA is ~ 10.3 deg C per volt. This output was recorded using the Fylde Data Acquisition unit The response time for this thermometer is low because of the very small sensor diameter. It was intended to estimate this by observing the temperature decay when the sensor is temporarily heated by a short pulse. Unfortunately the facility for doing this in the TSI instrument did not appear to work. Therefore the time constant is estimated using a heat transfer correlation for a cylinder. With this small diameter, the Reynolds number is much smaller than 1, so the flow is laminar and unseparated. The Nusselt number is evaluated using Churchill and Bernstein's equation:

$$\mathrm{Nu} = 0.3 + \frac{0.62\,\mathrm{Re}_D^{1/2}\,\mathrm{Pr}^{1/3}}{\left[1+(0.4/\mathrm{Pr})^{2/3}\right]^{1/4}}$$

Since the temperature fluctuations are small, the temperature sensitivity of fluid properties are not taken into account. All fluid properties are evaluated at 25 deg C. From the Nusselt number definition, the heat transfer coefficient (h) can be derived, which is then used to calculate the time constant as shown below.

$$\tau = \frac{\rho_w C_w D_w}{4h}$$

where the density (ρ_w) and specific heat (C_w) are values for tungsten.

Figure 7 shows that the time constant reduces with increasing pressure. Due to the much higher thermal conductivity of helium, the cold wire has a slower response in a nitrogen environment. Therefore, the biggest time constant occurs at 1 bar pressure in nitrogen gas and zero flow speed. The time constant is still 1.2 ms, which is small enough for temperature measurements to be considered instantaneous at the operating frequencies used in this study

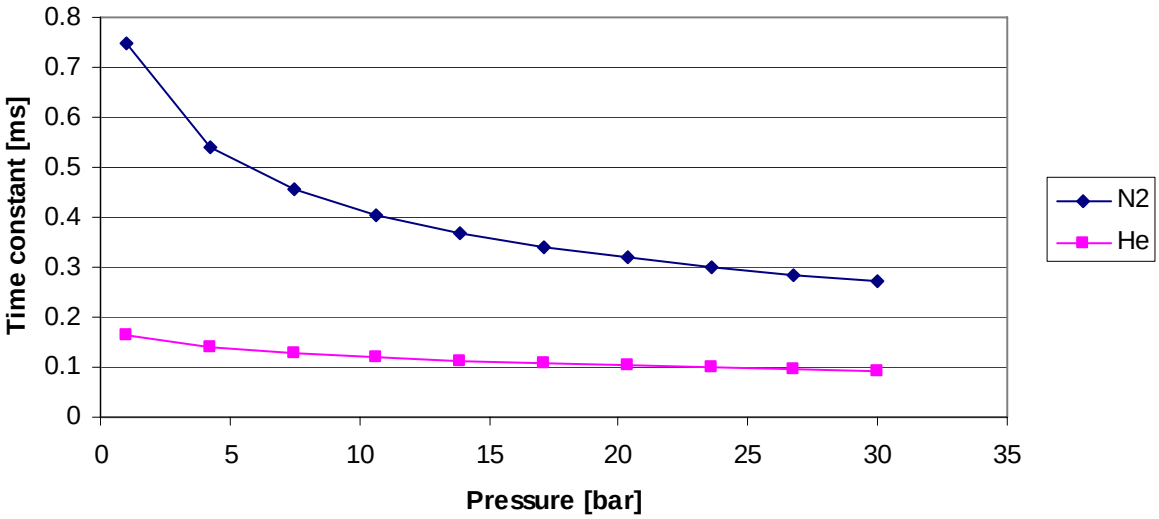

Figure 7. Estimated time constant of cold wire at 0.5 m/s flow velocity.

The complete probe assembly was installed into the compression test rig using a redesigned compression space plate and a housing that provided a seal on the OD of the 4.6 mm probe support. The housing was designed to allow the probe to be positioned in different radial locations within the compression volume but for the results given here the probe was positioned radially at the centre and axially about 4.5 mm away from the regenerator. The installation of the probe and probe housing are shown in Figure 8.

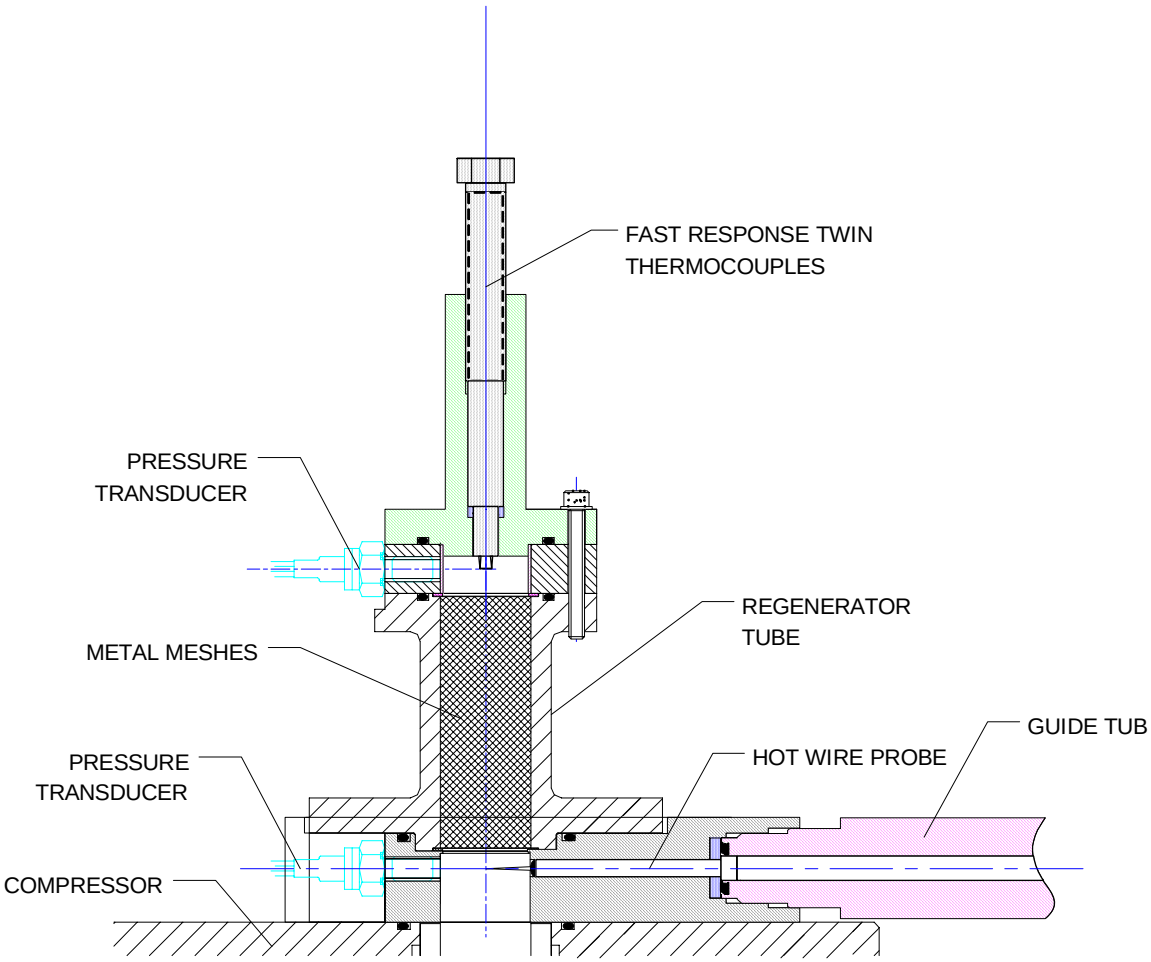

Figure 8. Installation Details for Pressure Transducers and Thermometers

Gas Temperature Measurements

The gas temperature variation was measured over a wide range of conditions for the two gases, nitrogen and helium. The ranges covered were:

Pressure:	1 to 26 bar
Frequency:	8.6 to 53 Hz
Stroke:	4 to 14 mm

It was not possible to obtain complete coverage of the strokes for all pressure and frequency combinations because the motor was largely running off resonance and the coil current had to be limited to prevent the coil overheating.

Overall the measurements revealed a surprisingly complex variation in temperature profiles. Part of the variation that is seen with stroke is likely to be due to the varying time that the sensor spends in the tidal gas flow that is flowing in and out of the regenerator. As the sensor is approximately 4.5 mm away from the regenerator, the sensor would be expected to respond to the tidal flow only for small periods if the stroke is small (e.g. 6 mm). When the stroke rises to 14 mm then the tidal flow will dominate the temperature profile.

It has not been possible to provide a comprehensive explanation for all that has been observed. There is some overlap between the nitrogen and helium temperature profiles but there are also regimes where the nitrogen and helium data were found to be quite distinct. The most general observation that was common to both sets of data, was that whilst cycle to cycle repeatability for the temperature could be very variable this was not reflected in the pressure or piston displacement values which were very repeatable and generally sinusoidal.

Helium Results

The range of temperature profiles obtain with helium is fairly well illustrated in Figures 9 and 10 which show the variation for differing strokes. The results in Figure 9 represent the data with the lowest mass flows i.e. low frequency and pressure. It is seen that whilst the waveform becomes more distorted as the stroke increases up to the maximum of 14mm, there are no additional features in the waveform. It is possible however to detect discontinuities in the gradient for the 14 mm stroke.

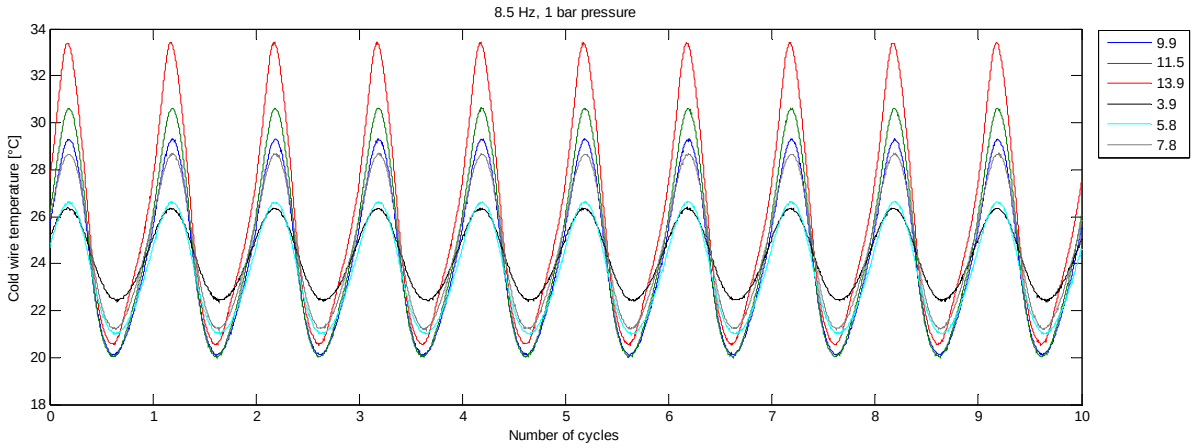

Figure 9. Fine Wire RT measurements: Helium, 1bar 8.5Hz for different strokes (mm)

In Figure 10 the results are shown for a pressure of 5 bar, still with a low frequency of 8.5 Hz. The waveform has acquired the feature of an extra minimum in the low temperature end. At higher frequencies the temperature profile changes but it still retains the same general features as is shown in Figure 11.

At the highest pressures and strokes the waveform starts to show a distinct lack of repeatability with apparent high frequency components as is shown in Figure 12. It is seen that the second peak is quite abrupt and that there are signs of instability.

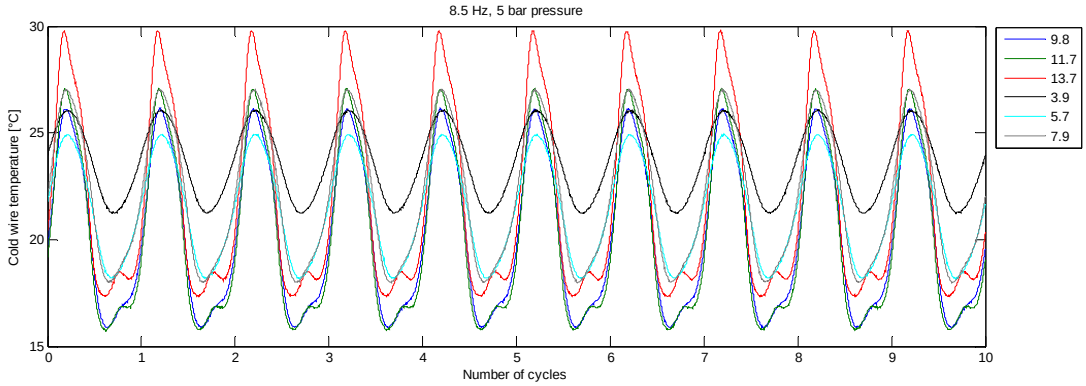

Figure 10. Fine Wire RT measurements: Helium, 5bar, 8.5Hz for different strokes (mm)

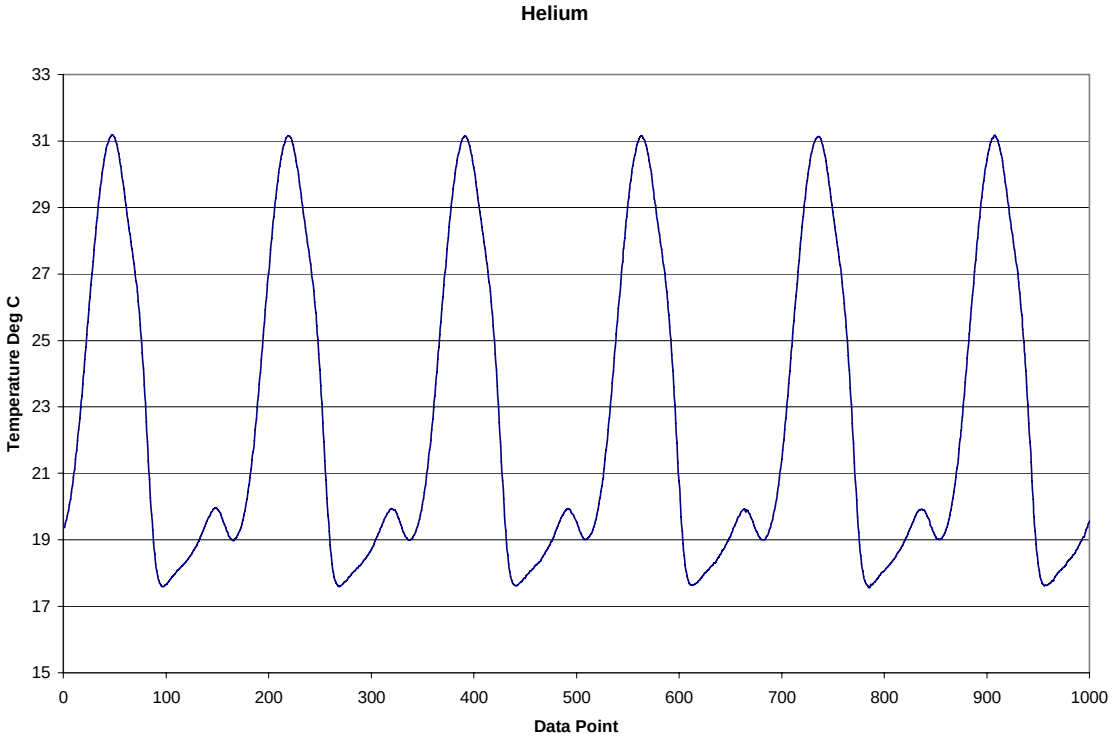

Figure 11. Fine Wire RT measurements: Helium, 3bar, 29 Hz, stroke = 14mm

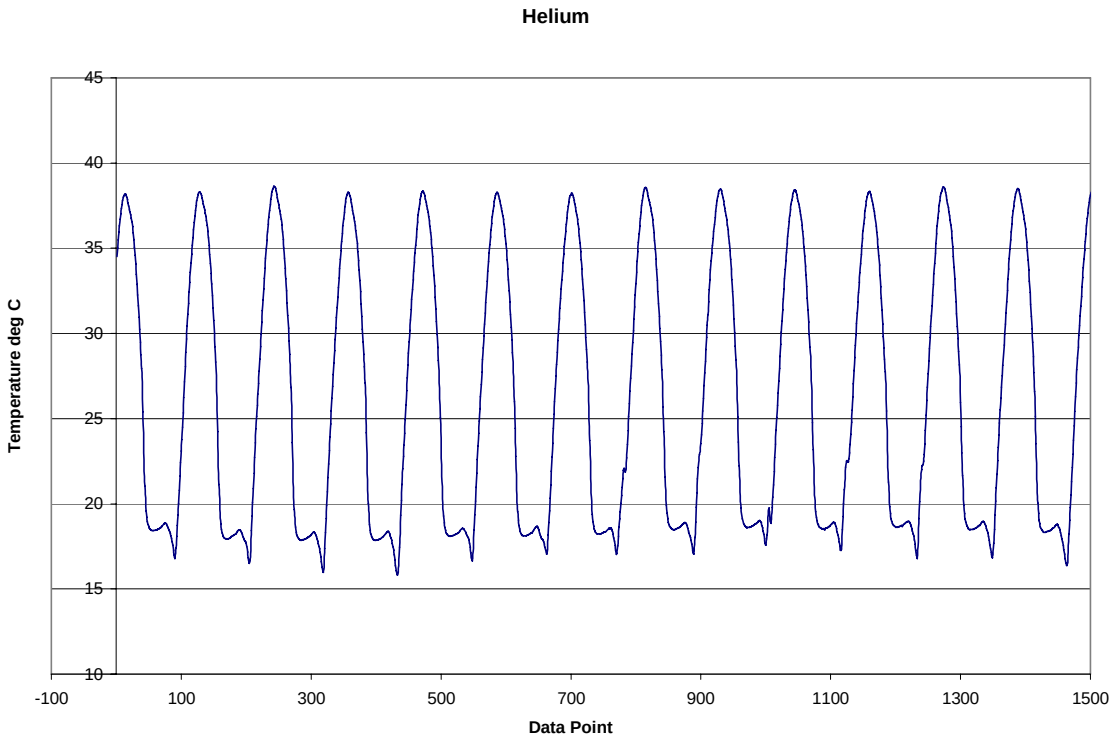

Figure 12. Fine Wire RT measurements: Helium, 21bar, 44 Hz, stroke = 14mm

Essentially the behaviour can be summarised as follows:

- At the lowest pressures the temperature variation is basically sinusoidal with distortion increasing with stroke and some sign of a discontinuity in the gradient
- As the pressure is increased, the waveform distortion is also increased until a second minimum appears in the lower temperature region. Discontinuities in the gradient also become more obvious.
- The results do not allow the transition to be pin-pointed because the next pressure investigated was 3 bar and the double minima appear to be established for 14 mm.
- As the frequency and pressure is increased the second minimum remains but its shape and position change
- At the highest pressures, frequencies and strokes the second minima becomes increasingly abrupt. Also the waveform show signs of instability with high frequency components becoming apparent.

Nitrogen Results

The low pressure nitrogen results are found to be fairly similar to the high pressure results for helium. Figure 13 shows the nitrogen results for a pressure of 1 bar and frequency of 8.6 Hz which have very clear similarities with the helium results at 5 bar shown in Figure 10.

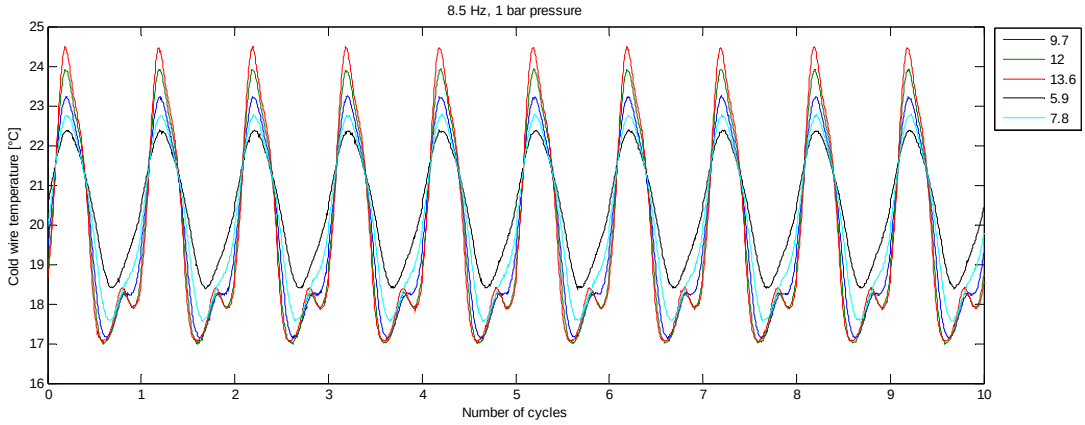

Figure 13. Fine Wire RT measurements: Nitrogen, 1bar, 8.5Hz for different strokes (mm)

With increasing pressure the nitrogen results are similar to the higher pressure helium results with the double minima feature being retained but changing shape and showing a sharper discontinuity. The high frequency components and reduction in repeatability also set in, but this time increase to the point where in a few cases the waveforms becomes very unstable and unrepeatable. For these results the behaviour appears chaotic and is characterized by both the presence of high frequency components and a lack of any repeatable waveform. In the 8.5Hz example shown in Figure 14, there are frequency components as high as 250Hz. The pressure variation for this set of data points is shown in Figure 15. It will be seen that there is no sign of this instability in these results. Unfortunately the current limit imposed on the motor did not allow higher strokes to be investigated for this pressure and frequency.

It might be expected that this unstable behaviour might be associated with some flow transition and would also be discernible in some combination of stroke and pressure for higher frequency data. This was not found to be the case – the only examples of this extreme instability occur in the low frequency data i.e. at 8.5 or 18 Hz.

For the highest combinations of pressure frequency and stroke there is variability between cycles, but there are still features of the waveform that remain consistent. Figure 16 shows the waveform for nitrogen for such conditions. It will be seen that it is remarkably similar to the high pressure, high frequency results for helium shown in Figure 12

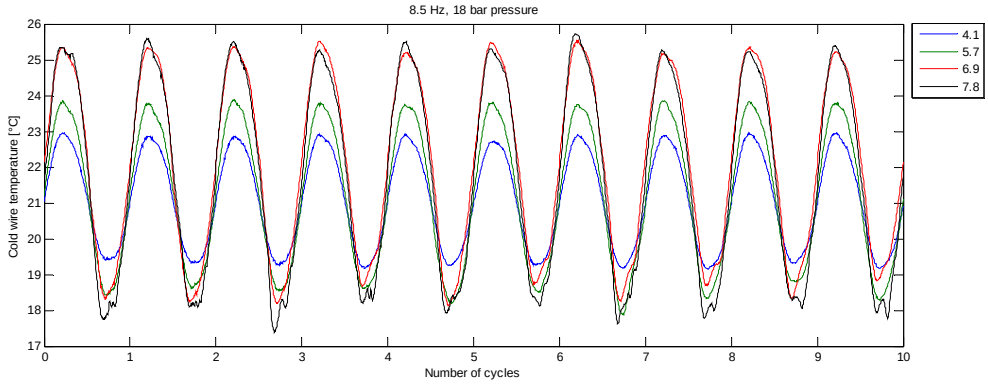

Figure 14. Fine Wire RT measurements: Nitrogen, 18bar, 8.5Hz

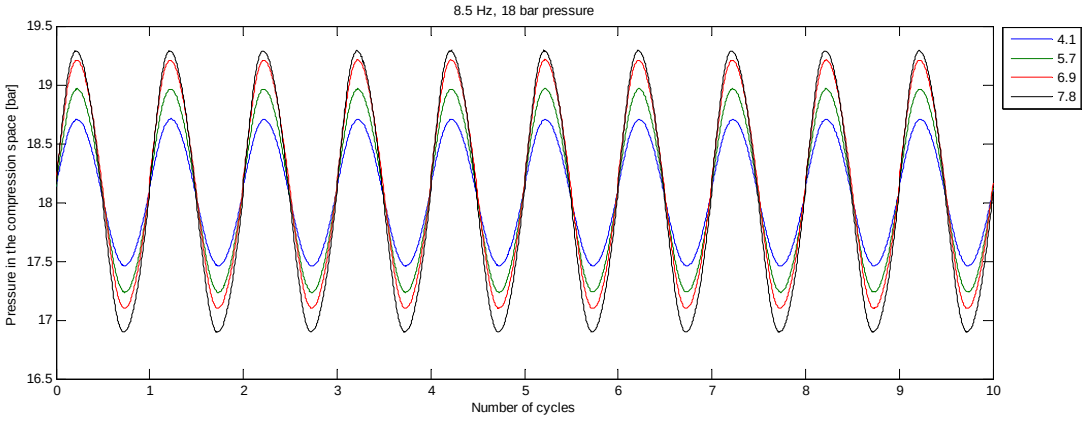

Figure 15. Pressure measurements: Nitrogen, 18bar, 8.5Hz

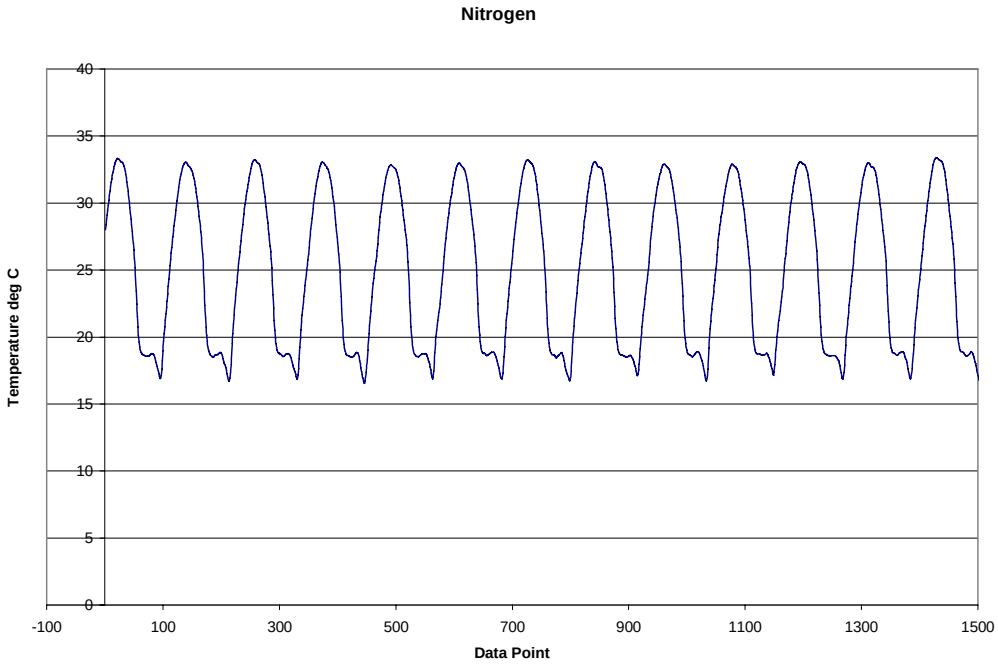

Figure 16. Fine Wire RT measurements: Nitrogen, 26bar, 43Hz, stroke = 14mm

Summary

These results tend to support the idea that there are two effects controlling the temperature behaviour: Thermal diffusivity along an axial temperature gradient and the transition from laminar to turbulent flow.

Thermal Diffusivity

Firstly for both gases the low stroke temperatures appear to be roughly sinusoidal. As the stroke increases additional features begin to appear; initially in the form of gradient discontinuities, ultimately with the appearance in many results of an additional minimum in the low temperature half of the cycle. The additional minimum always appears for the nitrogen results but for the helium results it is absent in the lowest pressure measurements.

A tentative conclusion that may be drawn is that the thermometer is measuring the temperature of two distinct volumes of gas and that the sudden changes in gradient that are generally observable correspond to the transition from one volume to another. The interesting thing to note is that the transition becomes more abrupt at higher pressures and frequencies. If the mixing in the compression volume was increasing with increasing pressure and frequency then it would be expected that the increased heat transfer would tend to smooth out the transition. The observation that the transition becomes more distinct suggests that the heat transport is less effective. A possible explanation for this is that the gas remains stratified and that the axial temperature gradient is enhanced because the thermal diffusion is reduced. Higher pressure reduces thermal diffusivity and if the frequency is higher then there is also less time for the heat conduction to occur. For the low pressure, low frequency, helium results it appears that the thermal diffusion is sufficient to largely smooth out any transition. This is not seen in the corresponding nitrogen results as its thermal diffusion is substantially lower (by a factor of >8):

Thermal Diffusivity for Helium @ 1 bar, 300 K = 1.8×10^{-4} m^2/s
Thermal Diffusivity for Nitrogen @ 1 bar, 300 K = 2.1×10^{-5} m^2/s

Transition from Laminar To Turbulent Flow
The evidence for transition from a laminar to a turbulent regime is the contrast in the temperature waveform stabilities. In the low pressure results, particularly for helium, the waveforms are very repeatable and show no sign of randomness or instability. In the high pressure results, particularly for nitrogen, there is very significant variability and in a few instances with high pressure nitrogen we appear to observe almost chaotic behaviour displaying significant high frequency components. These results suggest that the helium measurements are mainly in a laminar regime with a tendency to turbulence only at the highest pressures. With the nitrogen results it appears that they start off in a laminar regime but these changes more quickly to being turbulent.

7 MEASUREMENTS MADE USING COMPENSATED THERMOCOUPLES

Fast temperature measurements using a compensated thermocouple technique have been successfully implemented in IC engines (Kar[6]). The technique has the advantage of allowing substantially more robust sensors to be used whilst still achieving an adequate time response. Although the Stirling cooler environment is less hostile than an IC engine, this advantage still has practical significance as the alternative of using very fine wire sensors will always give handling and endurance problems.

In the IC engine application the temperature variations measured were generally quite large in comparison with the variations expected in the compression test rig volumes. As the signal to noise ratio is a significant factor in determining the degree of compensation that can be achieved, the challenge in this application is to see whether an adequate response is possible with the low signal levels expected in this application.

Description of Thermocouples and Installation
In the measurement of a fluid using a solid sensor there is always a delay between the change in fluid temperature and its detection by the sensor. This is due to the time taken for the sensor to reach thermal equilibrium with the gas and this delay is determined by the thermal

mass and heat transfer rate. For fast response times the sensor size is reduced to a minimum so as to improve the ratio of heat transfer to thermal mass. For sensors that are required to follow gas temperatures with frequency components of ~ 100Hz very fine sensors (such as the 3.8 micron resistance thermometer described above) are required.

Sensors that are too large will show an attenuated and delayed variation with higher frequency components increasingly filtered out. In principle, if the time constant function is known it is possible to reconstruct the original gas temperature by compensating for the delay.
The compensated thermocouple technique used here achieves this compensation by positioning two thermocouples with different time constants such that they see the same temperature variation. The outputs from the sensors undergo signal processing to extract a reconstructed gas temperature. It was found that the signal to noise ratio needed to be improved in order for the technique to give satisfactory results. This was done by sampling many cycles and using ensemble averaging.

The thermocouple assembly is shown in Figure 17. The two thermocouples are arranged in cross formation with a separation of approximately 0.1 mm. The sensor assembly is positioned centrally in the top flange of volume C such that the ceramic support is approximately level with the flange. The distance between the thermocouple junctions and the top flange is around 3.5 to 4 mm.

A comprehensive report that gives much more detail about the probes and the different signal processing schemes used is attached as appendix 2.

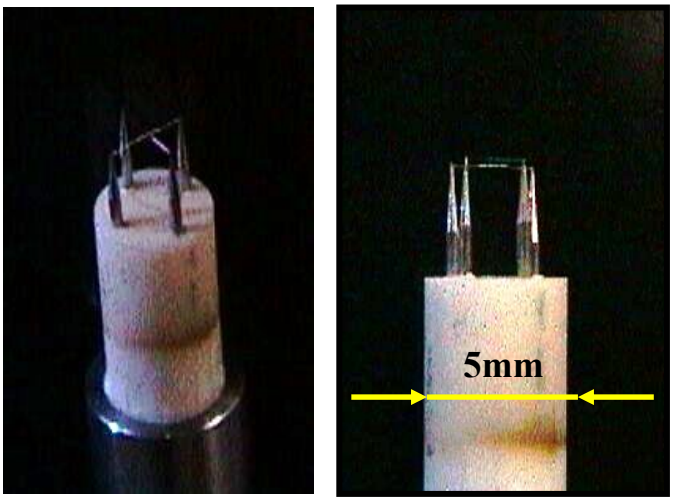

Figure 17. Pictures of thermocouple probe (courtesy of Prof. Moriyoshi).
Left: 3D view showing two fine thermocouples are in a cross configuration.
Right: Side elevation

Results and Discussion
Reconstructed temperatures were calculated using various types of estimator. Two techniques using difference equations were found to be most satisfactory. These were the Kalman filter and the recursive least squares estimators and will be denoted by ZOH-KF and ZOH-LS respectively. Figure 18 shows the direct thermocouple outputs with both reconstructed temperatures for one operating condition. The temperature variation for the fine wire resistance thermometer positioned at the other end of the regenerator is also shown for comparison.

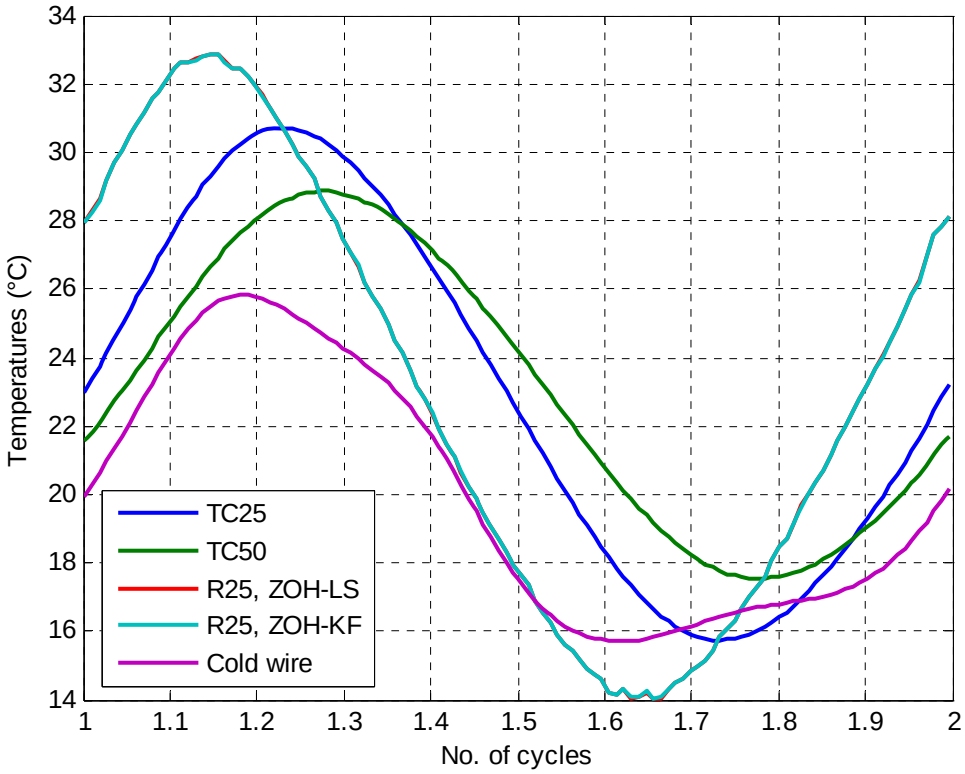

Figure 18. Record of the raw and compensated thermocouple temperatures and cold wire temperatures (i.e. at either side of regenerator). The sampling frequency was decimated to 1.25 kHz.Helium gas, 5 bar fill pressure, 10 mm stroke at 8.6 Hz. Note that the two "R25, ZOH.." traces are virtually identical.

Similar reconstructed temperatures for a wide range of operating conditions are given in appendix 2. It is noted that for all the results the two reconstructed temperatures appear to agree very well with each other.

Although we do not have any means for directly corroborating the reconstructed values some model tests were performed on the reconstructions and we can also look to see if the general features are plausible.

The model tests are described in detail in appendix 2. The discussion here will be limited to just the physical implications. A few features of the reconstructed temperatures are worth commenting on:

- Firstly it is observed that the phases of the reconstructed temperatures are in advance of the raw thermocouple data and are close to the phases of the fine wire RT temperatures.

- Secondly it is observed that the peak to peak temperature variation is significantly higher than for the fine wire thermometer. This suggests that the thermodynamic processes occurring are closer to adiabatic.

- Finally the peak to peak temperature variation can be used together with the peak to peak pressure to infer a mean polytropic constant. These have been calculated for a number of the helium results with the finding that the polytropic constant is ~1.6 for low frequencies and pressures with the values decreasing as frequency and pressure increase. These results suggests that there is increased mixing with higher Reynolds numbers.

These observations do not prove that the technique has any specific accuracy but they do at least confirm that the results are feasible.

Conclusions
The model tests (appendix 2) and the experimental observations support the general conclusion that the temperature reconstruction is useful provided that the varying temperature is sufficiently repeatable to allow ensemble averaging.

8 DESCRIPTION OF POWER LOSS MEASUREMENTS

The power determined from the integral of $P.dV$ in the compression space is the total power input to the gas and includes various components. The purpose of this analysis is to extract from the power measurements the contribution that is not accounted for in present models. These residual values can then be investigated to see how they vary with changing operating parameters.

The components that make up the total input power to the gas are:

- Seal Loss
- Flow Friction losses associated with flow through the regenerator
- Known thermal diffusion losses that correspond to boundary layer losses in the simple gas spring configuration. These will be referred to as *Boundary Gas Spring Losses*
- Residual values that make up the unaccounted compression loss. These will be referred to as *Residual Compression Losses*

Seal Loss (P_{sloss})
Power is expended by pumping gas backwards and forwards through the clearance seal. It can be calculated from:

$$P_{sloss} = \oint p.\frac{dV}{dt}$$

Where p is the pressure difference and $\frac{dV}{dt}$ is volume flow rate for the seal.
If the pressure variation is sinusoidal with an amplitude p_1, and laminar flow is assumed with a constant radial clearance of τ, then the power expended is given by:

$$P_{\text{sloss}} = \frac{\pi d_{\text{p}} \tau^3}{24 \mu L_{\text{p}}} p_1^2 \qquad \text{(Laminar flow through an annulus is assumed)}$$

where d_p is piston diameter, L_p is piston length and μ is gas viscosity.

Although it is possible to obtain a more accurate value by using instantaneous pressure values, this was not considered necessary for these measurements and the simple expression given above was used for all the results given here.

Flow Friction Losses (P_{floss})

The power loss associated with the flow through the regenerator is found by evaluating $P_{floss} = \oint p.\frac{dV}{dt}$ for the length of the regenerator. As the volume flow varies significantly from one end of the regenerator to the other, this is done by calculating local power loss values and then integrating along the length of the regenerator.

The power loss for flow through an element *dx* of the regenerator is given by

$$dP_{floss} = u(x).p_d(x).A_x$$

where p_d is the pressure difference across the element *dx*, *u(x)* is the flow velocity and A_x is the flow area.

For flow in plain square mesh the friction factor generally has the form:

$$f = \frac{a}{N_R} + b$$

where N_R is the local Reynolds number and *a* and *b* are constants denoting the laminar and turbulent components respectfully

If a linear velocity gradient is assumed then it is shown in Appendix 1 that for sinusoidal variations the mean power loss is given by:

$$P_{floss} = \frac{A_x.L}{D_h.u_d}.\left[\frac{\theta.}{3}.(u_0^3 - u_L^3) + \frac{\psi}{4}.(u_0^4 - u_L^4)\right]$$

where u_0 and u_L are the velocity amplitudes at either end of the regenerator, L is length of regenerator, D_h is hydraulic diameter for regenerator mesh and θ, ψ and u_d are given by:

$$\theta = \frac{a.\mu}{D_h}, \qquad \psi = b.\rho \text{ and } dx = -\frac{L}{u_d}.du(x) \qquad \mu \text{ is gas viscosity}$$

The gas velocities at either end of the regenerator can be calculated from the compression volumes as follows:

For Volume C peak gas velocity out of regenerator is given by (see appendix 1)

$$u_L = \frac{1}{A_x}.\left(\frac{V_c}{V_a + V_b + V_c}\right).\left(\frac{dV_a}{dt}\right)$$

For Volume B peak gas velocity into regenerator is given by

$$u_0 = \frac{1}{A_x}.\left(\frac{V_b}{V_a + V_b + V_c}\right).\left(\frac{dV_a}{dt}\right) + u_L$$

V_a, V_b, and V_c are volumes of Volumes A, B and C respectively. (Variations in pressure and temperature are relatively small. They not affect volume flows very much and were not taken into account)

Finally the amplitude for the pressure difference across the regenerator can be calculated from

$$\Delta p_{0-pk} = \frac{L}{D_h.u_d}.\left[\frac{\theta.}{2}.(u_0^2 - u_L^2) + \frac{\psi}{3}.(u_0^3 - u_L^3)\right]$$

Values for *a* and *b* could have been taken from the literature but there is a significant amount of variation between different correlations and it was decided to see if values could be deduced by investigating how they affected the loss correlation obtained.

It was found that the best correlation for nitrogen gave a friction factor correlation of

$$f = \frac{31}{N_R} + 0.25$$

For helium the best correlation gave a friction factor correlation of

$$f = \frac{31}{N_R} + b$$

where the correlation was not sensitive to the value of *b*. (Note: The coefficient *b* relates to the turbulent component of the pressure drop. For the helium results the Reynolds numbers were low and the pressure drop was dominated by the laminar component)

The correlation used to calculate the flow losses was

$$f = \frac{31}{N_R} + 0.25$$

This is similar to expressions quoted in the literature for packed mesh.

Boundary Gas Spring Losses (P_{Bgloss})
The losses associated with thermal diffusion through a boundary layer are the principal losses that occur in a simple gas spring geometry as described in the 1993 paper by Kornhauser and Smith[4] and investigated in Los-FR2. In the more complicated configuration investigated here these losses will still occur wherever there is a boundary layer and a pressure driven varying temperature.

The boundary layer gas spring loss will not be exactly the same as for the simple gas spring configuration but it will be assumed that the expression derived for the gas spring (Kornhauser and Smith[4]) will give a reasonable estimate. The equation used is:

$$P_{Bgloss} = \frac{\pi}{2}.p_0 V_0.\left(\frac{p_a}{p_0}\right)^2.\frac{(\gamma-1)}{\gamma}.\frac{1}{y}.\left(\frac{\cosh(y).\sinh(y)-\sin(y).\cos(y)}{\cosh^2(y)-\sin^2(y)}\right)$$

Where p_0 and V_0 are mean values of pressure and volume and p_a is the pressure amplitude. The parameter y is a dimensionless number that is defined by

$$y = \left(\frac{Pe_\omega}{8}\right)^{1/2}$$

The Peclet number used here is defined by:

$$Pe_\omega = \frac{\omega.D_h^2}{\alpha_0}$$

where D_h is the hydraulic diameter: $D_h = 4V_0 / A_0$ and α_0 is the thermal diffusivity.

Using these equations the Boundary Gas Spring loss was calculated for the three separate volumes and a total Boundary Gas Spring loss was calculated as the sum of these components.

$$P_{Bgloss}(Total) = P_{Bgloss}(VolA) + P_{Bgloss}(VolB) + P_{Bgloss}(VolC)$$

It is noted that the Peclet number for Volumes A and C was typically in the range 10 to 100 indicating that the heat transfer in these volumes is tending toward the adiabatic. In contrast the Peclet number in Volume B, the regenerator, is low (~0.5) confirming that the heat transfer regime is close to isothermal.

Residual Power Loss (P_{Rloss})
The unaccounted power loss is calculated from the total power and the components described above:

$$P_{Rloss} = P_{In} - (P_{sloss} + P_{floss} + P_{Bgloss})$$

Table 3 gives values for a range of operating parameters to give an idea of the magnitudes of these various components.

Table 3. Breakdown of Losses

Operating Conditions	Total Power Input into gas	Calculated Seal Loss	Calculated Flow Friction Loss	Calculated Boundary Gas Spring loss	Residual Loss
Helium 1 bar Stroke 4 mm Freq 8.6 Hz	6.74 mW	0.075 mW 1.1%	2.91 mW 43.2%	0.201 mW 2.98%	3.56 mW 52.82 %
Helium 21 bar Stroke 14 mm Freq 44 Hz	3455 mW	417 mW 12.07 %	1088 mW 31.49%	13 mW 0.376%	1937 mW 56.06 %
Nitrogen 1 bar Stroke 4 mm Freq 8.6 Hz	6.43 mW	0.335 mW 5.21%	2.74 mW 42.61%	0.043 mW 0.669%	3.32 mW 51.63%
Nitrogen 26 bar Stroke 11 mm Freq 53 Hz	4799 mW	428 mW 8.93%	1954 mW 40.72%	37 mW 0.77%	2379 mW 49.58%

Discussion of The Residual Loss (P_{ndLoss})

The residual values calculated are actual power losses. In order to look at what factors might determine these losses it is necessary to transform them into a non-dimensional form. This was done by dividing the residual power loss by a nominal power calculated from the product of frequency, peak to peak pressure and swept volume.

$$P_{ndLoss} = \frac{P_{Rloss}}{f.\Delta p.\Delta V}$$

The values of P_{ndLoss} are plotted against frequency for helium and nitrogen at different pressures in figures 19 and 20. These plots show an obvious difference between the results for the two gases. For helium the non-dimensional loss is fairly constant for the 1 and 5 bar measurements. For the 18 bar measurements there is decrease in non-dimensional loss with frequency. In contrast all the nitrogen measurements show an increase in non-dimensional loss with frequency.

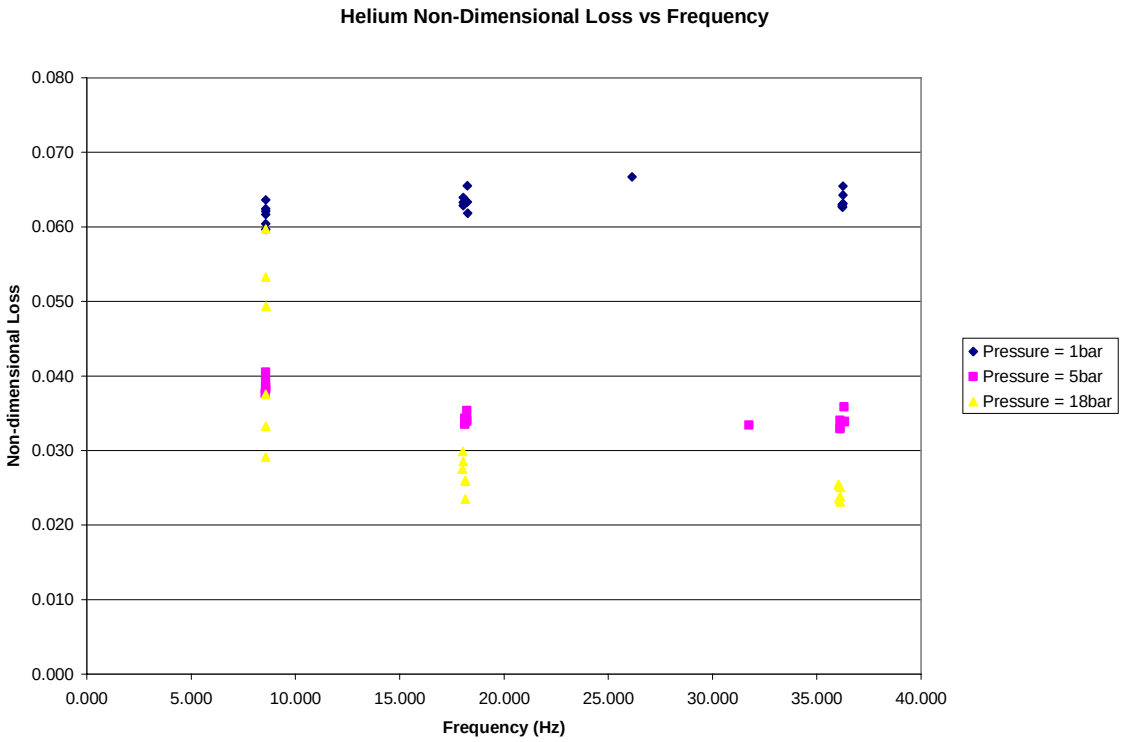

Figure 19. Helium: Variation of Non-Dimensional Loss with Frequency for Different Fill Pressures

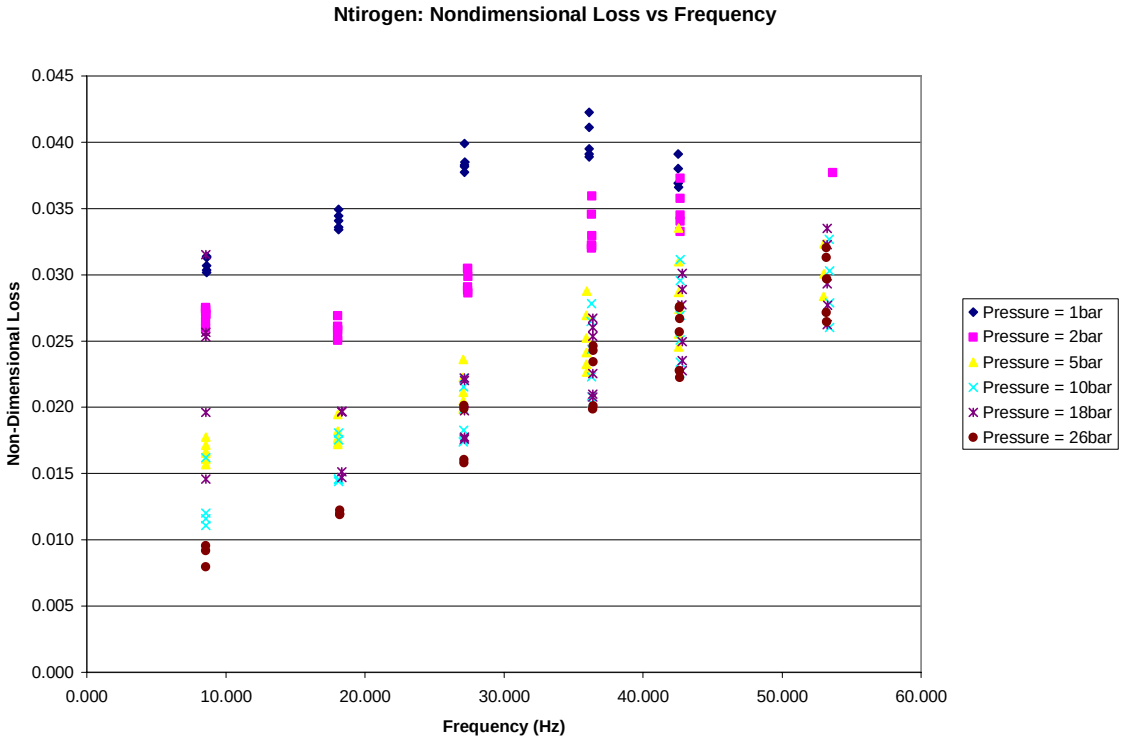

Figure 20. Nitrogen: Variation of Non-Dimensional Loss with Frequency for Different Fill Pressures

Initial Investigation of Loss Dependence

Attempts to pursue a more thorough dimensional analysis are described below but initially it was found useful to assume a dependence on Reynolds number and investigate the residual loss with respect to the varied parameters. The Reynolds number assumed is defined as:

$$N_R = \frac{\rho.v.D_h}{\mu}$$

where ρ and μ are density and viscosity evaluated for compression space, v is piston velocity and D_h is hydraulic diameter for compression space.

A parameter Z is defined by

$$Z = \left(\frac{P_{ndLoss}}{f^{k1}.s^{k2}.p^{k3}} \right)$$

where f, s and p are frequency stroke and pressure respectively.

Values of $Log(Z)$ were plotted against respective values of $Log(N_R)$. Indices *k1*, *k2* and *k3* were varied to find values that gave the best correlation of the data points.

Helium Results

Figure 21 shows a graph of $Log(P_{ndLoss})$ plotted against $Log(N_R)$ for helium (with *k1*, *k2* and *k3* = 0). Figure 22 shows a graph of $Log(Z)$ plotted against $Log(N_R)$ for helium. The values of *k1*, *k2* and *k3* that gave the best fit are:

k1=0.3 *k2*=0.3 *k3*=0

I.e. the non-dimensional loss is a function of piston velocity i.e. proportional to $v^{0.3}$
It will be seen that a very respectable straight line fit is achieved from points that originally had a lot of scatter.

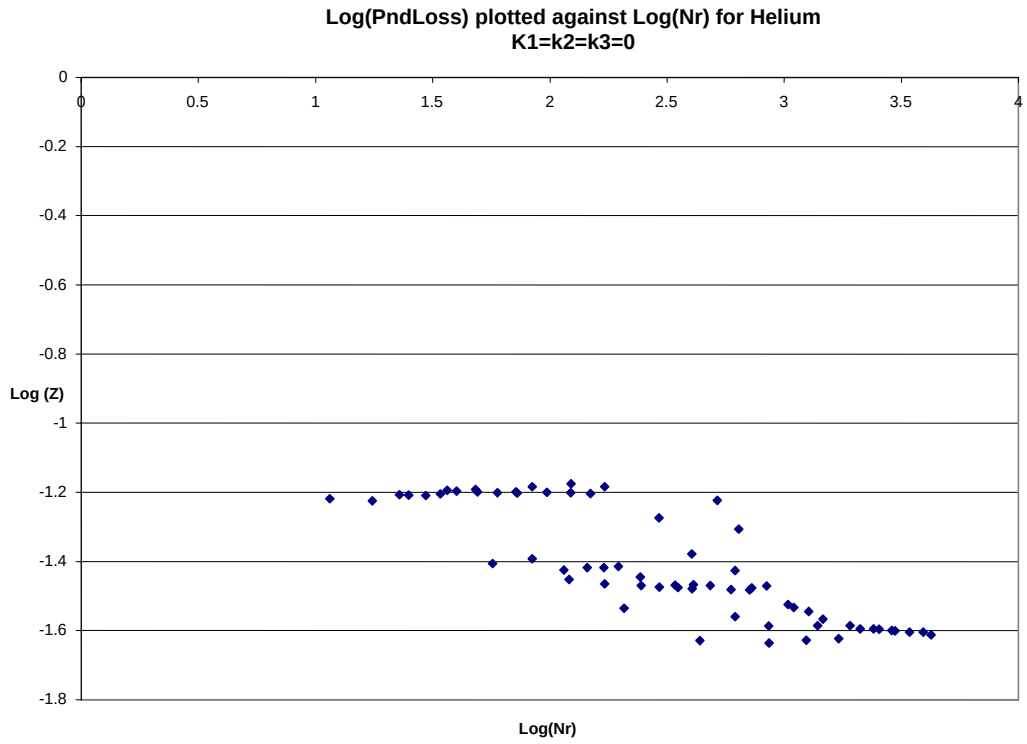

Figure 21. Helium: Log(Z) plotted against Log(Nr) for k1=k2=k3=0

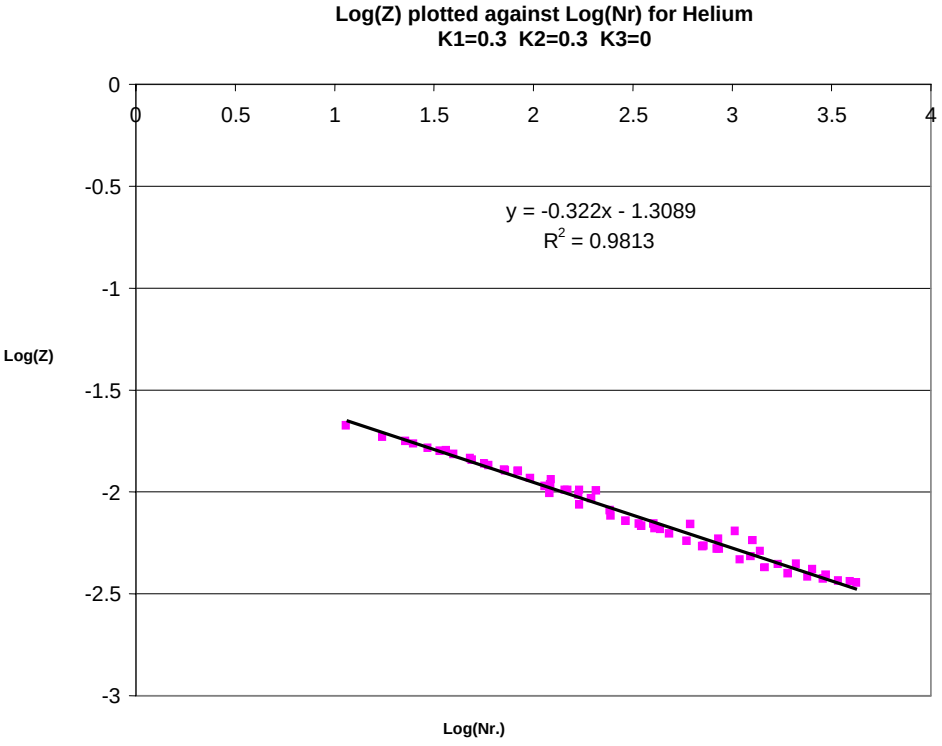

Figure 22 Helium: Log(Z) plotted against Log(Nr) for k1=k2=0.3 and k3=0

Nitrogen Results

Figure 23 shows a graph of $Log(P_{ndLoss})$ plotted against $Log(N_R)$ for nitrogen (with *k1*, *k2* and *k3* = 0). Figure 24 shows a graph of $Log(Z)$ plotted against $Log(N_R)$ for nitrogen for values of

$$k1 = k2 = 0.3 \quad \text{and} \quad k3 = 0$$
$$k1 = k2 = 0.5 \quad \text{and} \quad k3 = 0$$
$$k1 = k2 = 0.7 \quad \text{and} \quad k3 = 0$$

and the values that gave the best fit:

$$k1 = 0.7 \qquad k2 = 0.4 \qquad k3 = 0.1$$

The results are plotted again for the best fit in Figure 25.

It will be seen that forcing dependence on only velocity does not give a good correlation. A significantly better correlation is achieved with a different dependence on the parameters.

The conclusion to be drawn is that the behaviour of nitrogen and helium is different.
It is also noted that the good correlation is not for a single straight line, instead there are two regions which look reasonably linear but which have different gradients. The Reynolds number at which there is this apparent transition in behaviour is ~ 3000.

It is noted that for the nitrogen results the optimum values of *k1*, *k2* and *k3* were not as clear cut as for the helium values but this may well be because we are dealing with two regimes that have a differing dependence on flow parameters.

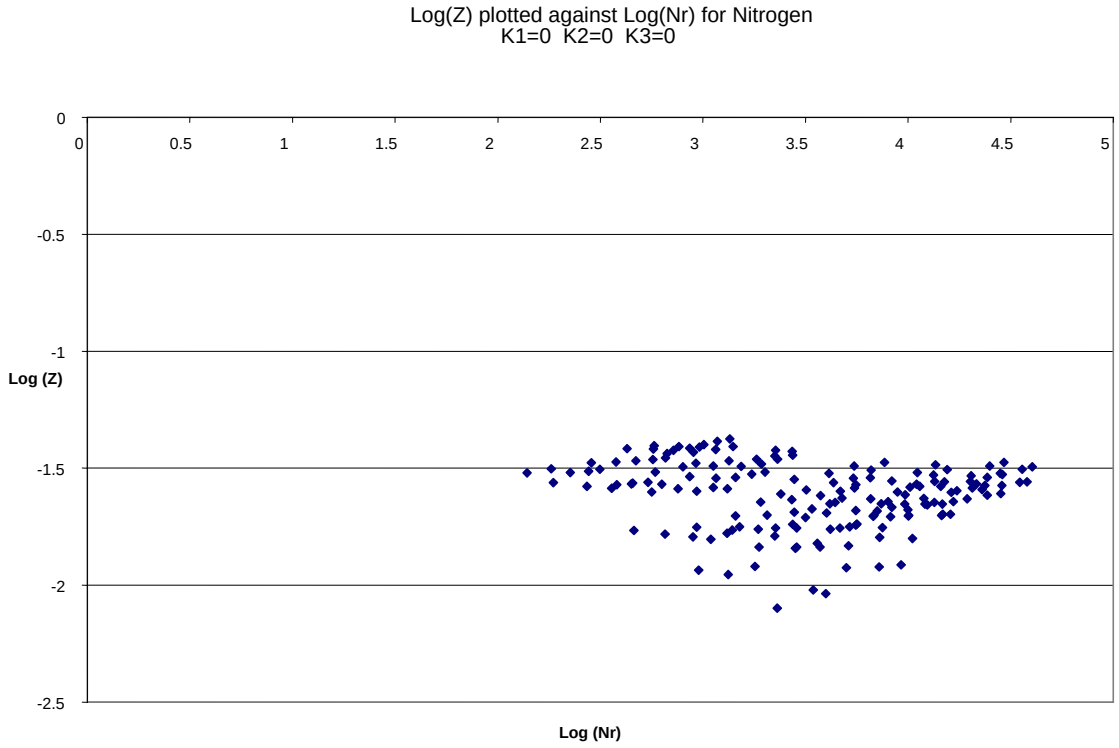

Figure 23. Nitrogen: Log(Z) plotted against Log(Nr) for k1=k2=k3=0

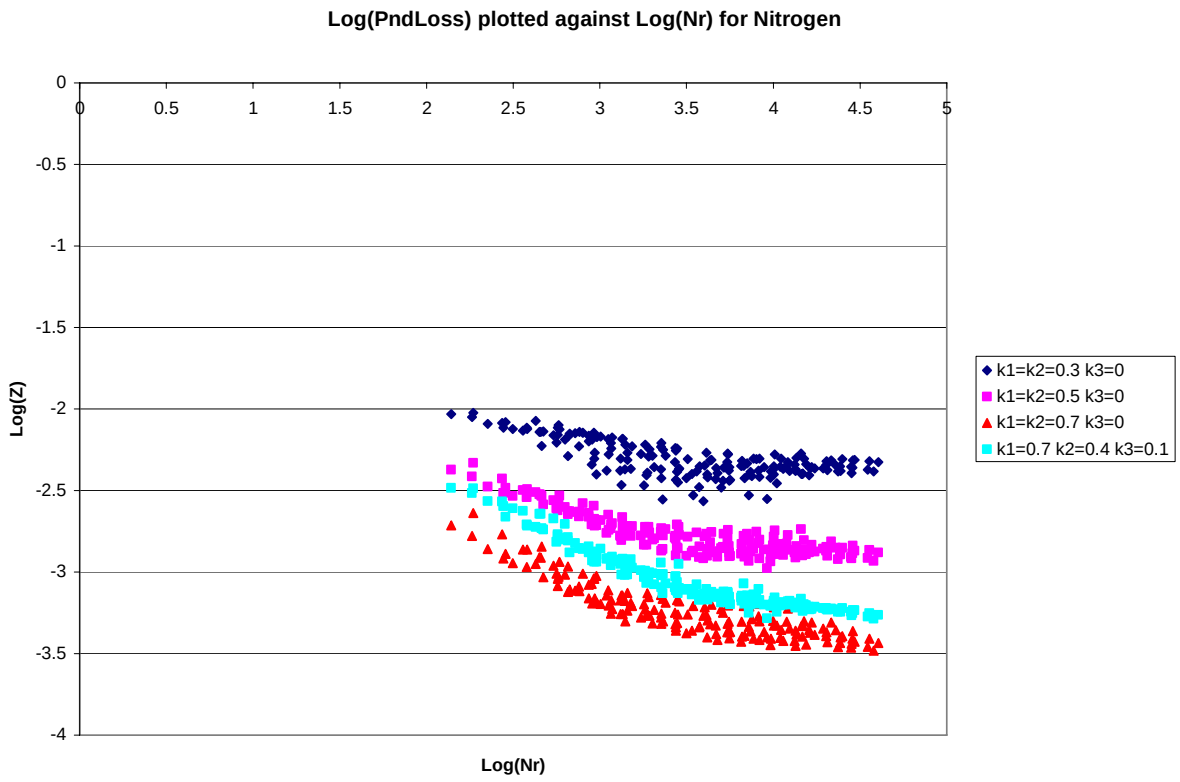

Figure 24. Nitrogen: Log(Z) plotted against Log(Nr) for k1=k2=k3=0

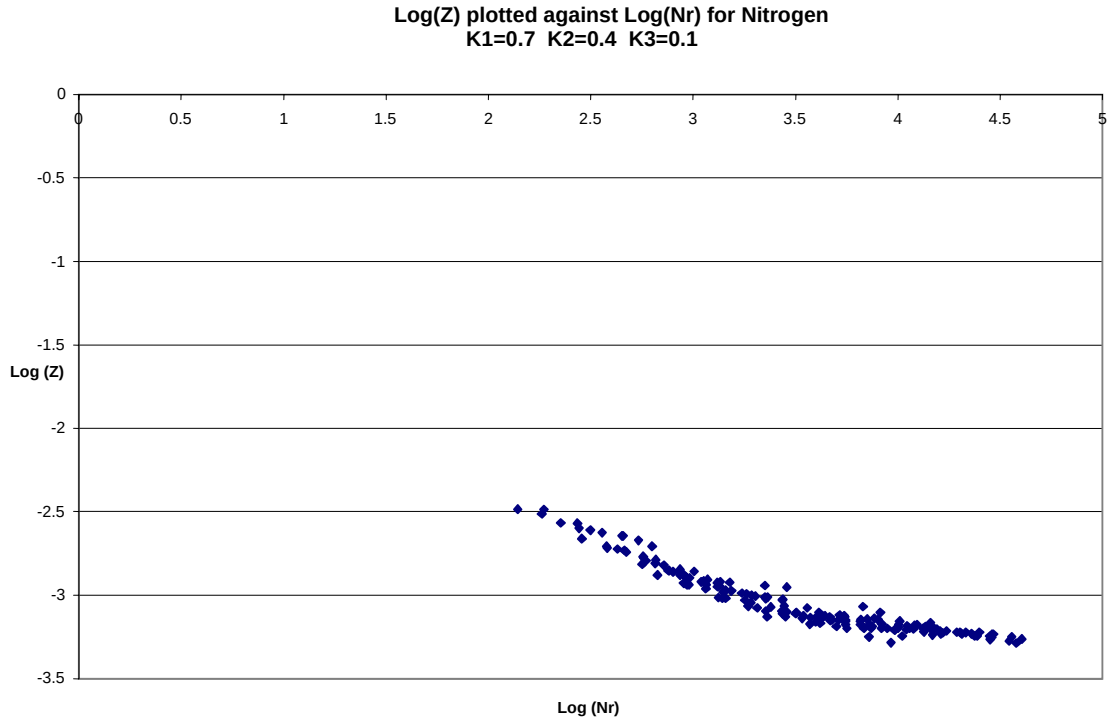

Figure 25. Nitrogen: Log(Z) plotted against Log(Nr) for k1=0.7 k2=0.4 and k3=0.1

Comments on Results
The initial conclusions to be drawn from these results are:

- There is a very strong dependence on the Reynolds number.
- Two regimes could be identified in the nitrogen results with a fairly well defined transition at a Reynolds number of 3000.
- The helium results only just extended up to Reynolds number values of 3000 so it not possible to discern a transition at this point.
- The dependence on frequency and stroke is quite marked for both helium and nitrogen but the magnitudes vary significantly. There appears to be no dependence on pressure for the helium results and for nitrogen the dependence was marginal.

Nature of Residual Loss
So far we have just referred to a Residual Loss without any comment as to its origin. The work described does not attempt to model a new mechanism but it is nonetheless desirable to at least speculate as to the nature of this extra loss.

In general terms power can be dissipated in this type of test rig by three mechanisms:

- Flow friction
- Irreversible heat transfer
- Work output

The only significant flow friction mechanisms are in the seal and regenerator and these have been adequately accounted for. The test rig has only one component that can transfer work and that is the piston which is the source of the power input. It therefore looks likely that our residual loss is caused by an irreversible heat transfer mechanism that is additional to the Boundary Gas Spring Loss.

If we look closely at the tidal gas that spends some of its time in the compression space and some of the time in the regenerator we see that there is an abrupt change in heat transfer conditions as gas moves from one component to the other. This discontinuity will in general cause a significant irreversible heat transfer and is regarded as a strong candidate for our missing loss. The mechanism will be briefly described here with reference to the boundary layer loss that is well documented.

Figure 26 shows a representation of a simple gas spring at four piston positions. It is assumed that the boundary layer is relatively thin so that we can regard the gas piston as having a lossless adiabatic core with a thin lossy boundary layer.

If we start with the piston midway in its compression stroke we will assume that the core temperature is roughly the same as the temperature of the walls and that the heat transfer will be close to zero (A). As we proceed with the compression the core gas temperature increases and heat is transferred from the gas boundary layer into the wall. This heat transfer continues during maximum compression Fig 25 (B) until we reach midway in the expansion stroke (C)

where the heat transfer is again close to zero. If we continue with the expansion then the core temperature becomes lower than the wall temperature and heat transfer is reversed with heat returning from the wall into the boundary layer. This heat continues until we finish the cycle at the midpoint of the compression stroke (A).

Overall we can be sure of three things:

- The mean gas temperature remains constant hence there is no net energy flow into the gas.
- The net heat transferred from the gas to the wall is not zero. It must be equal to the energy input into the gas in the form of work for energy to be conserved.
- The power absorbed is a direct result of the irreversible heat transfer occurring in the boundary layer.

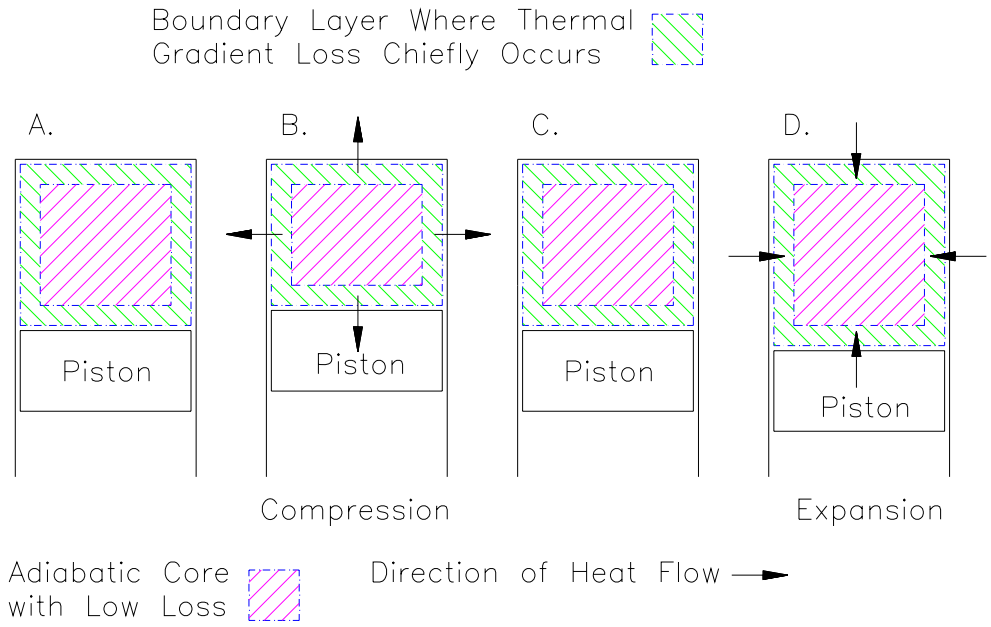

Figure 26. Boundary Layer Gas Spring Loss Mechanism.

If we now look at Figure 27 we see that tidal gas movement between the compression space (assumed adiabatic) and the regenerator is shown for four points in a cycle. At point A the gas envelope is mainly contained within the regenerator and will be at the regenerator temperature and roughly the maximum cycle pressure. As the pressure (A to C) decreases the gas envelope expands and moves from the regenerator to the adiabatic volume whilst also tending to cool. While gas is in the regenerator it will absorb heat and remain isothermal; as soon as gas enters the adiabatic volume it will undergo adiabatic expansion and its temperature will reduce. Different elements of gas will undergo differing amounts of cooling with the result that a temperature gradient will be set up and irreversible heat transfer will occur with the adiabatic gas volume. On the compression stroke (C to A) the flow is reversed and elements of gas will be moving from the adiabatic volume into the regenerator whilst tending to heat up. Heat transfer within the adiabatic gas will continue, but in addition there

will tend to be an irreversible transfer of heat between the gas entering the regenerator and regenerator matrix. Whilst it is possible that the gas temperature of the adiabatic gas is synchronised so that it reaches the regenerator temperature just as it enters the regenerator, this will not be the general case.

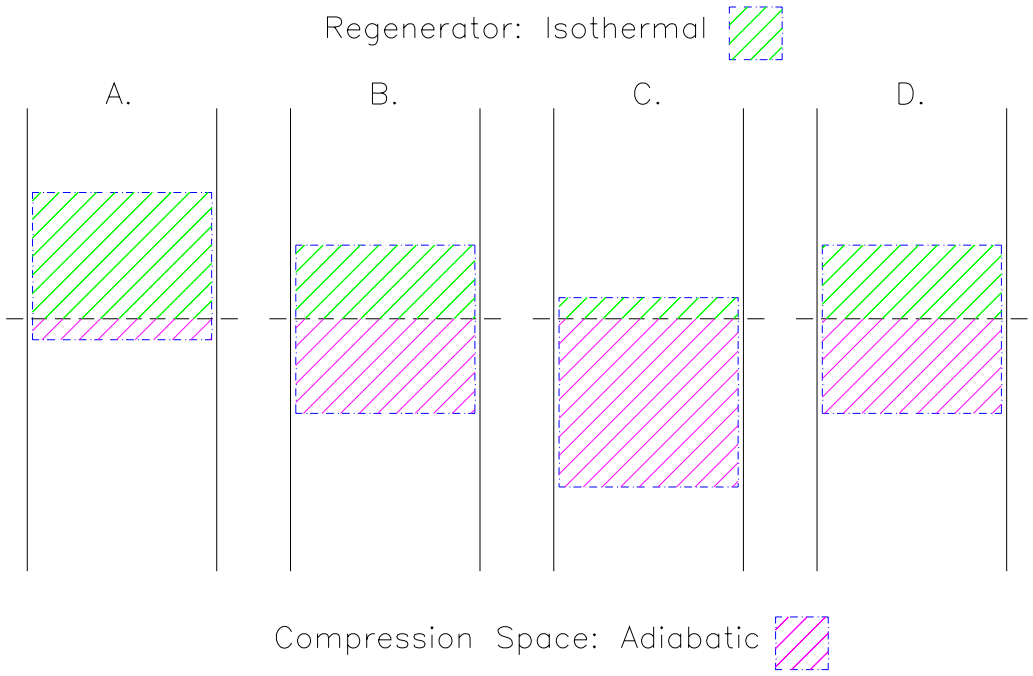

Figure 27. Tidal Gas Spring Loss Mechanism

We can identify three distinct aspects which will tend to produce irreversible heat transfer and therefore compression losses:

- Conduction of heat within the adiabatic volume driven by the temperature gradient. This effect is analogous to the heat conduction in the boundary layer gas spring loss and will be governed by the thermal diffusivity.

- Transfer of heat as above but amplified by convection. If the gas remains stratified i.e. unmixed then this will not occur. As soon as there is significant mixing then this effect is likely to become dominant in the way that turbulent heat transfer is dominant in steady flow heat transfer.

- Transfer of heat from gas to regenerator matrix as gas enters the regenerator.

From the above it is seen that there is an obvious mechanism for irreversible heat transfer and with two additional components, it is substantially more complicated than the mechanism occurring in a simple Boundary Layer gas spring. An appropriate term for this effect is a "*Tidal Gas Spring Loss*"

Dimensional Analysis

The correlations obtained above are surprisingly good if they really represent the loss outlined above. However, to be of any real use it is desirable to formulate these correlations in a non-dimensional form. As a starting point an analysis is pursued with the more obvious parameters listed below in table 4

Table 4. Parameters used in Dimensional Analysis

Variable	Symbol	Units
Frequency	f	s^{-1}
Viscosity	μ	$kg.m^{-1}.s^{-1}$
Density	ρ	$kg.m^{-3}$
Hydraulic Diameter	D_h	m
Velocity	v	$m.s^{-1}$
Thermal Diffusivity	α	$m^2.s^{-1}$
Gamma (ratio of specific heats)	γ	none

The ratio of specific heats is dimensionless and is assumed to form its own non-dimensional group. There are three fundamental dimensions: mass (kg), length (m) and time (s). There are assumed to be six variables, hence there will be three non-dimensional groups.

Repeating variables are chosen to be density ρ, velocity v and hydraulic diameter D_h. The non-dimensional groups $P(1)$, $P(2)$ and $P(3)$ will then have the forms:

$$P(1) = \rho^{a1}.v^{b1}.D_h^{c1}.\mu^{d1} \qquad P(2) = \rho^{a2}.v^{b2}.D_h^{c2}.\alpha^{d2} \qquad P(3) = \rho^{a3}.v^{b3}.D_h^{c3}.f^{d3}$$

The indices are found by equating dimensions, the three dimensionless groups are:

$$P(1) = \frac{\rho.v.D_h}{\mu} \qquad P(2) = \frac{v.D_h}{\alpha} \qquad P(3) = \frac{f.D_h}{v}$$

Hence the non-dimensional loss factor is expected to have a form:

$$P_{ndLoss} = K.f(\gamma).\left(\frac{\rho.v.D_h}{\mu}\right)^{n1}.\left(\frac{v.D_h}{\alpha}\right)^{n2}.\left(\frac{\omega.D_h}{v}\right)^{n3} + other\ terms$$

These dimensionless groups can be identified as:

$$P(1) = \frac{\rho.v.D_h}{\mu} \qquad \text{Reynolds Number} \qquad N_R$$

$$P(2) = \frac{v.D_h}{\alpha} \qquad \text{Peclet Number} \qquad N_{Pe}$$

$$P(3) = \frac{\omega.D_h}{v} \qquad \text{Strouhal Number} \qquad N_{Str}$$

The formulation of Peclet number can be improved to avoid disguising the density dependence in the thermal diffusivity. The thermal diffusivity is defined by:

$$\alpha \text{ is given by } \alpha = \frac{K}{\rho.c_p}$$

K is thermal conductivity and C_p is specific heat capacity

If we substitute this in the expression above we obtain

$$P(2) = \frac{v.D_h}{K}.\rho.c_p = \rho.v.D_h.\frac{c_p}{K}$$

Comparing this with the Reynolds number we see that both dimensionless groups have the variables ρ, v and D_h to the same power and that the other parameters are substantially constant for the gases concerned. The result is that for individual gases the Peclet number and Reynolds number will exhibit the same parameter dependence – in effect we only have one dimensionless group. In fact the ratio of Reynolds number to Peclet number defines another dimensionless group that is frequently used in heat transfer problems, the Prandtl number N_{Pr}:

$$N_R = N_{Pe} * N_{\mathrm{Pr}}$$

The Prandtl is typically equal to 0.7 for most gases. The difference between the values for nitrogen and helium is small and would not account for significant differences in their behaviour.

If we now attempt to use these dimensionless groups to correlate the helium data we hit an immediate problem. In the initial analysis given above we found that the non-dimensional loss was proportional to the Reynolds number and $v^{0.3}$. The Reynolds number is unchanged and we need to find a combination of the dimensionless groups that will give the required velocity dependence. With the only the three groups given here this does not seem possible and the conclusion to be drawn is that we are missing at least one important variable.

If the Mach number is invoked this will allow the velocity dependence to be expressed in terms of the velocity of sound. However for the velocities encountered in this investigation compressibility effects appear fairly unlikely.

In the discussion above concerning possible loss mechanisms in tidal gas flow we did not consider how the phase between pressure variation and mass flow might influence the loss. The likelihood is that it is a significant parameter and it may be that the apparent dependence on velocity is an expression of this. Taking the modelling or dimensional analysis further to investigate this is beyond the scope of the work reported here and we will have to conclude that whilst there does seem to be effects that can be well correlated the determining parameters have yet to be fully identified.

9 OVERALL SUMMARY AND CONCLUSIONS

The most interesting feature of this work is the general agreement between the resistance wire thermometry results and the power loss measurements. Both sets of results exhibit changes in flow behaviour consistent with the idea of a laminar to turbulent transition. Furthermore a region of transition defined by a Reynolds number suggested by the power measurements is reasonably supported by the thermometer results. In addition the resistance wire thermometry results changes in temperature profile are consistent with thermal diffusivity effects. It is also clear that the gas is quite stratified in the low pressure results and that this stratification is still present to a lesser extent in the high pressure results that are thought to turbulent.

A simple dimensional analysis confirms that the thermal diffusion effects should be determined by a Peclet number whilst the transition from laminar to turbulent should be determined by a Reynolds number. For the Peclet and Reynolds numbers defined it is found that they have the same dependence on the parameters varied i.e. pressure, frequency and stroke. The use of gases with different physical properties should allow differentiation of these groups but this could not be done here with the limited results available

The more detailed conclusions that can be drawn are:

- Cyclic temperature measurements were made for the gas in the fixed cylindrical volume (Vol C) attached to the end of the regenerator. The thermometer used was of a novel type that used two relatively slow thermocouples and a compensation technique to reconstruct the actual gas temperature. The measurements made with the compensated thermocouples did not give any information about the compression losses occurring in this gas spring configuration. However they did show that this technique could be considered in this type of application, provided that the noise levels were low enough. For the measurements described here the noise could only be sufficiently reduced by ensemble averaging. This would be a limitation in circumstances where the waveform is not very repeatable.

- Cyclic temperature measurements were made for the gas in the top of the compression volume (Vol A) adjacent to the end of the regenerator. The thermometer used was a resistance thermometer that used very fine wire to give a rapid response.

- The temperature profiles measured showed a range of shape and repeatability depending on the gas used and also on the stroke, frequency and pressure.

- A significant part of the stroke dependence appears to be due to the portion of time in which the thermometer was sensing the tidal gas flow and the proportion attributable to the gas which always remains in the compression space.

- This sensing of two distinct gas volumes is supported by the apparent gradient discontinuities that can be seen in the profiles. There are no corresponding discontinuities in the pressure waveforms.

- The variation in the gas temperature waveforms appear to be due to two effects:
    - Changes in the axial temperature gradient as the thermal diffusion varies.
    - A tendency with increased pressure towards waveform variability, instability and the presence of high frequency components, this suggests a transition to a more disordered regime: perhaps Laminar to Turbulent.

- The helium results tended to mainly occupy the ordered laminar regime. The nitrogen results appeared to straddle both.

- A few high pressure, low frequency nitrogen results showed extreme instability that could be described as chaotic – no repeatable waveform was discernible. It is possible that these results just happened to straddle a laminar/turbulent transition but with the limited data available this conclusion must be regarded as tentative.

- The power loss measurements showed that a loss existed that could be correlated by a combination of Reynolds number and the experimental parameters pressure, frequency and stroke. Attempts to formulate this in a non-dimensional form were not successful suggesting that key parameters may not have been invoked. One effect in particular that needs closer attention is the effect of phase angle between mass flow and pressure variation.

10 FUTURE WORK

For this investigation into compression losses to be continued two areas of work stand out:

- Further experimental measurements repeating resistance wire thermometry and power loss measurements for different gases and operating conditions. These would concentrate on the transitional regimes already identified to provide a better experimental description.

- A goal to establish a model for these proposed Tidal gas Spring Losses appears to be very important aspiration. It will remain difficult to make much sense of the results without a model to act as a framework.

11 REFERENCES

[1] Cryogenics Group, Oxford University, "An Investigation of Certain Thermodynamic Losses in Miniature Cryocoolers". Final report for USAF AFRL Contract FA8655-04-1-3011, Los-FR1 Jan 2005

[2] Cryogenics Group, Oxford University, "An Investigation of Certain Thermodynamic Losses in Miniature Cryocoolers". Final report for USAF AFRL Contract FA8655-04-1-3011, Los-FR2 Feb-2006

[3] Kornhauser, A.A., Smith, J.L., "A Comparison of Cylinder Heat Transfer Expressions Based on prediction of Gas Spring Hysteresis Loss", Fluid Flow in Heat Transfer and Reciprocating Machinery, ASME 1987

[4] Kornhauser A.A., Smith, J.L., "The Effects of Heat Transfer on Gas Spring Performance", Journal of Energy Resources Technology, Vol. 115 pp. 70-75, ASME, 1993.

[5] Lee, K.P., "A Simplistic Model of Cyclic Heat Transfer Phenomena in Closed Spaces." 18th IECEC, 1983

[6] Kar, K.C., "Three-Thermocouple Technique for Fluctuating Temperature Measurement", D. Phil Thesis, University of Oxford, 2004

APPENDIX 1: PRESSURE DROP IN REGENERATOR

BACKGROUND EQUATIONS

Kays and London

Shear Stress given by:

$$\tau = \frac{f.G^2}{2.\rho}$$

f is friction factor G is mass flow rate per area (i.e mass flux) = $u.\rho$

ρ is fluid density

$G = u.\rho$ where u is fluid velocity

$$\tau = \frac{f.\rho.u^2}{2}$$

$dP.A_x = \tau.A_w$ $A_x = \frac{Vol}{L}$ $A_w = \frac{4.Vol}{D_h}$ $\frac{A_w}{A_x} = \frac{4.L}{D_h}$

A_x is flow area A_w is wetted area Vol is wetted volume

D_h is hydraulic diameter L is regenerator length

$$dP = \tau.\frac{A_w}{A_x} = \tau.\frac{4.L}{D_h} \qquad dP = \frac{f.\rho.u^2}{2}.\frac{4.L}{D_h} \qquad dP = \frac{(f.\rho.u^2).2.L}{D_h}$$

For flow through mesh friction factor has form

$$f = \frac{a}{N_R} + b \qquad N_R = \frac{\rho.u.D_h}{\mu}$$

APPLICATION TO COMPRESSION LOSS RIG

Power Loss

Flow velocity and hence pressure drop varies along length of regenerator. It is therefore necessary to evaluate pressure drop power loss for small length dx and then integrate over length of regenerator. It will be assumed that flow velocity varies linear along length of regenerator

$$u(x) = u_0 - \frac{x}{L}.u_d \qquad \text{for } x=L \qquad u(x)=u_L$$

u_0 is velocity at entrance to regenerator, u_d is velocity difference across regenerator

For length of regenerator dx with fluid velocity $u(x)$ and pressure drop $P_d(x)$, power dissipated is given by:

$$dW = u(x).P_d(x).A_x$$

Substituting expressions from above

$$P_d(x) = \left(\frac{a.\mu}{\rho.u(x).D_h} + b\right).\frac{\rho.u(x)^2.2.dx}{D_h} = \frac{2}{D_h}.\left(\frac{a.\mu.u(x)}{D_h} + b.\rho.u(x)^2\right).dx$$

$$dW = \frac{2.A_x}{D_h}\left(\frac{a.\mu.u(x)^2}{D_h} + b.\rho.u(x)^3\right).dx$$

Let $\theta = \frac{a.\mu}{D_h}$, $\psi = b.\rho$ and $dx = -\frac{L}{u_d}.du(x)$

Then Power integrated over length of regenerator is given by:

$$W = -\frac{2.A_x}{D_h}.\frac{L}{u_d}\int\left(\theta.u(x)^2 + \psi.u(x)^3\right)du(x) = -\frac{2.A_x}{D_h}.\frac{L}{u_d}.\left[\frac{\theta.u(x)^3}{3} + \frac{\psi.u(x)^4}{4}\right]$$

evaluated over velocity limits u_0 and u_L

$$W_{peak} = \frac{2.A_x.L}{D_h.u_d}.\left[\frac{\theta.}{3}.(u_0^3 - u_L^3) + \frac{\psi}{4}.(u_0^4 - u_L^4)\right]$$

Where u_0 and u_L are the peak velocity amplitudes at either end of the regenerator
The above doesn't take account of the time variation. In principle this expression can be integrated for sinusoidal velocities. However as the pressure drop increases the velocity will reduce hence it is considered that the power variation will be rounded off and quadratic dependence on power is a good approximation. The mean power is then related to the maximum instantaneous power by:

Mean power = 0.5 *(maximum instantaneous power)

Hence

$$W_{mean} = \frac{A_x.L}{D_h.u_d}.\left[\frac{\theta.}{3}.(u_0^3 - u_L^3) + \frac{\psi}{4}.(u_0^4 - u_L^4)\right]$$

Estimation of Peak Gas Velocities
Total of gas is assumed to be constant over cycle i.e. leakage past seal is neglected

$m_{tot} = m_{va} + m_{vb} + m_{vc}$ $\qquad$ $m = \frac{M.P.V}{R.T}$ for each gas volume

M is mass of 1 mole $\quad P$ is pressure $\quad V$ is volume
R is universal gas constant $\quad T$ is temperature

We need to evaluate the peak values of max volume flux $\dot{V}$ at the boundaries between the volumes. The peak velocities can then be calculated from

$$u = \frac{1}{A_x}.\dot{V}$$

The volume fluxes are calculated from the mass variations $\frac{dm}{dt}$ in each volume.

$$\dot{V} = \frac{1}{\rho}.\frac{dm}{dt}$$

For the volumes that are constant

$$\frac{dm}{dt} = \frac{M.V}{R.T}.\frac{dP}{dt} \qquad \dot{V} = \frac{1}{\rho}.\frac{M.V}{R.T}.\frac{dP}{dt} = \frac{V}{P}.\frac{dP}{dt}$$

Effect of temperature variation is assumed to be small and mean temperature for all volumes at maximum gas velocity is assumed to be equal.

Pressure variation is driven by volume variation caused by piston can be calculated from

$$m_{tot} = \left(\frac{M}{RT}\right).(V_a + V_b + V_c).P \qquad P = \left(\frac{M}{RT}\right).\left(\frac{m_{tot}}{V_a + V_b + V_c}\right)$$

Differentiating the only variable is compression volume V_a

$$\frac{dP}{dt} = -m_{tot}.\left(\frac{M}{RT}\right).\left(\frac{1}{V_a + V_b + V_c}\right)^2.\left(\frac{dV_a}{dt}\right) = -P.\left(\frac{1}{V_a + V_b + V_c}\right).\left(\frac{dV_a}{dt}\right)$$

For Volume c peak gas velocity out of regenerator is given by

$$u_L = \frac{1}{A_x}.\left(\frac{V_c}{V_a + V_b + V_c}\right).\left(\frac{dV_a}{dt}\right)$$

For Volume b peak gas velocity into regenerator is given by

$$u_0 = \frac{1}{A_x}.\left(\frac{V_b}{V_a + V_b + V_c}\right).\left(\frac{dV_a}{dt}\right) + u_L$$

Pressure Drop across Regenerator

Total Pressure drop is given by integral of pressure drop along length of regenerator

$$P_d(x) == \frac{2}{D_h}.\left(\theta.u(x) + \psi.u(x)^2\right)dx$$

$$\Delta P = -\frac{2.L}{D_h.u_d}.\int\left(\theta.u(x) + \psi.u(x)^2\right)du(x) = -\frac{2.L}{D_h.u_d}.\left[\frac{\theta.u(x)^2}{2} + \frac{\psi.u(x)^3}{3}\right]$$

evaluated over velocity limits u_0 and u_L

$$\Delta P_{0-pk} = \frac{L}{D_h.u_d}.\left[\frac{\theta.}{2}.(u_0^2 - u_L^2) + \frac{\psi}{3}.(u_0^3 - u_L^3)\right]$$

APPENDIX 2: REPORT ON COMPENSATED THERMOCOUPLE RESULTS

1 Thermocouple compensation

1.1 Introduction

Two fine wire thermocouples of different diameters were installed after the regenerator exit. These are R type thermocouples (Platinum/Pt-13% Rhodium) with nominal diameters of 25 and 50 microns. The junctions were specially made by percussion welding. Traditionally, the junctions were created by spot welding, which has a diameter 2-2.5 times bigger than the diameter. The bigger the diameter of a junction, the bigger the thermal inertia, and so reduces the time response. Percussion welding can form a junction no bigger than the original diameter, realizing the full potential of the fine wires. Each welded thermocouple was inspected under the microscope. The wire diameter has to be uniform within 10% for it to be accepted.

The fine wires were supported by four prongs made of the same thermocouple materials as shown in Figure 1. The wires are arranged in a X configuration with the junctions situated at the centre of the probe. The finer wire is raised slight above the thicker wire, so that the junctions are separated by 0.1 mm.

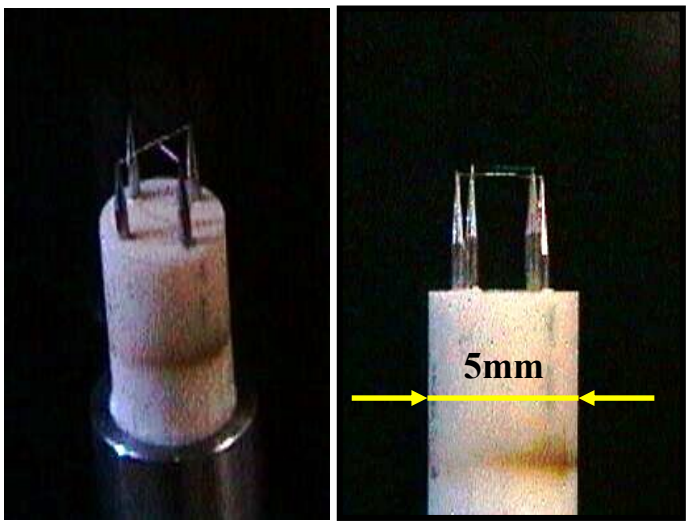

Figure 1 Pictures of thermocouple probe (courtesy of Prof. Moriyoshi). Left: 3D view showing two fine thermocouples are in a cross configuration. Right: Side elevation

Even though very fine thermocouples were used in the experiment, the time response was still insufficient to measure the gas temperature accurately. Figure 2 illustrates this point. The temperature variations in a cycle are plotted. TC25 and TC50 represented the 25 and 50 micron thermocouple temperatures respectively. The cold wire temperature is also plotted for comparison. The cold wire was installed in the compression space, 4.5 mm upstream of the regenerator entry. Since the response of the cold wire is at least 100 times faster than the thermocouple, the measured temperature may be regarded as instantaneous.

The beginning of the cycle is defined as zero piston displacement when the piston is moving up. The cold wire temperature peaks at about 1/4 of the cycle, when the piston has the maximum displacement. This means the temperature rise is mainly due to compression.

However, the peak temperatures of TC25 and TC50 occur later and at different parts of a cycle with different magnitude. TC50 has smaller peak and lags behind TC25. The results strongly indicate that the TC25 and TC50 are not fast enough to response to the changes in the gas temperature. This section will explain the theory of thermocouple compensation techniques and how they are being applied to the measurements. The quality of compensation will be evaluated by model validation.

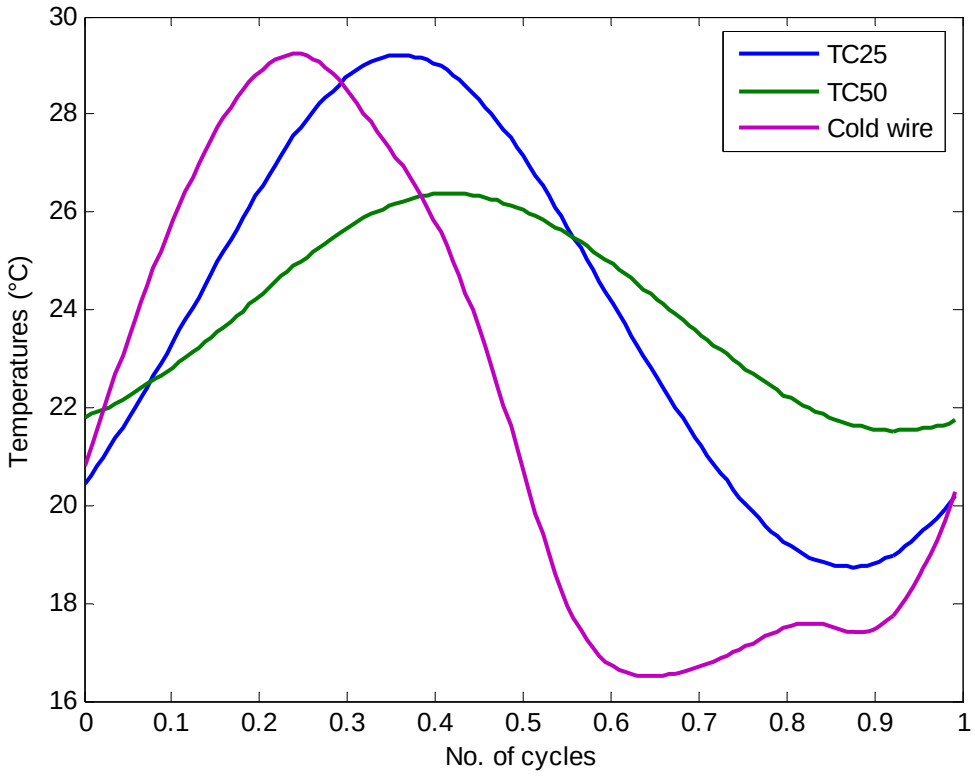

Figure 2 Typical results. Helium gas, 5 bar fill pressure, 10 mm stroke at 36 Hz.

1.2 Theory

A well designed thermocouple (convective heat transfer is dominant compared to conductive and radiative heat transfer) can be modelled as a first-order lag system, in which the time constant (τ) defines how fast a thermocouple will response to a change in temperature. The response may be described mathematically as

$$T_g = T + \tau \frac{\mathrm{d}T}{\mathrm{d}t} \qquad 1)$$

where:

T_g is the temperature of the environment
T is the thermocouple measured temperature
t is time

Hoshino [1] investigated the effect of conduction on the thermocouple temperature under Stirling engine operating conditions. The simulation results have shown that if the length-to-diameter ratio (L/d) of a thermocouple is bigger than 40-80, the conduction effect is negligible. The exact value depends on the convective heat transfer rate. The lowest L/d of the thermocouple probe is 65, so the conduction effect is expected to be small. Given the maximum thermocouple temperature swing observed is about 10 K, and the regenerator

housing and other connected components were more or less at the average thermocouple temperature. There was only ~5 K temperature difference at about 300 K to drive the radiative heat transfer process. Therefore, the radiation heat transfer is also expected to be small.

When the gas temperature changes with time, Eq. 1 states that the measured and the gas temperatures will be different. This difference is called the dynamic error due to finite heat transfer between the gas and the thermocouple. The dynamic error can be minimised by having smaller thermocouples, and materials with smaller density and specific heat, but it cannot be totally eliminated. In the process of thermocouple compensation, the time constant is not minimised, instead it is being estimated by some means. Then the gas temperature can be back calculated from the measured temperature and its time derivatives. Unfortunately, the time constant is not a property of the thermocouple, but depends on parameters that can affect the heat transfer, such as gas density, Reynolds number and thermal conductivity, etc.

The time constant may be estimated analytically using established Nusselt correlations for the appropriate geometry, e.g. Collis-William's equation [2]. This method has limited use because:

- Nusselt correlations are derived in steady flow, so they may not work in an oscillatory flow as found in Stirling engines.
- Flow velocity is required, which is often not available.
- Some fluid and material properties are functions of temperature.

The alternative is to measure the time constant by creating a step change in thermocouple temperature in the test flow. By observing the temperature decay, the time constant is the time required for the junction temperature to decease to 63.2% of the difference between the initial and final temperatures. The step change is usually achieved by passing an electric current through the thermocouple wire. Some researchers [3] found that the heat transfer characteristic is different when the thermocouple is subject to internal heating rather than external heating (when it is working as a thermometer). Since the time constant varies with flow conditions, it needs to be measured for every test flow condition and this can be rather time consuming. When the flow is constantly changing with time, only an average time constant can be measured. The accuracy of the compensation will be determined by the range of the time constant. It may be acceptable for some applications, but may be not for others.

The latest development has been in two-thermocouple techniques. These techniques allow the time constant to be estimated *in situ*. No heating or cooling is involved. In some techniques the instantaneous time constants can be estimated, as opposed to an average value from the empirical method. The key assumption of these techniques is that the two thermocouples are subjected to the same temperature. This may be violated in the case of a steep temperature gradient. The model validation section later on will verify this assumption. Many two-thermocouple techniques have been proposed: Cambray [4], Tagawa *et al.* [5, 6, 7], Forney and Fralick [8], Hung *et al.* [9, 10] and Kar *et al.* [11]. This report will only give a brief overview of these techniques. For more details, please refer to [11, 12 and 13]. The most important distinction between these techniques is whether the time constant is assumed to be time invariant. A time invariant assumption requires the environment conditions not to change with time.

Let subscript 1 and 2 denote the first and second thermocouples respectively. The thermocouple equations are:

	$$T_g(t) = T_1(t) + \tau_1(t)\frac{dT_1(t)}{dt}$$	2)
	$$T_g(t) = T_2(t) + \tau_2(t)\frac{dT_2(t)}{dt}$$	3)

and,

	$$\alpha = \frac{\tau_1(t)}{\tau_2(t)} \neq 1$$	4)

Cambray [4] assumed α in Eq. 4 is known *apriori*, Eqs. 2 and 3 can be solved simultaneously for τ_1:

	$$\tau_1(t) = \frac{T_2(t) - T_1(t)}{dT_1/dt - \alpha\, dT_2/dt}$$	5)

There is a singularity in this solution when the denominator approaches zero. Moreover, the evaluation of the time derivatives will invariably amplify any measurement noise in the signals, this will tend to make the equation ill-defined over a region. The result is unphysical and erratic time constant estimates. The measurement noise can be handled by least square methods [5, 6, 9, 13]. Instead of equating Eq. 2 and 3, these methods seek to minimise the difference between T_{g1} and T_{g2} in a least square sense in N number of samples.

	$$\xi = \frac{1}{N}\sum_{i=1}^{N}\left(T_{g1} - T_{g2}\right)^2$$	6)

This occurs when

	$$\frac{\partial \xi}{\partial \tau_1} = 0; \frac{\partial \xi}{\partial \tau_2} = 0$$	7)

For which the solution for the time constants is

	$$\tau_1 = \frac{\sum G_2^2 \sum (G_1 \Delta T) - \sum (G_1 G_2) \sum (G_2 \Delta T)}{\sum G_1^2 \sum G_2^2 - \left[\sum (G_1 G_2)\right]^2}$$ $$\tau_2 = \frac{\sum (G_1 G_2) \sum (G_1 \Delta T) - \sum G_1^2 \sum (G_2 \Delta T)}{\sum G_1^2 \sum G_2^2 - \left[\sum (G_1 G_2)\right]^2}$$	8)

In Eq. 8, the following abbreviation has been used to make the equations easier to interpret: $\frac{1}{N}\sum_{i=1}^{N} = \sum$; $\Delta T = T_2 - T_1$; $G_1 = \frac{\mathrm{d}T_1}{\mathrm{d}t}$ and $G_2 = \frac{\mathrm{d}T_2}{\mathrm{d}t}$.

To track the changes in the time constants, N is set to be smaller than the total number of samples. It is apparent that the choice of N is a compromise between fast tracking and noise rejection. In the limits when $N = 1$, the estimation become a recursive algorithm. O'Reilly *et al.* [14], Kar *et al.* [11], and Grys and Minkina [15] applied various recursive algorithms for time constant estimation. The major difference in the algorithms lies in which estimators they used. For example, Kar *et al.* used a Kalman filter, while Grys and Minkina employed the popular least mean squares and recursive least square estimators. Since recursive algorithm will be applied in this work, their theories will be covered fully in Analysis method section.

1.3 Scope

This work focuses on both nitrogen and helium data at a fixed stroke of 10 mm. Three filling pressures (1, 5 and 18 bar) and three frequencies (8.6, 18 and 36 Hz) have been investigated, that is a total of 9 operating points for each gas. A longer stroke is not considered, as there is no experimental data for some pressures and/or frequencies due to limits on the maximum input voltage or current to the compressor.

1.4 Analysis Methods

The general flow of the analysis method is illustrated in Figure 4. The amplified thermocouple voltages were digitised and recorded using the Flyde data acquisition system. As described in the data processing section, the voltages are corrected for amplifier's zero voltages and sampling delay, and finally calibrated to temperatures. The calibrated temperature has an uncertainty of 0.2 K.

1.4.1 Ensemble averaging

The thermocouple has a low sensitivity (about 5 μV/K). To improve the signal-to-noise ratio, ensemble averaging has been employed. It has been found that interference especially from the mains is effectively eliminated. However, the results will be limited to "average" conditions; cyclic variability cannot be investigated. This would not be a serious limitation as the measured temperatures are highly repeatable, e.g. see Figure 3.

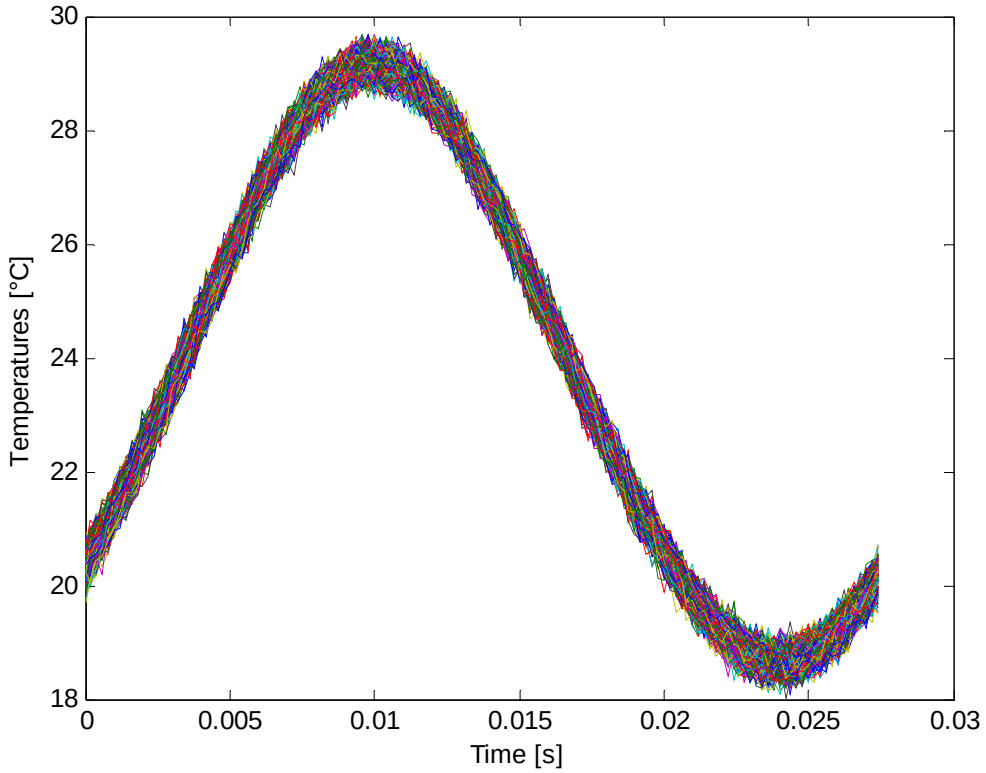

Figure 3 Thermocouple temperatures (TC25) for 360 cycles, 5 bar fill pressure, 10 mm stroke at 36 Hz.

The ensemble averaged temperatures are extended by joining the end of cycle to the beginning three times, so that there are 3 cycles of data. There are several reasons for doing so:

- Some filters have lead-in and lead-out periods, in which the filtered signal is meaningless. Extending the data will give all the lead-in in the first cycle and the lead out in the third cycles, leaving the second cycle free of filtering errors.
- At high frequency cyclic frequency conditions, there are not enough data points in a cycle for the Gaussian smoothing filter to work.
- The time derivatives of temperatures are usually calculated by central difference (3-point scheme). This is not possible for the first and the last data points. Having two redundant cycles will overcome this problem.

A fixed number of samples were collected for each experiment, irrespective of the cyclic frequency. Therefore, the higher the cyclic frequency, the fewer data points each cycle has, and the greater the number of cycles. So at the lowest frequency (8.6 Hz), there are only 85 cycles. At 36 Hz, the number of cycles increases to 360. This effect will be discussed in detail later.

1.4.2 Time derivatives and low pass filtering

The time derivatives of temperatures are needed for some estimators and for temperature reconstruction. If low pass filtering is not required, they are evaluated by central difference. When low pass filtering is desired, the temperature signals are filtered by a Gaussian smoothing filter. The filter suppresses the high frequency noise by convolving the signal with a Gaussian kernel. The Gaussian kernel is defined by:

$$g(t) = \exp\left(-\lambda t^2\right) \tag{9}$$

where λ is a smoothing parameter that sets the cut-off frequency. Let the thermocouple signal be *x(t)*; the filtered signal $y(t)$ is then:

$$y(t) = x(t) \otimes g(t) \tag{10}$$

The time derivatives can be found easily by using the commutative law of convolution as follows:

$$\begin{aligned} \frac{\mathrm{d}\, y(t)}{\mathrm{d}\, t} &= \frac{\mathrm{d}\, x(t)}{\mathrm{d}\, t} \otimes g(t) \\ &= x(t) \otimes \frac{\mathrm{d}\, g(t)}{\mathrm{d}\, t} \end{aligned} \tag{11}$$

where $\mathrm{d}g(t)/\mathrm{d}t = -2\lambda t\exp(-\lambda t^2)$.

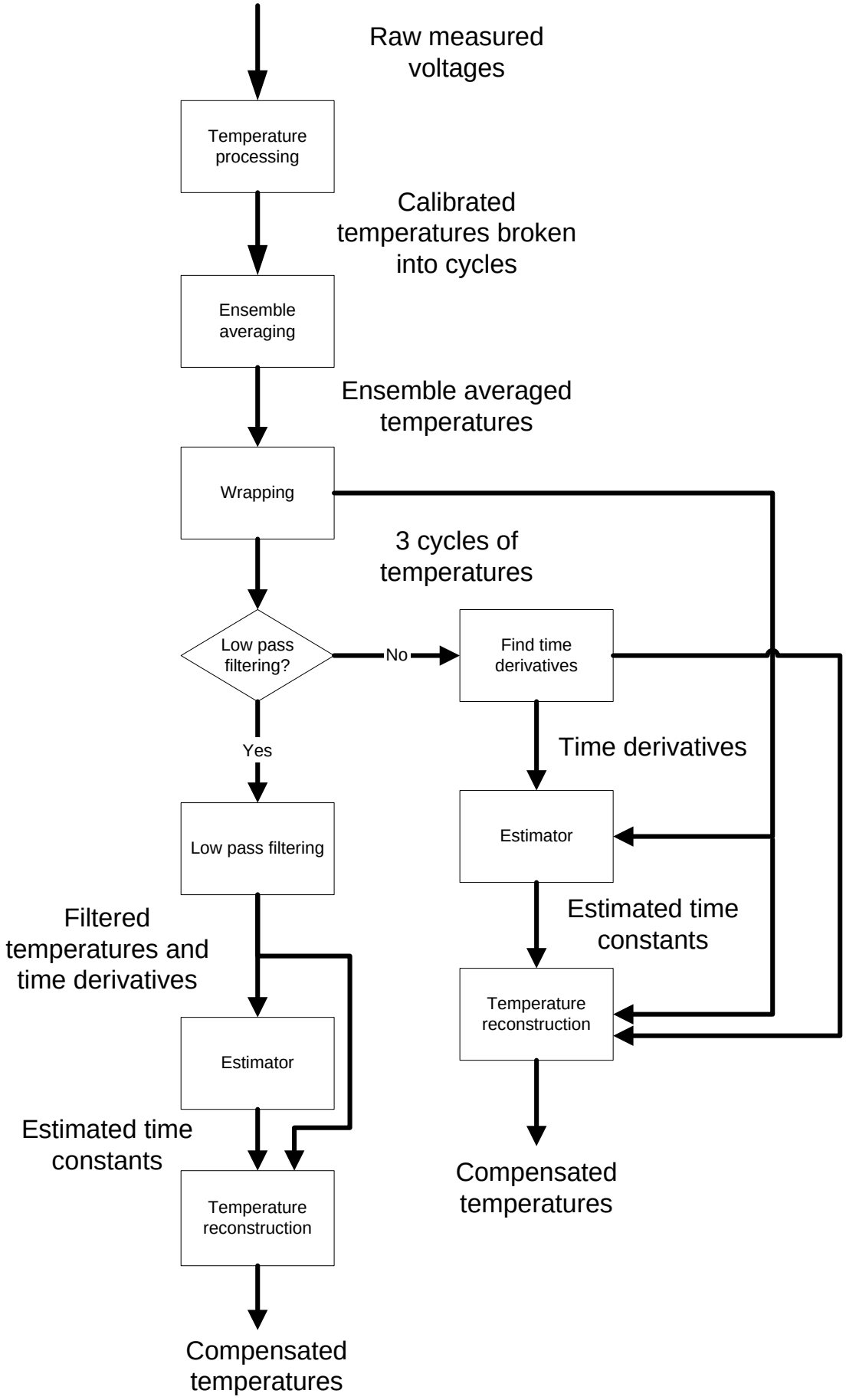

Figure 4 Analysis method flow chart

1.4.3 Estimators and model structure

It is unclear if the change in pressure and velocity in the regenerator exit can cause strong variations in the time constants. If so, the two thermocouple techniques must be able to track the changes by means of recursive algorithms. However, since these techniques have to place more emphasis on more recent samples than past samples, they are inherently more prone to noise and have bigger error (bias) in the estimation. Thus, in some case, an average time constant with small bias can be more accurate than a varying time constant with a big bias. It is therefore proposed to estimate an average time constant first. This will establish the benchmark with which the time varying results can be compared. In this way, any improvement/deterioration in accuracy can be assessed. Only if the time varying results show improvement in the model validation will they be accepted.

The response equations (Eqs. 2 and 3) can be expressed in a matrix-vector form:

$$T_1(k) - T_2(k) = \begin{bmatrix} -\dfrac{\mathrm{d}T_1(k)}{\mathrm{d}t} & \dfrac{\mathrm{d}T_2(k)}{\mathrm{d}t} \end{bmatrix} \begin{bmatrix} \tau_1 \\ \tau_2 \end{bmatrix} \qquad (12)$$

$$y = \mathbf{x}^{\mathrm{T}}\boldsymbol{\theta}$$

where k is the k^{th} sample in a discretised signal. The left hand side of the equation is called system output (y). The right hand side consists of a regressor ($\mathbf{x}$) and parameter vector ($\boldsymbol{\theta}$). This general form is well known in the system identification literature [16, 17]. Once the thermocouple equations are in this form, the time constants can be estimated by different estimators, such as a Kalman filter. Eq. 12 demonstrates one model structure in which the differential equations are used directly. Alternatively, the thermocouple equations can be modelled by difference equations [9], which yield another model structure:

$$T_2(k) - T_2(k-1) = \begin{bmatrix} T_1(k) - T_1(k-1) \\ T_1(k-1) - T_2(k-1) \end{bmatrix}^{\mathrm{T}} \begin{bmatrix} \dfrac{1-\exp(-t_s/\tau_2)}{1-\exp(-t_s/\tau_1)} \\ 1-\exp(-t_s/\tau_2) \end{bmatrix} \qquad (13)$$

where t_s is the sampling time which is equal to 1/sampling frequency (f_s).

Notice that Eq. 13 does not require time derivatives, so it may handle noise better. These two model structures will be considered and compared in the Results and Discussion section.

The estimators considered here are recursive least squares (RLS) with exponential forgetting factor and Kalman filtering (KF). Other methods which require a presumed ratio of time constant will not be used. The RLS estimator assumes white noise (v) in the measurement in Eq. 12, that is

$$y = \mathbf{x}^{\mathrm{T}}\boldsymbol{\theta} + v \qquad (14)$$

The RLS estimator seeks to minimize the following cost function

$$J = \sum_{i=1}^{N} \lambda^{N-i} \left(y(i) - x^{T}(i)\theta \right) \qquad (15)$$

The term in the bracket is the residual of the estimation. This is to be weighted by a forgetting factor λ. Tracking is attained by placing more importance on the more recent data than the past data. A data point is exponentially discounted as time increases with the forgetting factor (λ) defining the time constant of the exponential decay. As far as the estimator concerns, there are roughly $1/(1-\lambda)$ of data points which are effective (in memory). A lower value gives a

more rapid response in tracking the parameter vector. The value commonly used in industry is between 0.97 and 0.995. In the limit of $\lambda = 1$, all data points are remembered, so the estimator gives a constant parameter estimation.

It can be showed that the following recursive formulae estimate the parameter vector and minimise the cost function:

$$\hat{\theta}(k+1) = \hat{\theta}(k) + \mathbf{G}(t+1)\varepsilon(k+1)$$
$$\varepsilon(k+1) = y(k+1) - x^{\mathrm{T}}(k+1)\hat{\theta}(k)$$
$$\mathbf{G}(k+1) = \frac{\mathbf{P}(k)x(k+1)}{\lambda + x^{\mathrm{T}}(k+1)\mathbf{P}(t)x(k+1)} \qquad 16)$$
$$\mathbf{P}(k+1) = \frac{1}{\lambda}\left[\mathbf{I} - \mathbf{G}(k+1)x^{\mathrm{T}}(k+1)\right]\mathbf{P}(k)$$

where:

ε is the output (*apriori*) prediction error
G is time varying gain matrix
P is the covariance of parameter estimation error
I is the identity matrix
λ is the forgetting factor with a limit between zero and one

At the start of the estimation, the parameter vector is initialized to a zero vector and the covariance **P**(0) is assumed to be $10^4\mathbf{I}$, which is defined to be sufficiently large, so that fast convergence of the solution can be achieved.
In a Kalman filter, both measurement and the parameter vector have white noise with variances of σ^2(k) and **W**(k) respectively, which may change with time step. Note that there are two parameters in the parameter vector, so **W**(k) is a 2x2 matrix. The recursive formulae for the Kalman filter are similar to RLS, except the gain and covariance matrices are evaluated according to the noise variance as shown below.

$$\mathbf{G}(k+1) = \frac{\mathbf{R}(k+1)x^{\mathrm{T}}(k+1)}{\sigma^2_{\hat{y}}(k+1)}$$
$$\mathbf{P}(k+1) = \mathbf{R}(k+1) - \mathbf{G}(k+1)x(k+1)\mathbf{R}(k+1) \qquad 17)$$
$$\mathbf{R}(k+1) = \mathbf{P}(k) + \mathbf{W}(k+1)$$

where:

R is the covariance of the parameter vector.
$\sigma^2_{\hat{y}}$ is the estimated prediction variance. It is the sum of measurement noise variance (σ^2) and prediction variance due to uncertainty in the parameters (σ^2_θ) as defined in Eq. 18.

$$\sigma^2_{\hat{y}}(k) = \sigma^2(k) + \sigma^2_\theta(k)$$
$$\sigma^2_\theta(k) = x(k)\mathbf{R}(k)x^{\mathrm{T}}(k) \qquad 18)$$

The noise parameters are not assigned arbitrarily. They are estimated using Jazwinski's method [18]. The state noise covariance matrix is assumed to be an isotropic matrix, $\mathbf{W} = q\mathbf{I}$. The prediction variance (σ^2_{q0}) is calculated, assuming no state noise, i.e. $q = 0$ by:

$$\sigma^2_{q0}(k+1) = \sigma^2(k+1) + x(k+1)\mathbf{P}(k)x^{\mathrm{T}}(k+1) \qquad 19)$$

If σ_{q0}^2 is smaller than the prediction error (ε^2), the state noise is inferred to be non-zero. This logic can be implemented using a ramp function in Eq. 24.

$$h(x) = \begin{cases} x \ldots \text{if } x \geq 0 \\ 0 \ldots \text{otherwise} \end{cases} \quad (20)$$

Therefore, q can be updated according to:

$$q(k) = h\left(\frac{\varepsilon^2(k) - \sigma_{q0}^2(k)}{x(k)x^{\mathrm{T}}(k)} \right) \quad (21)$$

Eq. 18 shows that the estimated prediction variance is made up of the measurement noise and the component due to the uncertainty in the latent variables. Thus the measurement noise can be estimated by subtracting the second component from the prediction error as

$$\sigma^2(k+1) = h\left(\varepsilon^2(k+1) - x(k+1)R(k)x^{\mathrm{T}}(k+1) \right) \quad (22)$$

It can be proved that the observation noise estimated by Eq. 22 will maximize the likelihood of the observation in the next sample.

The Kalman filter is initialised with $q(0) = 1$, $\theta(0) = [0.5, 0.5]$, $\sigma^2(0)$ based on 40 dB signal-to-noise ratio. To estimate average time constants, system noise is zero always and σ^2 is fixed to have a 40 dB signal-to-noise ratio.

There are two model structures and two estimators forming a combination of 4 techniques. These techniques will be named according to the model structure and the estimator used.

A CT prefix will be used for any technique that uses the differential equations directly (Eq. 12). Techniques that use the difference equation will have a ZOH prefix. Kalman filter and recursive least squares estimators will be abbreviated as KF and LS respectively, and they form the suffix of a technique. For example, a CT-KF technique is a technique that uses the differential equations and estimates the time constants using Kalman filtering.

1.4.4 Temperature reconstruction

The gas temperature is reconstructed by applying Eq. 1 with the estimated time constants ($\hat{\tau}_1$ and $\hat{\tau}_2$). To make a distinction between the actual gas temperature (T_g) and the reconstructed temperature, a new symbol R is assigned to the reconstructed temperature in Eq. 23.

$$R_1(t) = T_1 + \hat{\tau}_1 \frac{\mathrm{d}T_1(t)}{\mathrm{d}t}$$
$$R_2(t) = T_2 + \hat{\tau}_2 \frac{\mathrm{d}T_2(t)}{\mathrm{d}t} \quad (23)$$

The assumption for two thermocouple techniques is that the two reconstructed temperatures should be equal, but not at every time step. Noise and other extraneous factors may prevent them being so. Most estimators assume that the difference is a white noise. By studying this difference (known as residual of the estimation), this assumption can be validated. Any departure from this assumption may indicate modelling error, biased time constant estimates, and unsteadiness in the thermocouples. These issues will be addressed in the model validation section.

1.5 Results and discussion

1.5.1 Preliminary evaluation of the data

Kar et al [11] pointed out that time constant estimation can be compromised by any DC offsets in the raw thermocouple voltages. This is why the amplifier zero voltages were monitored and the thermocouple was calibrated with the zero voltage taken off in advance. An acid test is to compare the cyclic means of the two thermocouple signals to see if there are any significant DC offsets, or any other unaccounted effects that violate the two thermocouple assumptions. For example, a very steep temperature gradient near the thermocouple probes will cause the two means to differ from each other. If so, the two-thermocouple techniques cannot be applied, and thermocouple compensation is not possible.

The results were very positive. The cyclic mean of the two thermocouple temperatures are differ by 0.4% for helium (typical) and 0.6% for nitrogen. In one case, the difference is as low as 0.01%. The cyclic mean of TC25 can be bigger or small than the one of TC50 in the nitrogen data. But the helium results have shown that the cyclic mean of TC50 is always bigger. Is this systematic difference genuine, or this is just a systematic error in the experiment? In some tests, especially large stroke at high pressure, the zero readings were not stable, so some judgment was made on what were the best values. Finally the comparison is not entirely foolproof. If the gas temperature is highly asymmetric - asymmetry here refers to dissimilar waveforms - above and below the mean level, it is possible for the attenuated thermocouple signals with different response times to have different means. This is because the attenuation is proportional to the rate of change of the signal, not the absolute signal level.

1.5.2 Estimated time constants

The time constants were estimated using the four techniques described, with and without low-pass filtering. Two helium results at 5 bar filling pressures are shown in Figures 5 and 6. The results at 8.6 Hz all show smaller time constants when low-pass filtering is not used. Many previous studies [7, 9, 19] have found that the effect of measurement noise is to introduce a bias, which tends to underestimate the time constants. Low-pass filtering reduces the noise level, so the bias is reduced accordingly.

Different techniques handle the measurement noise differently. Some will give a lower bias for the same noise level. Since low-pass filtering can reduce bias, the increase in the time constant after filtering can reveal how well a technique handle noise. The results in Figure 5 show that the ZOH-LS and ZOH-KF techniques are more tolerant to noise than their continuous time counterparts. It seems the model structure is a more important factor than the estimator in noise rejection.

The time constant estimates at 36 Hz cyclic frequency (Figure 6) are more consistent. The ZOH-LS and ZOH-KF both return the same estimates of 5.6 ms (within 0.1 ms) with and without filtering. The low-pass filtering does reduce the bias in Tagawa's technique and CT-LS technique, bringing the estimates to 5.6 ms as well. However, the increases in the time constants is very small (4%), which means the bias is small in the unfiltered case. In summary, the time constants at 36 Hz are unaffected by bias. All techniques give similar results and low-pass filtering makes little difference. It is of practical interests to find out why the estimation at 36-Hz is of high quality, as this may shed light on how to optimise the estimation process in other less ideal situations.

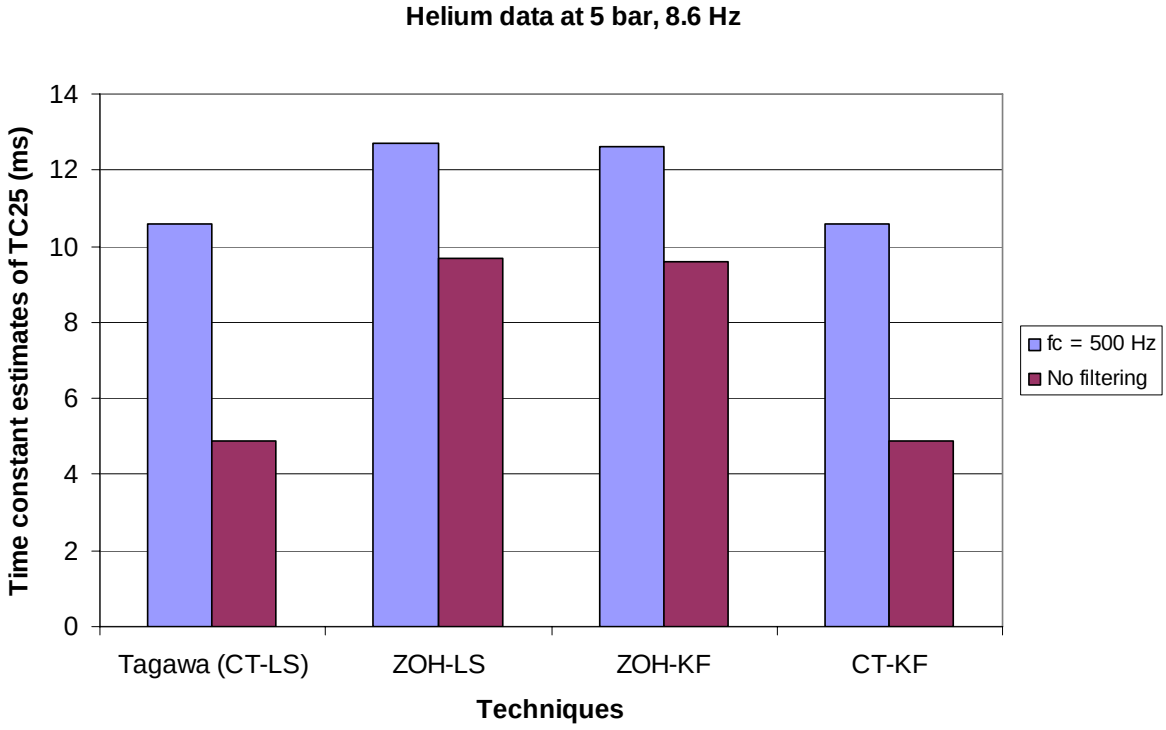

Figure 5 **Comparison of different two-thermocouple techniques. Helium gas, 5 bar fill pressure, 10 mm stroke at 8.6 Hz.**

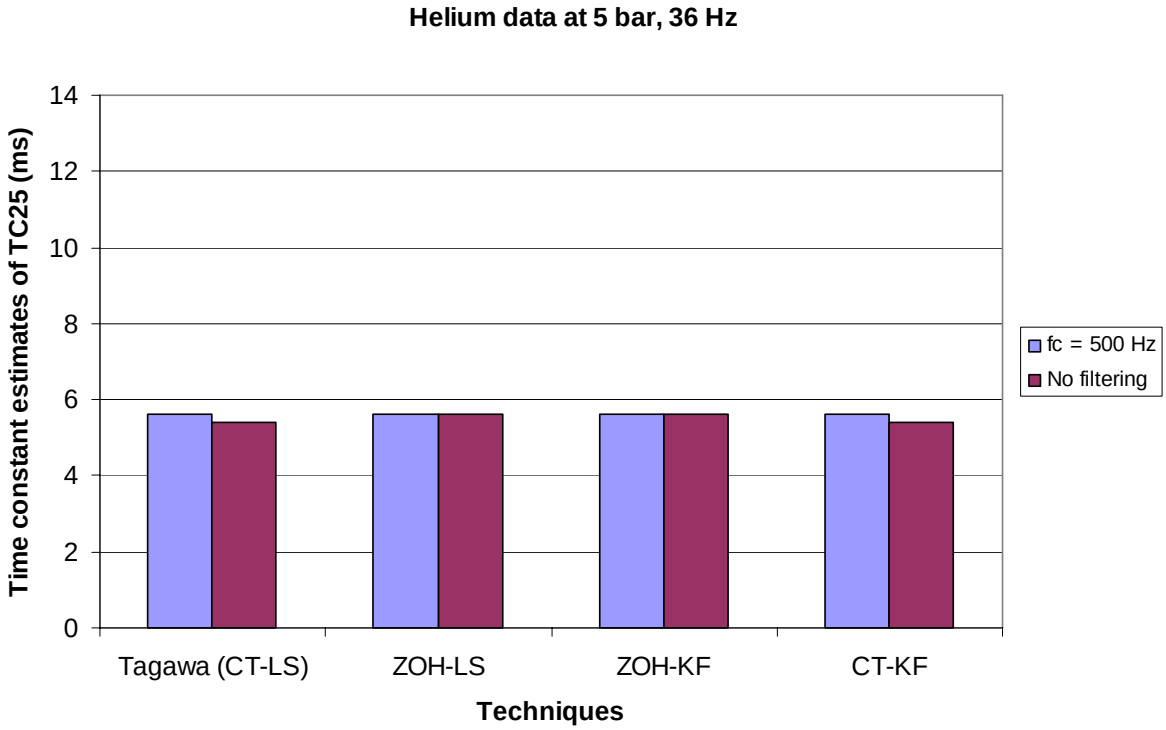

Figure 6 **Comparison of different two-thermocouple techniques. Helium gas, 5 bar fill pressure, 10 mm stroke at 36 Hz.**

The graphs in Figure 7 and Figure 8 can answer why the estimates at 36 Hz have small biases. The noise is imperceptible in the ensemble averaged temperatures. However, the two-

thermocouple techniques either make use of the time derivatives or the temperature difference between two time steps. Hence, noise in the time derivatives should be a better measure of the noise level. It is clear that the time derivatives at 36 Hz are much smoother, whilst at 8.6 Hz the time derivatives have lots of high frequency fluctuations, which are not physical. Obviously, the estimators will be more affected by noise at 8.6 Hz, i.e. subject to a lower signal-to-noise ratio, so yielding bigger biases as indicated by the difference between the estimates with and without filtering.

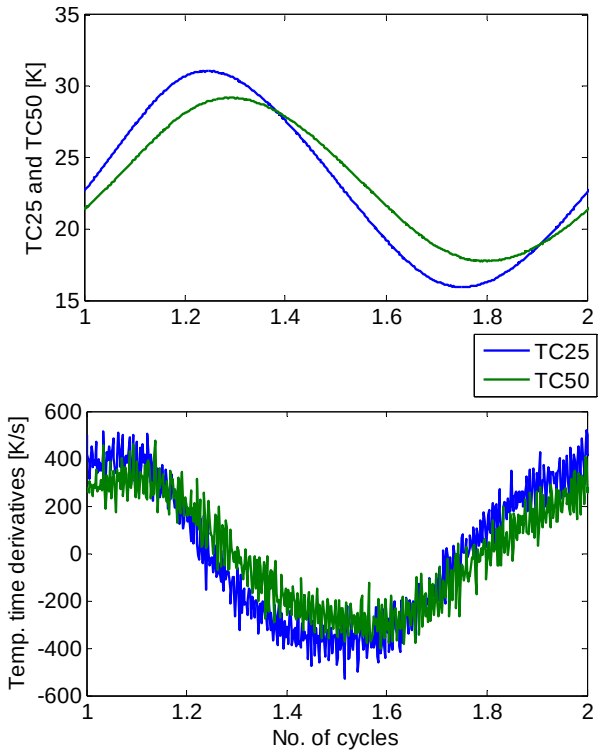

1.5.3

Figure 7 The ensemble averaged TC25 and TC50 temperatures and their time derivatives. Helium gas, 5 bar fill pressure, 10 mm stroke at 8.6 Hz.

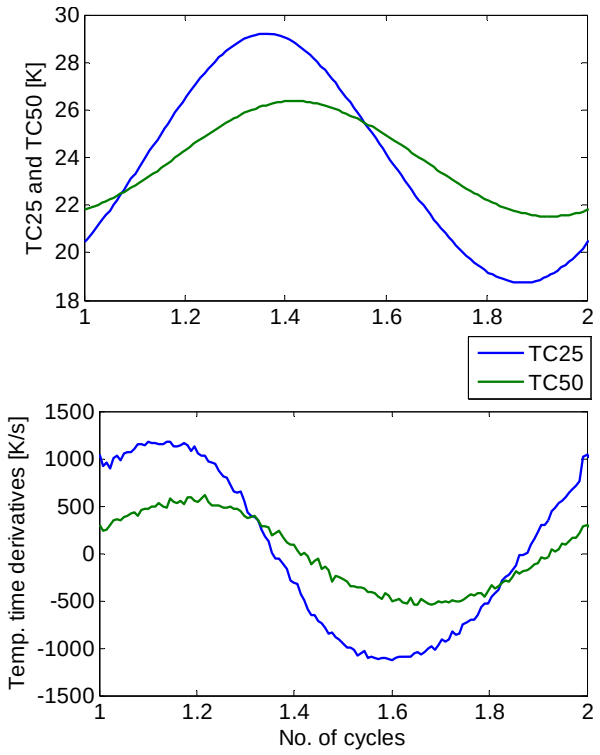

1.5.4

Figure 8 The ensemble averaged TC25 and TC50 temperatures and their time derivatives. Helium gas, 5 bar fill pressure, 10 mm stroke at 36 Hz.

There are several differences that can explain why the signal-to-noise ratio is higher at 36 Hz:

1. The sampling frequency and the total sampling time are fixed, so if the cycle frequency goes up, the number of samples per cycle goes down with a proportional increase in the number of cycles sampled. At 36 Hz, there are 360 cycles; each one has 138 samples versus 582 samples for each 85 cycle.
2. Consider the time constants for TC25, the time constant is about 12 ms at 8.5 Hz, which means the corner frequency is 13 Hz. At a cyclic frequency of 36 Hz, the time constant decreases to 5.7 ms, which means the corner frequency is now 28 Hz. The cyclic frequency is relatively closer to the corner frequency, so less attenuation and stronger signals are expected.
3. Recall that the signals are ensemble averages. There are about 4 times more cycles at 36 Hz than there at 8.6 Hz, so the signal-to-noise ratio should be double.

Amongst the above three points, it has been found that the first point is the most significant factor. When any finite difference schemes calculate time derivatives there needs to be a time step (h). For example at the time step k, a forward difference scheme calculates:

	$\frac{\mathrm{d}T(k)}{\mathrm{d}t} \cong \frac{T(k+1)-T(k)}{h}$	24)

Eq. 24 states that the time derivative is inversely proportional to h. In reality, there is also noise (e) present in T. It will be at least as big as in the numerator in Eq. 24. Thus,

	$\frac{\mathrm{d}T(k)}{\mathrm{d}t} \cong \frac{T(k+1)-T(k)}{h} + \frac{e}{h}$	25)

Therefore, any unwanted noise will also be scaled by h in the time derivative. If h is increased by lower the sampling rate, the noise level should be reduced accordingly. The sampling rate may be reduced by decimation. Decimation by a factor of r does not simply mean selecting every r^{th} sample. This is because doing so will introduce aliasing (signals below the Nyquist frequency in the original sampling rate is now above the new Nyquist frequency). To avoid aliasing, an anti-aliasing filter has to be applied as well.

The sampling rate of 8.5 Hz data is decimated by a factor of 4 by firstly applying an 8^{th} order Chebyshev filter with a cut-off frequency of 0.4 of the reduced sampling frequency (0.4 x 5000/4 = 500Hz). Only every 4^{th} data point in the filtered signals is retained. The low pass filter does not alter the phase of the signal, and the magnitude is at least 99.43% accurate. The time derivatives are recalculated and plotted in Figure 9. Indeed the time derivatives have much lower noise, and correspondingly the biases in the time constants are reduced or eliminated. As shown in Figure 10, a marked reduction in bias can be achieved just by halving the sampling frequency. This happens for the ZOH model structure, even though the time derivatives are not used directly. As the decimation factor increases, the estimate eventually reaches a stable value, which is identical to the value found by filtering. In addition, the ZOH model structure being more noise tolerant, settles to the stable value quicker than the continuous time model structure (Tagawa and Ohta's method). To be consistent, both model structures are processed using a least squares estimator, but the influence of the model structure does not change when a Kalman filter is used.

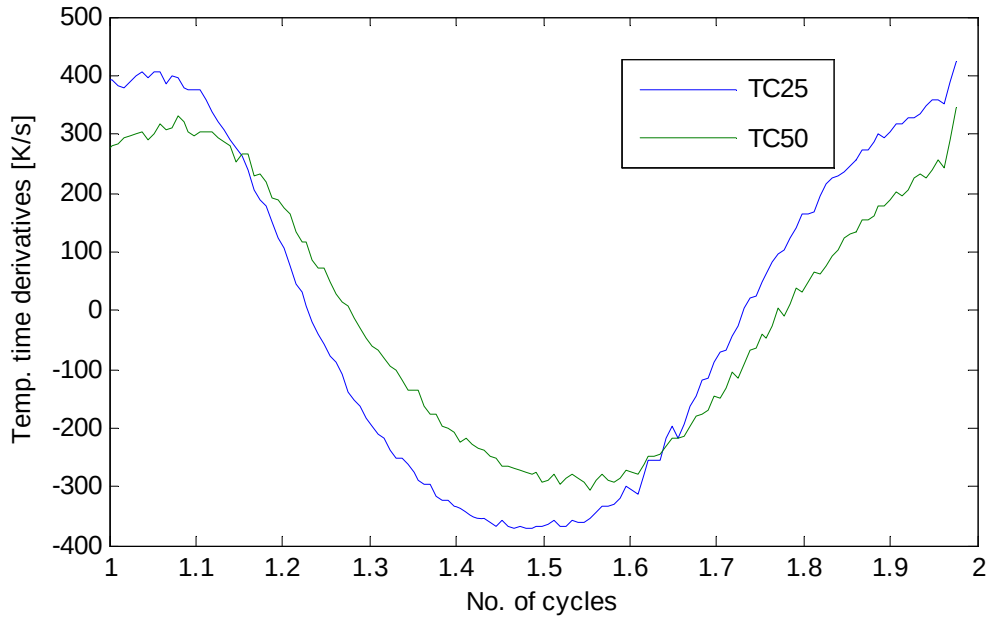

Figure 9 The time derivatives of TC25 and TC50 temperatures, decimated by 4 times. The sampling frequency is 1.25 kHz. Helium gas, 5 bar fill pressure, 10 mm stroke at 8.6 Hz.

Decimation was applied to the 18-Hz and 36-Hz data. The minimum decimator factors required to achieve a stable time constants were recorded. It was found that the decimation factors were inversely proportional to the cyclic frequency. For example, starting with a decimator factor of 1 at 36 Hz, it becomes 2 at 18 Hz, and 3 at 8.5 Hz. In other words, the sampling frequency increases in proportion with the cyclic frequency. These results suggest that the estimators can give unbiased estimations when the data points per cycle are equal to or smaller than certain values. Whilst it has been shown that decimation can increase the effective signal-to-noise ratio, it is desirable to keep decimation to a minimum (sampling frequency as high as possible), so that no genuine high frequency information is discarded. Also, the numerical error in calculating the time derivatives is in the order of h^2. Using too high a decimation will eventually lead to inaccurate evaluation of the time derivatives, and then the time constant estimates may diverge from the stable values as shown in Figure 11.

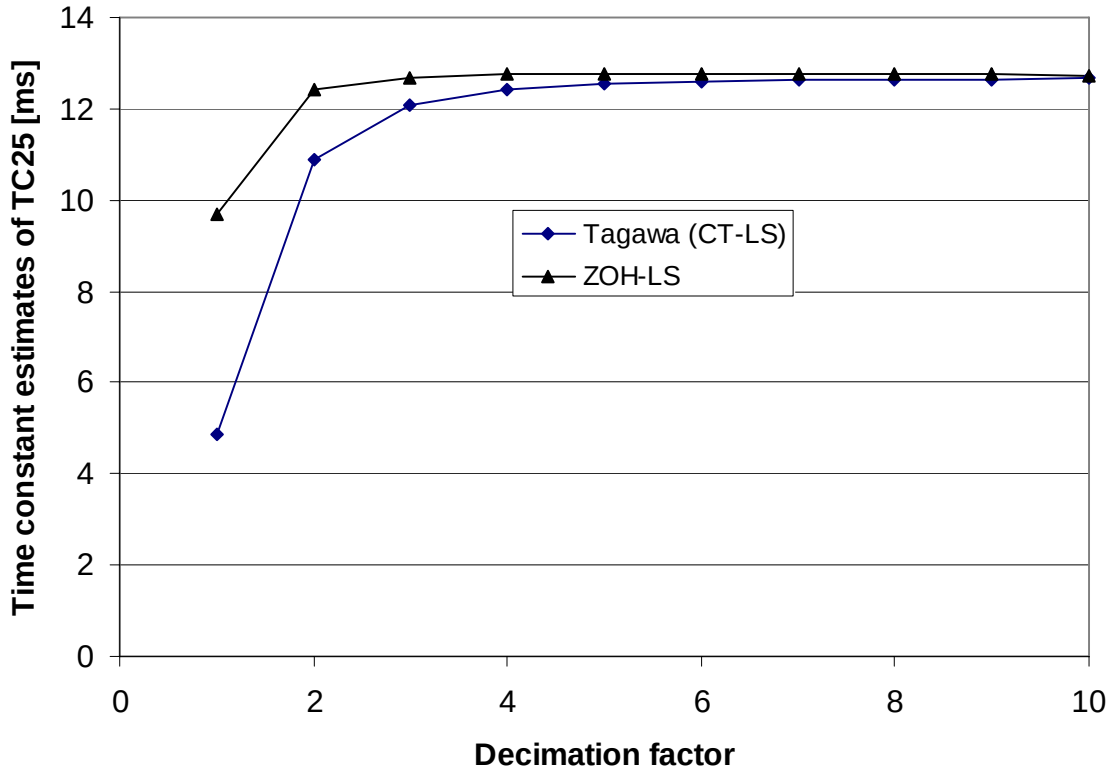

Figure 10 Time constant estimates of TC25 as a function of decimation factor. Helium gas, 5 bar fill pressure, 10 mm stroke at 8.6 Hz.

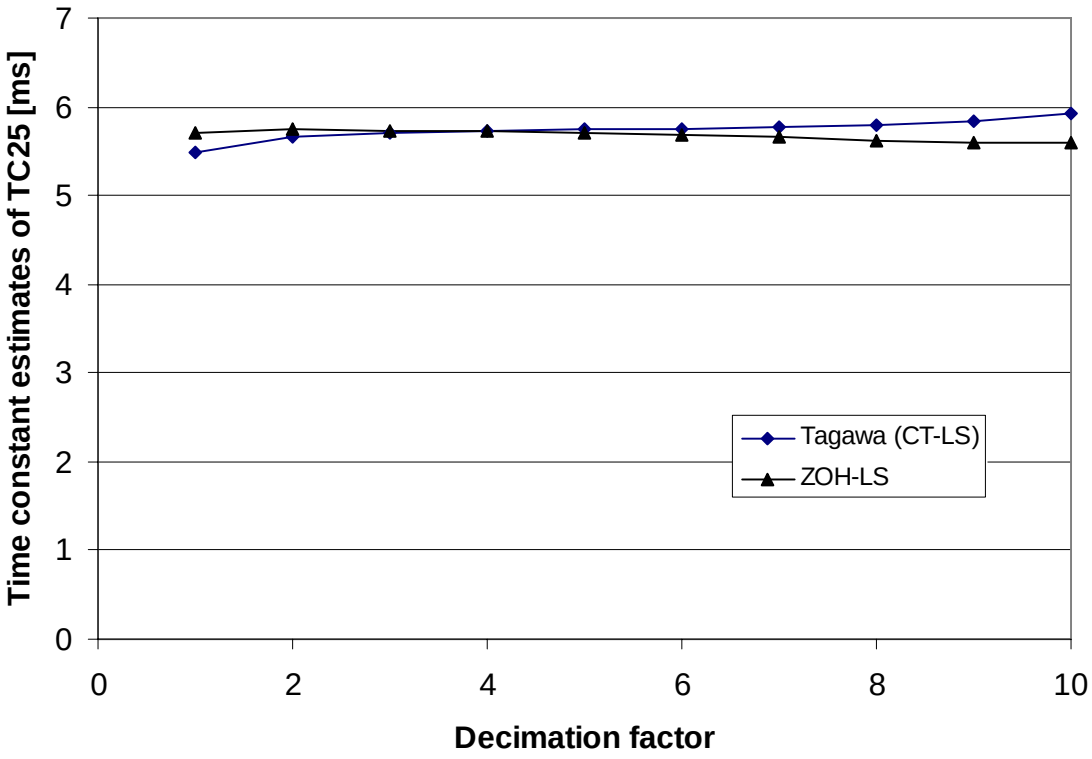

Figure 11 Time constant estimates of TC25 as a function of decimation factor. Helium gas, 5 bar fill pressure, 10 mm stroke at 36 Hz.

For each test condition, the time constants were estimated with from no decimation to 10 times decimation. The minimum decimator factor was noted when the estimates had settled to stable values. The helium results are summarised in Table 1. Only the ZOH-LS results are shown, since previous results have established that the ZOH structure handles noise better. The estimates of Kalman filtering (ZOH-KF) are within the uncertainty of the ZOH ones. All time constants settle within 0.1 ms when the decimation increases further than the stated values. The results show that the time constants decrease when the filling pressure increases and the cyclic frequency increases. The cyclic frequency seems to have a bigger effect.

Table 1 Time constant estimates using ZOH-LS technique in a helium environment. The uncertainty is +/-0.1 ms.

Fill pressure (bar)	Cyclic frequency (Hz)	Time constant of TC25 (ms)	Time constant of TC50 (ms)	Decimation factor used
1	8.6	13.2	28.0	5
5	8.6	12.7	22.8	4
18	8.6	7.4	15.4	2
1	18	8.6	22.1	2
5	18	7.3	17.1	2
18	18	6.2	15.0	3
1	36	8.4	23.6	3
5	36	5.6	14.8	2
18	36	5.7	14.5	2

Table 2 gives the nitrogen results. The magnitude of the time constants is 3 to 4 times bigger than that of helium. So, the raw temperature is a lot more attenuated. Probably due to the increases in time constant magnitude, there are more variations in the time constant estimates as the decimation factor increases. The uncertainty in Table 2 refers to the possible change in the estimates as the decimation factor varies. The response of time constants to fill pressure and frequency is not as clear as with helium. In particular, the time constants at 5 bar and 36 Hz are exceptionally high. The uncertainty is very high too.

Table 2 Time constant estimates using ZOH/LS technique in a nitrogen environment.

Fill pressure (bar)	Cyclic frequency (Hz)	Time constant of TC25 (ms)	Time constant of TC50 (ms)	Uncertainty (ms)	Decimation factor used
1	8.6	46.0	119.3	+0.0, -0.4	3
5	8.6	37.0	95.1	+0.1, -0.1	3
18	8.6	40.8	95.3	+0.0, -0.1	3
1	18	39.4	110	+0.2, -0.4	4
5	18	37.2	101.8	+0.1, -0.8	3
18	18	28.3	73.3	-0.0, -0.8	3
1	36	40.2	117	+0.0, -2.0	2
5	36	62	170	+0, -7	2
18	36	24.9	59.8	+0.0, -1.7	1

1.5.5 Reconstructed temperatures

Ultimately the time constant is used for finding the true gas temperature. The reconstructed temperatures are symbolised as R25 for TC25 and R50 for TC50. This is to avoid confusion with the actual gas temperature at the regenerator exit. The estimated values are listed in Table 1 and Table 2. The time derivatives are calculated using central difference scheme.

The reconstructed temperatures at three frequencies are plotted in Figures 13-15. Results at other conditions are given at the end of this report. The results for R25 and R50 are very similar (Figure 12), so only R25 are shown. Although the true gas temperature is not available, the accuracy of the reconstructed temperatures can be evaluated by the common features in these three plots. Firstly, the two techniques ZOH-LS and ZOH-KF give almost identical temperatures and this is an assurance of the quality of the reconstruction. Secondly, the peak reconstructed temperature is in phase with the cold wire temperature, which indicates the phase of the thermocouple signal has been corrected properly. Phase correctness is only true if the regenerator has little effect, i.e. the temperature changes are driven by compression. The reconstruction and cold wire temperatures are in phase in the first quarter of the cycle. This is when the piston is moving up, and gas mixing in compression space is not expected, so the regenerator cannot affect the cold wire temperature much.

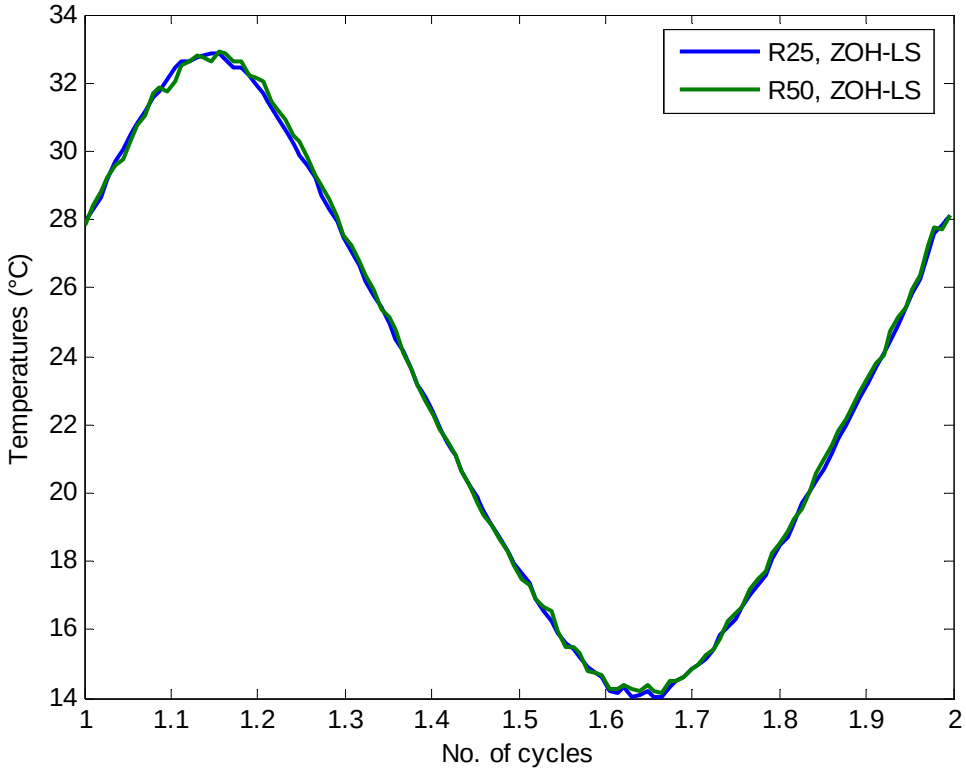

Figure 12 Reconstructed temperatures using ZOH-LS technique. Helium gas, 5 bar fill pressure, 10 mm stroke at 8.6 Hz.

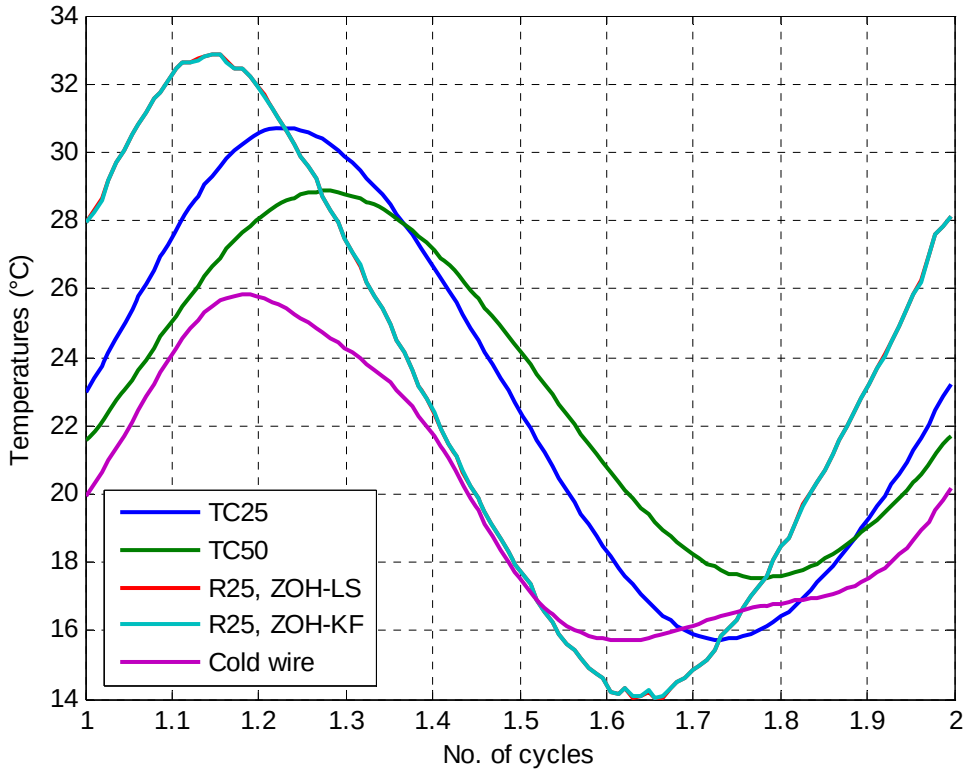

1.5.6

Figure 13 Comparison of the raw and compensated thermocouple and cold wire temperatures. The sampling frequency was decimated to 1.25 kHz. Helium gas, 5 bar fill pressure, 10 mm stroke at 8.6 Hz.

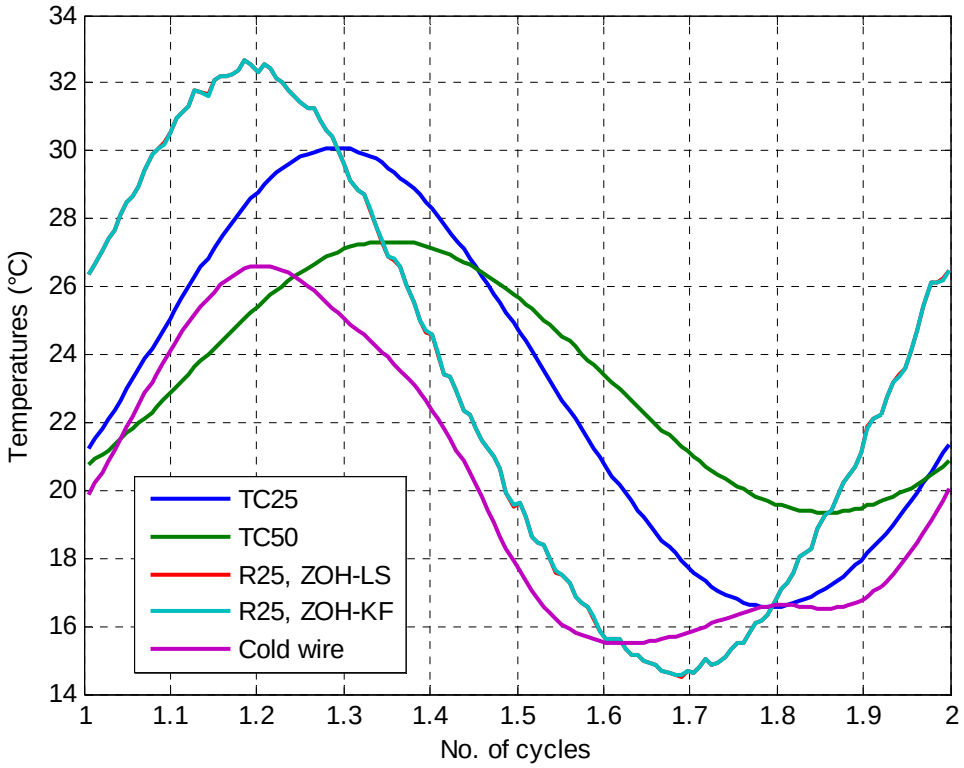

Figure 14 **Comparison of the raw and compensated thermocouple and cold wire temperatures. The sampling frequency was decimated to 2.5 kHz. Helium gas, 5 bar fill pressure, 10 mm stroke at 18 Hz.**

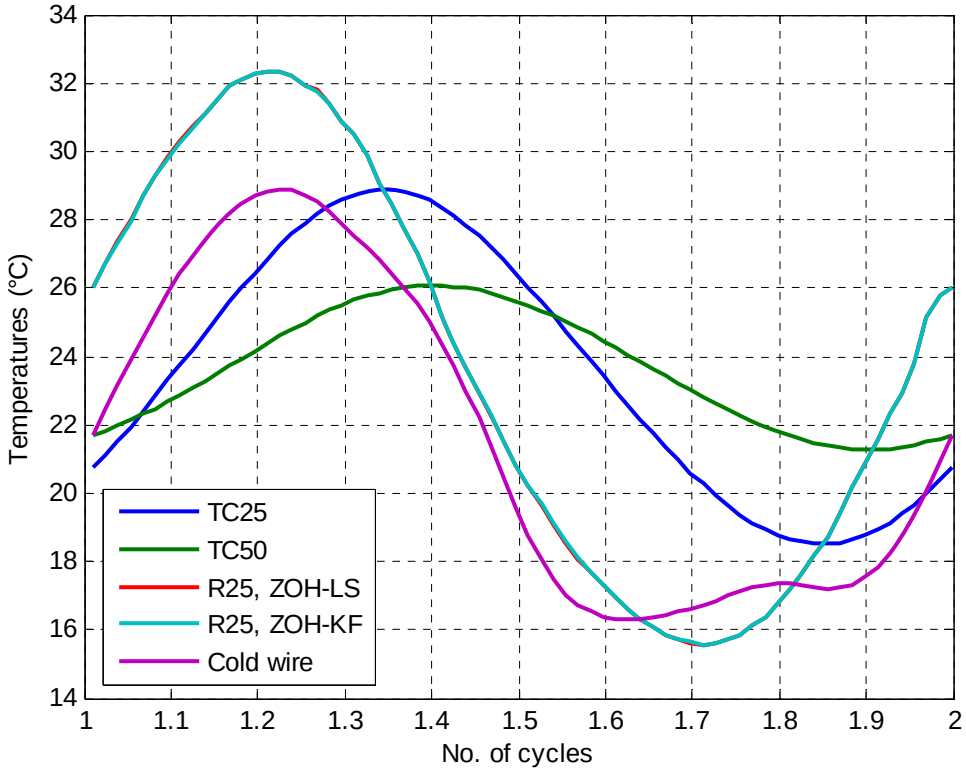

Figure 15 **Comparison of the raw and compensated thermocouple and cold wire temperatures. The sampling frequency was 2.5 kHz. Helium gas, 5 bar fill pressure, 10 mm stroke at 36 Hz.**

1.6 Model validation

The thermocouple measurements are compensated using the estimated time constant. In other words, these compensated signals are no longer real measurements. They are only valuable if they can be validated by some means. The obvious method is to compare them against the true temperature, but this is clearly impossible. In practice, the compensated signals can be indirectly validated by model validation. Model validation checks that the thermocouple models are sufficient to describe the response of the thermocouple and other assumptions made in the estimators. The important assumptions made in two-thermocouple techniques are summarised below:

- Convective heat transfer is dominant, such that a first order response equation is sufficiently accurate.
- The two thermocouples measure the same temperature field, i.e. the separation distance between them is small enough.
- Once the time constant estimate converges as the decimation factor increases, the estimate is optimal (least biased or unbiased).
- Measurement noise and the differences in the two reconstructed temperatures are due to white noise.
- The average time constants are sufficiently good that time varying techniques are not necessary.

The existence of noise means that R_1 and R_2 cannot be equalled at all time. If all the assumptions hold, the residual in the estimation will be non zero, and randomly distributed with zero mean, i.e. a white noise. Residual (*aposterior* prediction error) is defined as

	$\eta(k) = y(k) - x^{\mathrm{T}}(k)\hat{\theta}(k)$	26)

Model validation is essentially a white noise test. It finds the autocorrelation function of the residual, $\Phi_{\eta\eta}$. The autocorrelation function compares if the present sample (zero delay) to sample at a later time step (non-zero delay). If the residual is white noise, it should be uncorrelated to anything else except itself. So, the autocorrelation function whose value is normalised to the value at zero delay should be one at zero delay and zero everywhere else. In practice however, because the data sample is finite, this limits the noise bandwidth. The consequence is that the samples may be slightly correlated. A 95% confidence interval has been constructed to allow for the effect of finite data length. If the autocorrelation exceeds this interval, this means it is 95% certain that the residual is correlated (not white).

It has been deduced that when no decimation or low-pass filtering is applied, the time constant estimates tend to be biased due to the influence of noise. Figure 16 and Figure 17 compare the autocorrelation function of residual without and with decimation. The decimation selected was the minimum decimation required to achieve a stable time constants. The results clearly show that when the time constant was too low, there are dynamics in the residual (unaccounted system information) which are correlated. The function is always above the upper limit of uncertainty. After appropriate decimation is applied, the autocorrelation fluctuates around zero (except delay = 0), and the fluctuations are within the confidence interval. The residual can be accepted as white noise. This test also indicates that the thermocouple model is sufficiently accurate and that any effect of thermocouple separation is negligible.

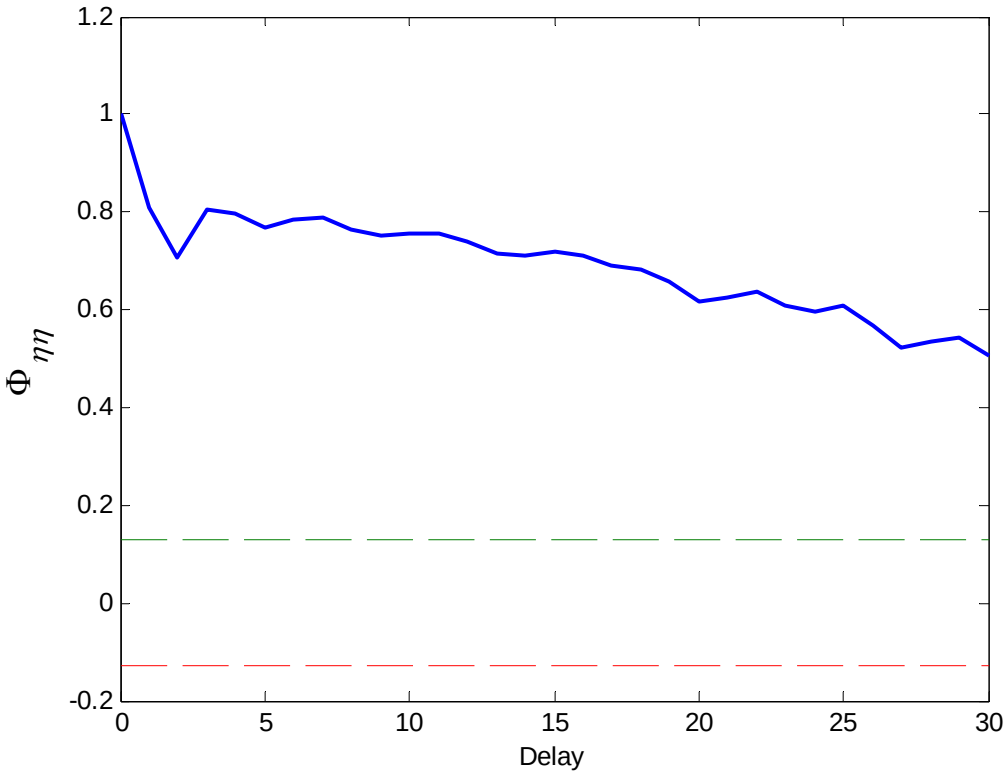

Figure 16 **Normalised Autocorrelation function of the residual for the CT-LS technique. Nitrogen gas, 1 bar fill pressure, 10 mm stroke at 8.6 Hz. No decimation was applied. The dotted lines show the 95% confidence interval within which the autocorrelation should lie if the residual is white noise.**

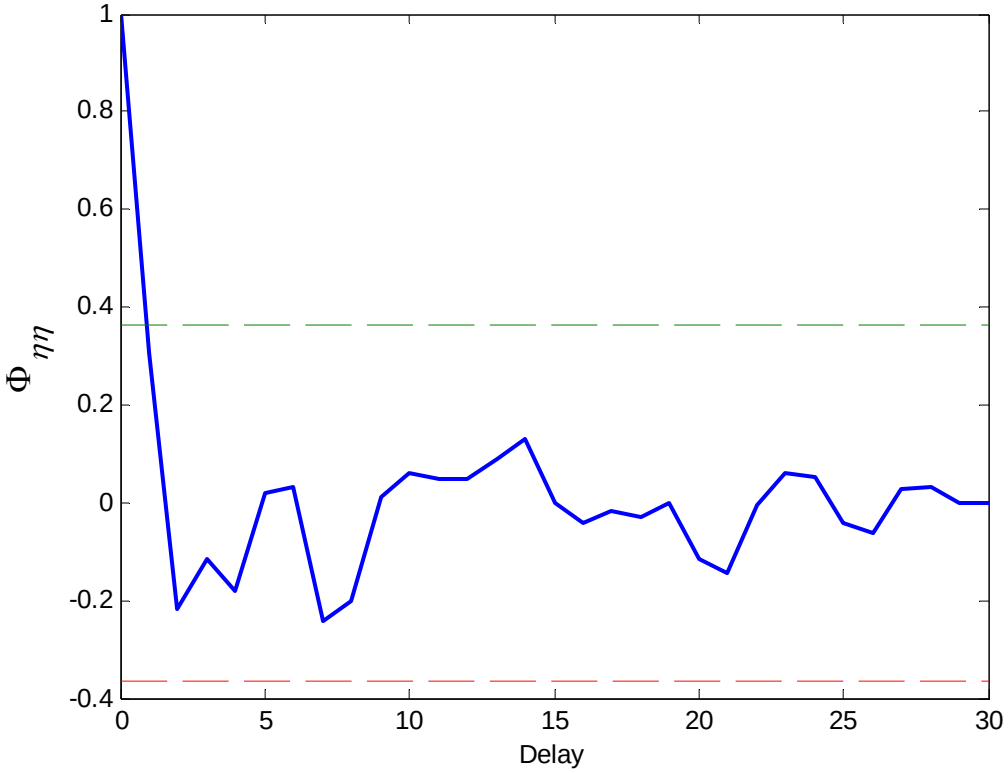

Figure 17 **Normalised autocorrelation function of the residual for the CT-LS technique. Nitrogen gas, 1 bar fill pressure, 10 mm stroke at 8.6 Hz. 8 times decimation was applied. The dotted lines show the 95% confidence interval within which the autocorrelation should lie if the residual is white noise.**

The results of the model validation are generally satisfactory at higher frequency and filling pressure, see Figure 18 for example. But, there are some marginal cases where the autocorrelation function exceeds the confidence intervals by a small amount. The case for nitrogen gas at 18 bar filling pressure at 8.6 Hz clearly illustrates this point (Figure 19). The marginal case should still be considered acceptable because there is a 5% probability that a genuine white noise fails the model validation. If the marginal tests are accepted, 8 out of 9 tests pass the model validation when nitrogen is used, but only 3 out of 9 tests pass for helium. Table 3 summarises the results for all tests. Amongst all the failed cases, there is a common feature – the autocorrelation function only fails at delay = 3. For all other delays the function is within the limits. An example of this failure is shown in Figure 20. The failure at delay = 3 means that the model does not account for the dynamics with a delay of 3. The results cannot pinpoint which assumption has been violated. For these cases, variable time constants were estimated instead of average values, the autocorrelation does not change much. This shows that the high correlation at delay =3 is not caused by the average time constant. Grys *et al.* [15] performed similar model validation, in which a least mean squares estimator was used. Interestingly the normalised autocorrelation function also has a distinct spike, but at delay = 2 (Figure 21). Nevertheless Grys *et al.* [15] still stated that "the autocorrelation lies inside the confidence interval". It is not apparent at this stage whether this feature in the autocorrelation is enough to jeopardise the two-thermocouple technique. Since the actual gas temperature is unknown, it is difficult to establish which other assumptions are to blame, and decide appropriate action. Therefore, it is recommended to proceed with caution. Without rigorous analysis, it seems likely that the conduction effect may play a role which the thermocouple model needs to take account of.

Table 3 Results of the model validation tests using average time constant estimation, ZOH-LS techniques results

Filling pressure (bar)	Cyclic frequency (Hz)	Helium results	Nitrogen results
1	8.6	Delay = 3 exceeds the limit	Acceptable
5	8.6	Delay = 3 exceeds the limit	Marginal
18	8.6	Delay = 2 and 3 exceed the limit	Marginal
1	18	Failed. The autocorrelation function appears to be periodic	Acceptable
5	18	Delay = 3 exceeds the limit	Delay = 3 exceeds the limit
18	18	Marginal	Marginal
1	36	Marginal	Acceptable
5	36	Acceptable	Acceptable
18	36	Delay = 3 exceeds the limit	Acceptable

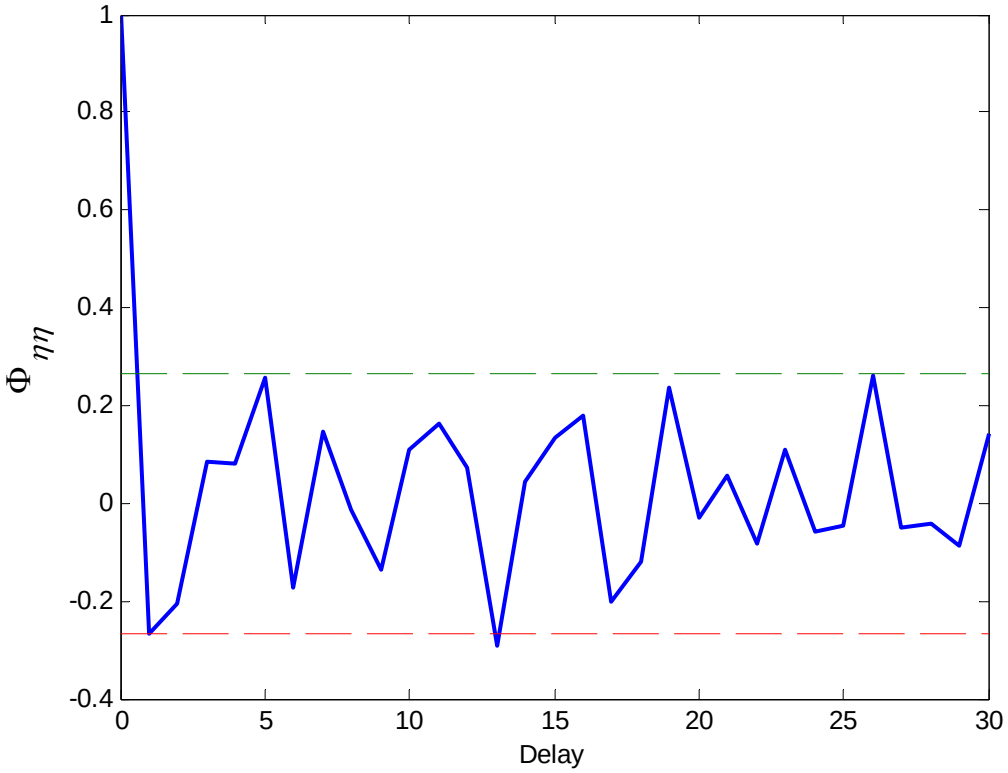

Figure 18 **Normalised autocorrelation function of the residual using ZOH-LS techniques. No decimation has been applied. Nitrogen gas, 18 bar fill pressure, 10 mm stroke at 36 Hz. The dotted lines show the 95% confidence interval within which the autocorrelation should lie if the residual is white noise.**

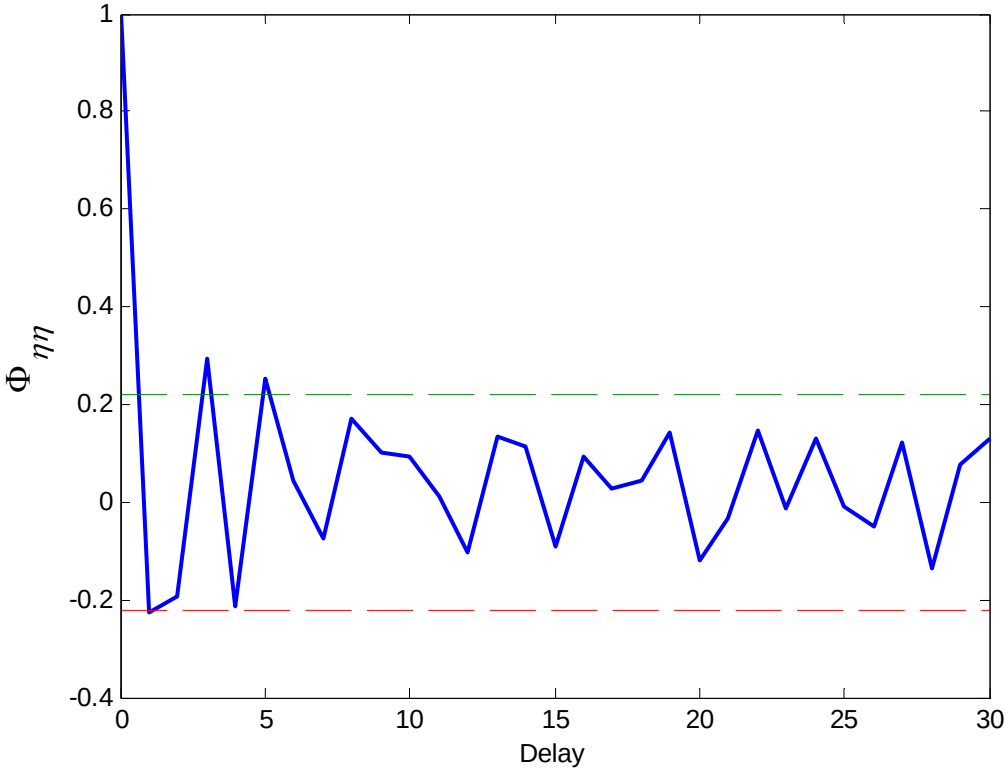

Figure 19 **Normalised autocorrelation function of the residual using ZOH-LS techniques. 3 times decimation has been applied. Nitrogen gas, 18 bar fill pressure, 8 mm stroke at 8.6 Hz. The dotted lines show the 95% confidence interval within which the autocorrelation should lie if the residual is white noise.**

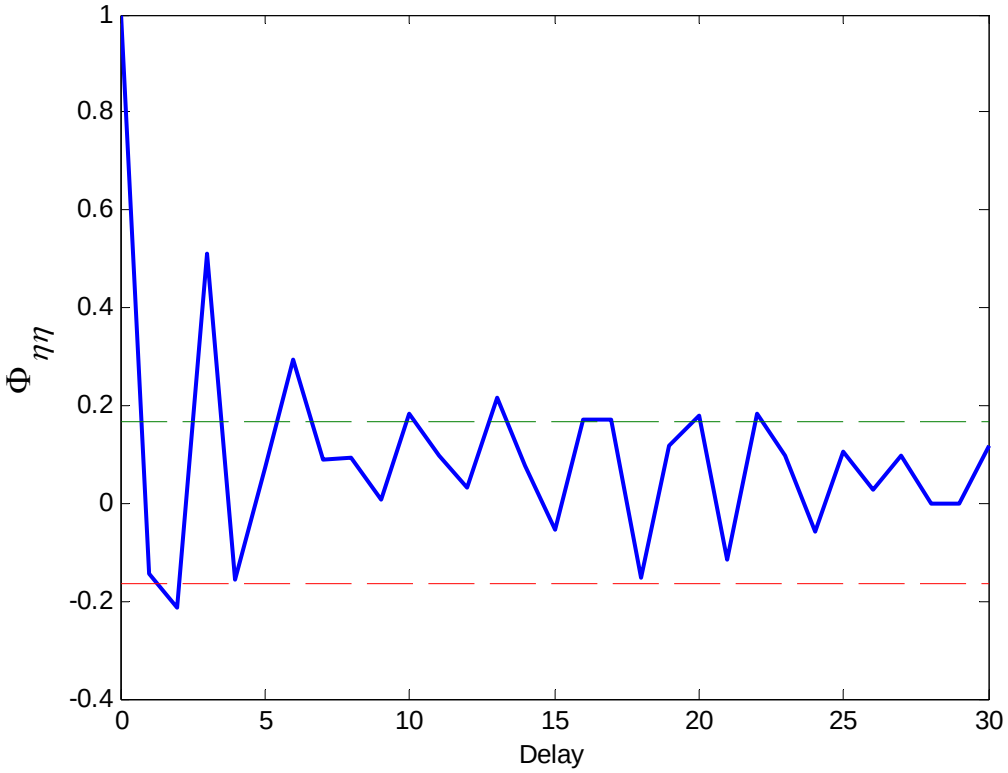

Figure 20 Normalised autocorrelation function of the residual using ZOH-LS techniques. 2 times decimation has been applied. Nitrogen gas, 5 bar fill pressure, 10 mm stroke at 18 Hz. The dotted lines show the 95% confidence interval within which the autocorrelation should lie if the residual is white noise.

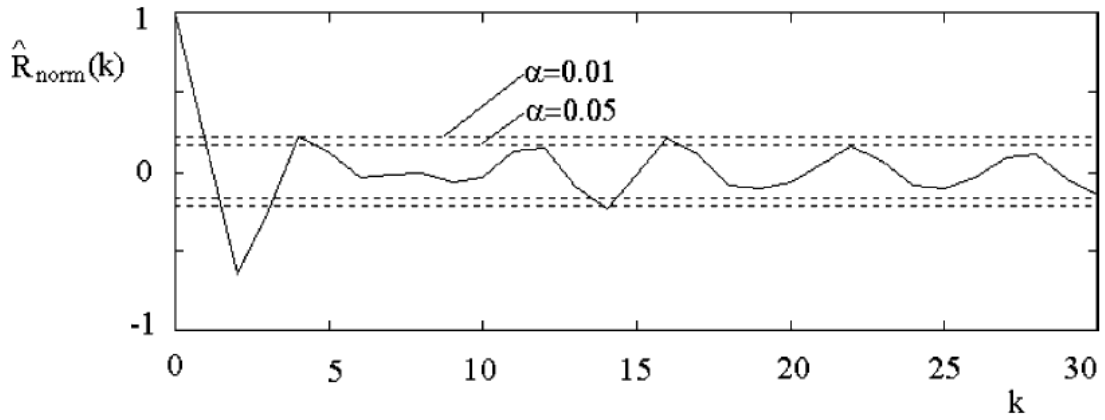

Figure 21 Normalised autocorrelation function of the residual from Gry et al. [15]. *k* represents delay and *α* is the error probability. 1-*α* indicates the width of the confidence interval.

The helium result at 1 bar pressure and 18 Hz deserves further discussion because it is the one that fails differently. The autocorrelation function shows regular oscillations in Figure 22. The confidence interval is consistently exceeded over a range of delays. This is in a sharp contrast to the case in which the autocorrelation is unusually high at delay = 3. Therefore, the time constants and the reconstructed temperature at this condition may be unreliable and are ignored accordingly.

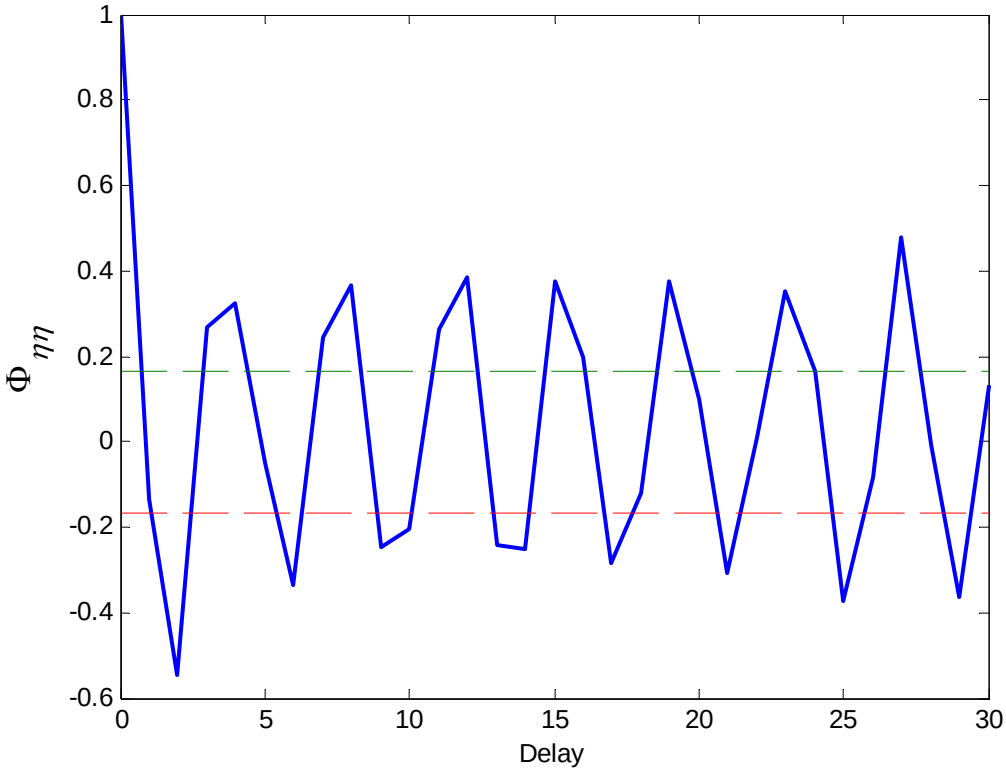

Figure 22 Normalised autocorrelation function of the residual using ZOH-LS techniques. 2 times decimation has been applied. Helium gas, 1 bar fill pressure, 10 mm stroke at 18 Hz. The dotted lines show the 95% confidence interval within which the autocorrelation should lie if the residual is white noise.

1.7 Conclusions

The following conclusions can be drawn from the thermocouple compensation work:

- Although very fine thermocouples were used in the experiment, thermocouples of different diameters still had different responses, which suggested the time response was still insufficient to measure the gas temperature accurately.
- The cyclic variability is found to be low. This makes ensemble averaging possible without losing much information.
- Low-pass filtering reduces bias in time constant estimation, so comparing the results with and without low-pass filtering can reveal the noise tolerance of different techniques. The results show that model structure is more important in noise rejection than the types of estimator used. The ZOH model structure is far superior to the continuous time (CT) model structure.
- Low noise as found in high cyclic frequency results has prompted the fact that any unwanted noise will be scaled by the time step in the time derivation. So, an effective way to reduce noise is to reduce the sampling frequency by decimation.
- It has been found that the time constant estimates converge as the decimation factor increases. The stable value allows a minimum decimation factor to be determined, above which an unbiased time constant estimate can be obtained.
- The time constants are found to decrease when the filling pressure increases and the cyclic frequency increases. The cyclic frequency seems to have a bigger effect.
- The magnitude of the time constants in a nitrogen environment is 3 to 4 times bigger than that in helium.

- Features in the reconstructed temperatures, e.g. the peak temperature in phase with the cold wire temperature, suggest that the compensation is physically sound.
- 8 out of 9 nitrogen results pass the model validation test, but only 3 out of 9 helium results pass. Most of the failure can be characterised by abnormally high autocorrelation at delay = 3.
- Variable time constants were estimated for the results which fail the model validation test. However, the autocorrelation does not change much when compared to the average time constant cases.

1.8 Reference

1. Hoshino, T., Watanasirisuk, P., Ibrahim, M. and Simon T. (2004) Dynamic temperature measurements in Stirling cycle machines using two-thermocouple technique. 2nd International Energy Conversion Engineering Conference (Rhode Island), Aug 16-19, AIAA 2004-5559.
2. Collis, D. C. and Williams, M. J. (1959) Two-dimensional convection from heated wires at low Reynolds numbers. *J. Fluid Mech*. **6**, 357-384.
3. Petit, C., Gajan, P., Lecordier, J. C. and Paranthoen, P. (1982) Frequency response of fine wire thermocouple. *J. Phys. E.: Sci. Instr*. **15**, 761-764.
4. Cambray, P. (1986) Measuring thermocouple time constants: a new method. *Combustion Science and Technology*, **45**, 221-224.
5. Tagawa, M. and Ohta, Y. (1997) Two-Thermocouple Probe for Fluctuating Temperature Measurement in Combustion- Rational Estimation of Mean and Fluctuating Time Constants. *Combustion and Flame*, **109,** 540-560.
6. Tagawa, M., Shimoji, T., and Ohta, Y. (1998) A two-thermocouple probe technique for estimating thermocouple time constants in flows with combustion: in situ parameter identification of a first-order lag system. *Review of Scientific Instruments*, **69**(9), 3370-3378.
7. Tagawa, M., Kato, K., and Ohta, Y. (2003) Response compensation of temperature sensors: frequency-domain estimation of thermal time constants. *Review of Scientific Instruments*, **74**(6), 3171-3174.
8. Forney, L. J. and Fralick, G. C. (1994) Two wire thermocouple: Frequency response in constant flow. *Review of Scientific Instruments*, **65**(10), 3252-3256.
9. Hung, P. C., Irwin, G., Kee, R. and McLoone, S. (2005) Difference equation approach to two-thermocouple sensor characterization in constant velocity flow environments. *Review of Scientific Instruments*, **76**, 024902.
10. Hung, P. C., Kee, R. J., Irwin G. W. and McLoone, S. F. (2007) Blind deconvolution for two-thermocouple sensor characterization. *Journal of Dynamic Systems, Measurement, and Control*, **129**, 1-13.
11. Kar, K., Roberts, S., Stone, R., Oldfield, M. and French, B. (2004) Instantaneous exhaust temperature measurement using thermocouple compensation techniques. *SAE Journal of Fuels and Lubricants,* **4**, 652-673.
12. Kar, K. (2004) Three-Thermocouple Technique for Fluctuating Temperature Measurement. PhD Thesis, University of Oxford.
13. Kee, R. J., Hung, P., Fleck, B., Irwin, G., Kenny, R., Gaynor, J. and McLoone, S. (2006) Fast response exhaust gas temperature measurement in IC engines. SAE 2006 World Congress (Detroit), Apr 3-6. Paper no 2006-01-1319.
14. O'Reilly, P.G., Kee, R.J., Fleck, R., and McEntee, P.T. (2001) Two-wire thermocouples: a nonlinear state estimation approach to temperature reconstruction. *Review of Scientific Instruments*, **72**(8), 3449-3457.

15. Grys, S. and Minkina, W. (2002) Fast temperature determination using two thermometers with different dynamical properties. *Sensors and Acutators A*, **100**, 192-198.
16. Johansson, R. (1993) System modeling Identification. Prentice-Hall, Englewood Cliffs, New Jersey.
17. Haykin, S. (2002) Adaptive filtering theory. Prentice-Hall, Upper Saddle River, New Jersey.
18. Jazwinski, A. H. (1969) Adaptive filtering. *Automatica*, **5**, 475-485.
19. Kar, K., Swain, A., Raine, R., Roberts, S., and Stone, R. (2006) Cycle-by-cycle variations in exhaust temperatures using thermocouple compensation techniques. SAE 2006 World Congress (Detroit), Apr 3-6. Paper no 2006-01-1197.

1.9 Appendix

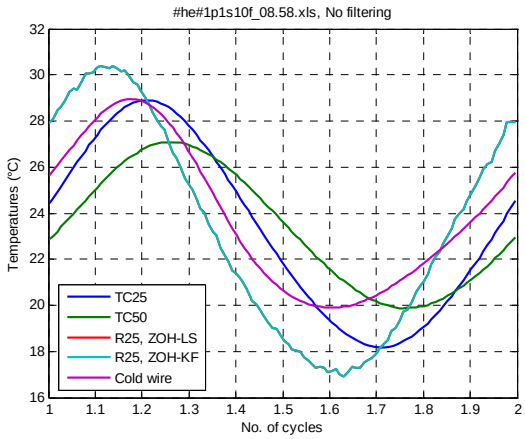

Helium gas, 1 bar fill pressure, 10 mm stroke at 8.6 Hz.

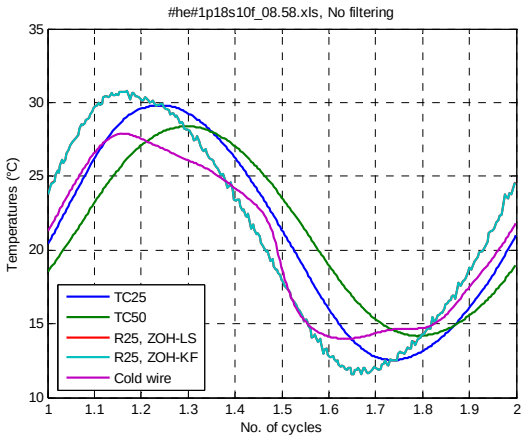

Helium gas, 18 bar fill pressure, 10 mm stroke at 8.6 Hz.

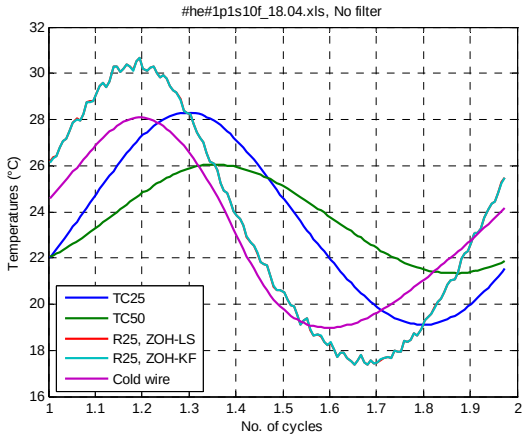

Helium gas, 1 bar fill pressure, 10 mm stroke at 18 Hz.

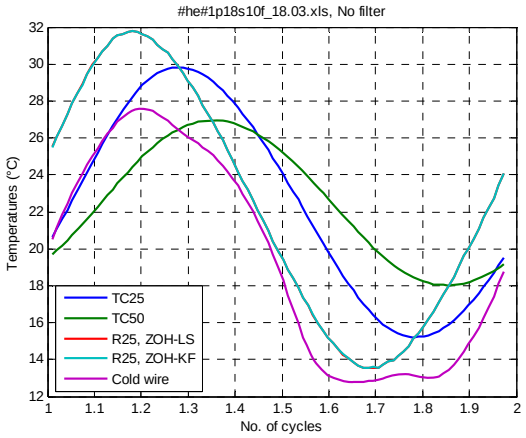

Helium gas, 18 bar fill pressure, 10 mm stroke at 18 Hz.

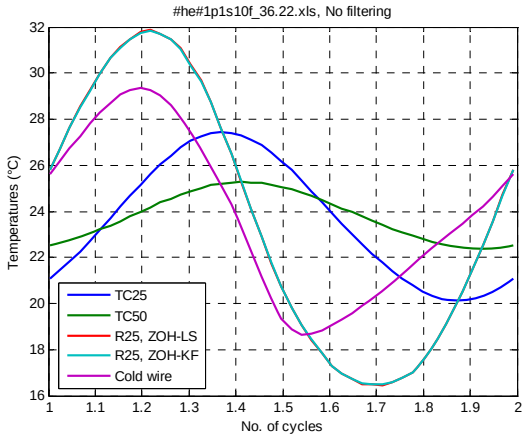

Helium gas, 1 bar fill pressure, 10 mm stroke at 36 Hz.

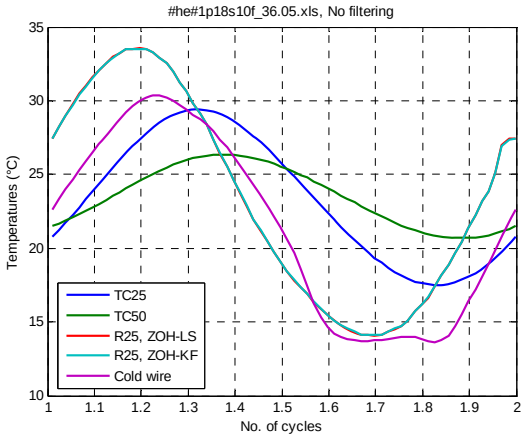

Helium gas, 18 bar fill pressure, 10 mm stroke at 36 Hz.

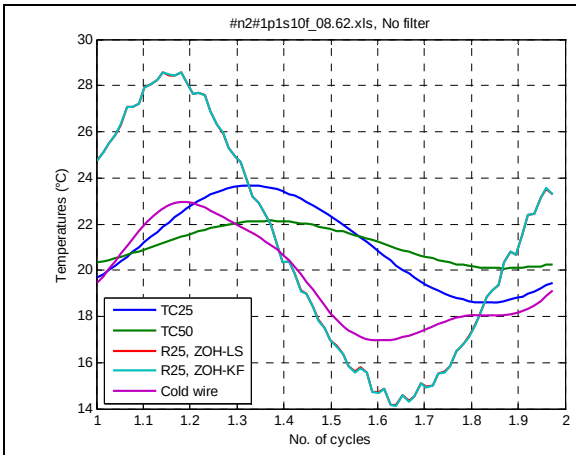

Nitrogen gas, 1 bar fill pressure, 10 mm stroke at 8.6 Hz.

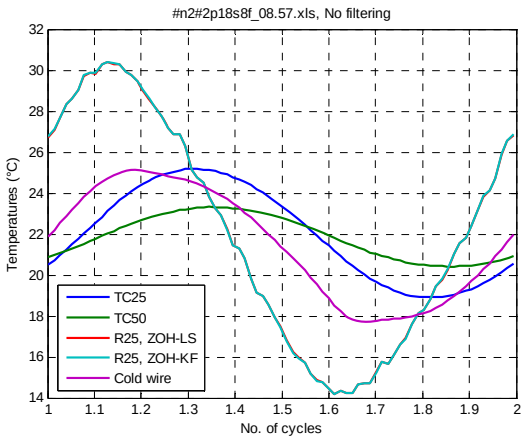

Nitrogen gas, 18 bar fill pressure, 8 mm stroke at 8.6 Hz. 10 mm was not achievable.

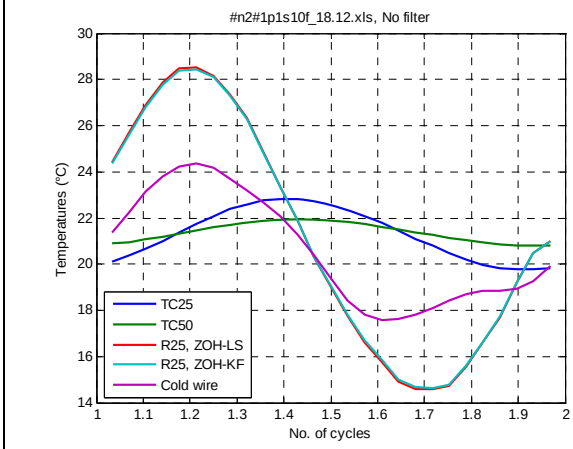

Nitrogen gas, 1 bar fill pressure, 10 mm stroke at 18 Hz.

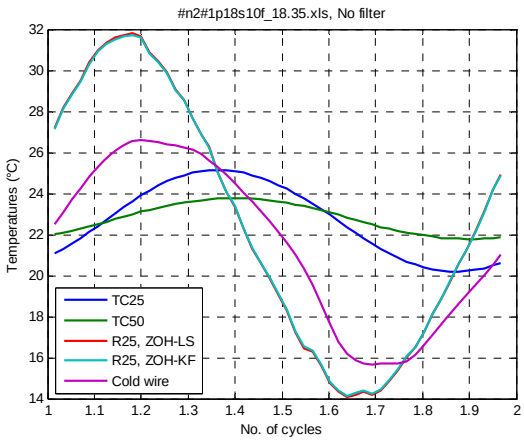

Nitrogen gas, 18 bar fill pressure, 10 mm stroke at 18 Hz.

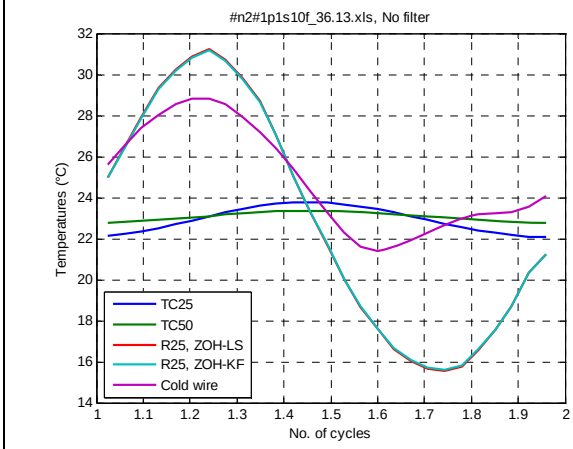

Nitrogen gas, 1 bar fill pressure, 10 mm stroke at 36 Hz.

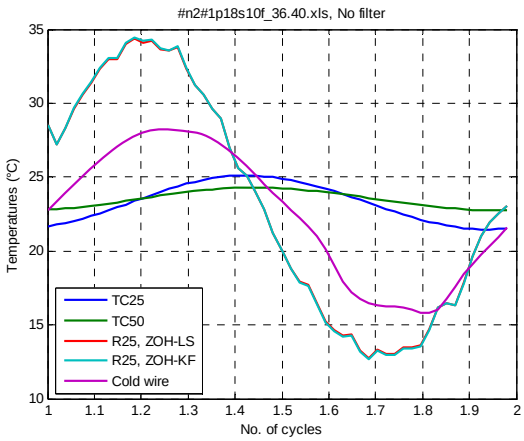

Nitrogen gas, 18 bar fill pressure, 10 mm stroke at 36 Hz.

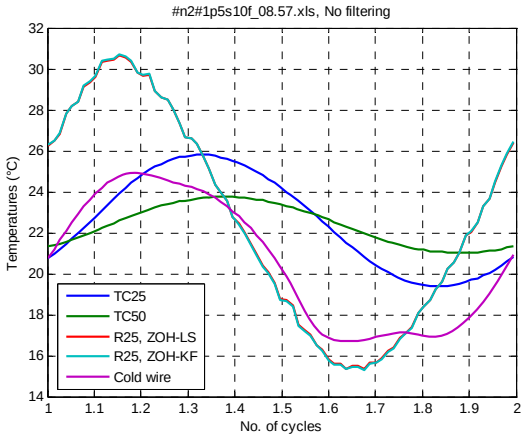

Nitrogen gas, 5 bar fill pressure, 10 mm stroke at 8.6 Hz.

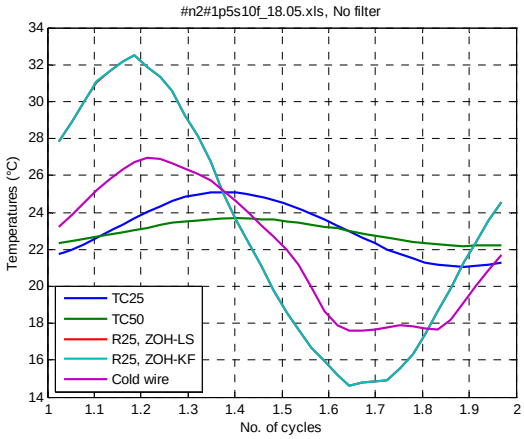

Nitrogen gas, 5 bar fill pressure, 10 mm stroke at 18 Hz.

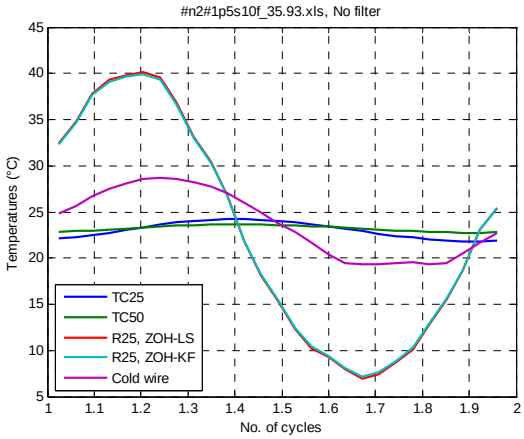

Nitrogen gas, 5 bar fill pressure, 10 mm stroke at 36 Hz.